University of Nevada, Reno

Development of Low Noise-Broadband Raman Amplification Systems Based on Photonic Crystal Fibers for High Capacity DWDM Networks

A thesis submitted in partial fulfillment of the

requirements for the degree of Master of Science in

Electrical Engineering

By

Abdelghafor Elgamri

Dr. Banmali Rawat (Thesis Advisor)

August, 2017

THE GRADUATE SCHOOL

We recommend that the thesis
prepared under our supervision by

ABDELGHAFOR ELGAMRI

Entitled

Development Of Low Noise-Broadband Raman Amplification Systems Based On Photonic Crystal Fibers For High Capacity DWDM Networks

be accepted in partial fulfillment of the
requirements for the degree of

MASTER OF SCIENCE

Dr.Banmali Rawat, Advisor

Dr. Ji Yoon, Committee Member

Dr. Micheal A.Webster, Graduate School Representative

David W. Zeh, Ph.D., Dean, Graduate School

August, 2017

Abstract

The increased demand from IP traffic, video application and cell backhaul has placed fiber routes under severe stains. The high demands for large bandwidth from enormous numbers from cell sites on a network made the capacity of yesterday's networks not adequate for today's bandwidth demand. Carries considered Dense Wavelength Division Multiplexing (DWDM) network to overcome this issue. Recently, there has been growing interest in fiber Raman amplifiers due to their capability to upgrade the wavelength-division-multiplexing bandwidth, arbitrary gain bandwidth. In addition, photonic crystal fibers have been widely modeled, studied, and fabricated due to their peculiar properties that cannot be achieved with conventional fibers.

The focus of this thesis is to develop a low-noise broadband Raman amplification system based on photonic crystal Fiber that can be implemented in high capacity DWDM network successfully. The design a module of photonic crystal fiber Raman amplifier is based on the knowledge of the fiber cross-sectional characteristics i.e. the geometric parameters and the Germania concentration in the dope area. The module allows to study different air-hole dimension and disposition, with or without a central doped area. In addition the design integrates distributed Raman amplifier and nonlinear optical loop mirror to improve the signal to noise ratio and overall gain in large capacity DWDM networks.

Acknowledgements

Praise be to ALLAH, his majesty for his uncountable blessings, and best prayers and peace be unto his best messenger Mohammed, his pure descendant, and his family and his noble companions.

Foremost, I would like to express my thanks to my advisor Dr. Banmali Rawat for his constant guidance and encouragement. Without his assistance this research would not have been possible. I would like to thank my thesis committee members, Dr. Yoon and Dr. M. Webster, for taking time from their schedules to contribute to my thesis. I would also like to thank my family and friends for their continual financial and moral support throughout my studies at the University of Nevada, Reno.

Table of Contents

List of Tables

List of Figures

List of Abbreviations

PCF	Photonic Crystal Fiber
OFC	Optical Fiber Conference
EDFA	Erbium-Doped Fiber Amplifier
DWDM	Dense Wavelength Division Multiplexing
FDTD	Finite Difference Time Domain
OSNR	Optical Signal to Noise Ratio
UPML	Uniaxial Perfectly Matched layer
ASE	Amplified Spontaneous Emission
DRS	Double Rayleigh Scattering
MPI	Multipath-Path interference
SRS	Stimulated Raman Scattering
DRA	Disturbed Raman Amplifier
SNR	Signal to Noise Ratio
NF	Noise Figure
BER	Bit Error Rate
PRBS	Pseudo Random Bit Sequences
NRZ	Non-Return –to-Zero
OOK	On Off Keying

NOLM	Nonlinear-optical loop mirror
SPM	Self-Phase Modulation
NALM	Nonlinear Amplification Loop Mirror
EMLs	Externally Modulated Lasers
DMLs	Directly Modulated Laser
HPCF	Hexagonal Photonic Crystal Fiber
FEM	Finite Element Method
FDTD	Finite-Difference Time-Domain
PWE	Plane Wave Expansion
PBG	Photonic Band Gab
SMF	Single Mode Fiber
SCW	Surface Capillary Waves
NZ-DSF	Nonzero Dispersion-Shifted Fiber
DCF	Dispersion-Compensation Fiber
HC-PCF	Hollow Core Photonic Crystal Fibers

Chapter-1
Introduction

After the arrival of optical fiber technology in the early 1970s, the use and demand of optical fibers has grown at a rapid rate. The increasing demand for bandwidth with high capacity for handling vast amount of information due to internet, multimedia, voice data and video has made fiber optics with its comparatively infinite bandwidth the only solution. The fiber optic industry has grown explosively in the last fifteen years and the analysts are expecting that the industry will keep growing at exponential rate for the coming decade and beyond.

Recently, there has been growing interest in fiber Raman amplifiers due to their capability to upgrade the wavelength-division-multiplexing bandwidth, arbitrary gain bandwidth which is determined by the pump wavelength only and the low noise figure. In the last few years photonic crystal fibers have been widely modeled, studied, and fabricated due to their special properties such as endless single- mode, high –nonlinearity, very high numerical aperture, strong birefringence multicore designs and unusual chromatic dispersion properties. The objective of this thesis is to develop and simulate a low noise amplification system for high capacity dense wavelength division multiplexing network based on photonic crystal fiber Raman amplifier.

1.1 History of Fiber Optics communication

The revolution of communication began when Samuel Morse (1791-1872) and other inventors developed the telegraph in the 1830s. In addition, he developed a code –Morse Code- that increased the bit rate to almost 10b/s and by using intermediate relay station, Morse was able to send the first long distance telegraph massage from Washington D.C to Baltimore,

Maryland in1844 [1]. By 1876 Graham Bell succeeded in using his “vibraphone” to remotely transmit his voice over the telephone for the first time [2]. This great invention was able to transmit the electrical signals in analog form over the transmission line creating worldwide telephone networks and dominating the communication systems for over a century.

The communication system had a noticeable improvement in the total capacity by using coaxial cables instead of twisted pairs. As a result a 3-MHz coaxial system capable of carrying 300 voice channels or a single TV channel was established in 1940 but the coaxial cable losses increased rapidly after 10 MHz, limiting the system bandwidth below 10 MHz [3]. Microwaves communication systems were introduced to overcome the high frequency loss limitations by using electromagnetic carrier waves operating at 1- 10 GHz frequency range as the transmitting signal. Coaxial cable systems evolved and reached a saturation point of 100 Mb/s bit rate with a limitation of small repeater spacing (1Km) increasing the total system cost. In general the Microwave communication systems allowed large distance spacing (50 km) but the carrier frequency of the signal limited their bit rate as well [4]. A commonly used way to measure the performance of commination systems is the bit rate – distance product, BL, where B is the bit rate and L is the distance between the repeaters. Figure 1.1 shows the improvement of the bit rate-distance product through the technological movement over 150 years span.

By the 1950s the researchers had realized that the bit rate-distance product could be exponentially increased if the electromagnetic waves were replaced by optical waves as the carrier of the transmitted signal. In 1966, after the invention of the laser, Charles K. Kao and George Hockam proposed the optical fibers as the transmission medium as they were capable of guiding the light the same way the coaxial cables guide the electricity [5]. In fiber optics, the optical signal is transmitted through hair-thin waveguide made of glass or plastic. The light

is guided in the fiber core which is surrounded by the cladding. The optical signal is trapped in the core due to total internal reflection phenomena between the core and the cladding. However that system suffered from 1000 dB/Km loss compared to (2-5) dB/Km loss for the coaxial cables at that time.

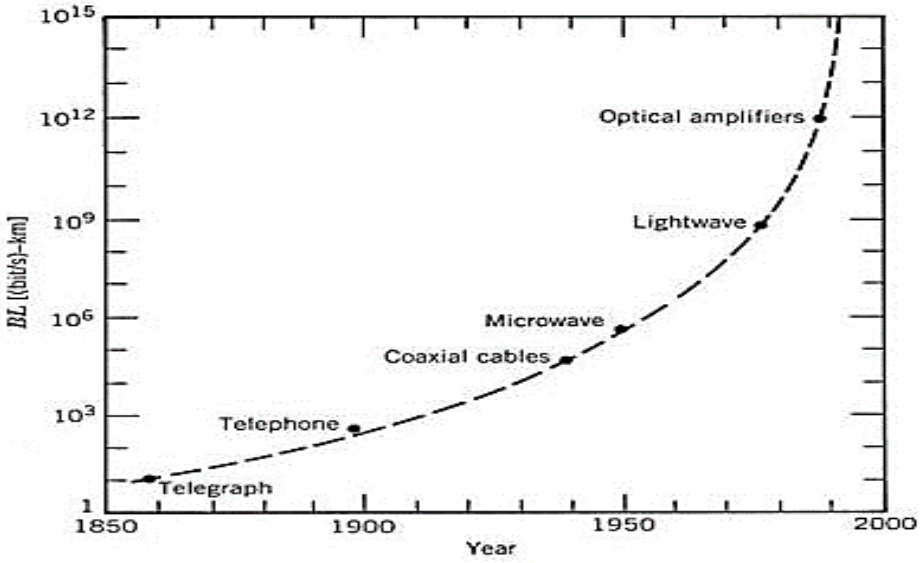

Figure1.1: The increasing in bit rate-distance product during the last century and a half.

In 1970, a 20dB/Km loss fiber was introduced when the operating wavelength was around 0.8μm. At the same time the continuous wave semiconductor lasers were developed .The dual availability of relatively low –less fiber and compact optical sources led to the first generation of fiber optics system with 45Mbit/s and 10 Km repeaters spacing [6]. Figure1.2 shows the improvement in optical fiber communication systems through technological enhancement during the period of 1974-1996.

1.2 Raman Amplifiers

In the telecommunication revolution in the early 1990s optical amplifiers have played a leading role when it was realized that the fiber optics system could operate over a large spans

by using internal light amplifier reducing the high cost of using electronic regenerations and converters. As shown in Figure 1.4 in early 1990s Erbium-doped Fiber amplifiers (EDFAs) were the focus of the researchers as it was suitable for the low loss wavelength spectrum (1530 to 1610 nm) of silica-based fibers [9]. In addition the high pump power required for Raman gain compared to EDFA small signal power combined with the lake of high power laser sources at suitable wavelength subsided the research in Raman amplifiers until the mid -1990s.

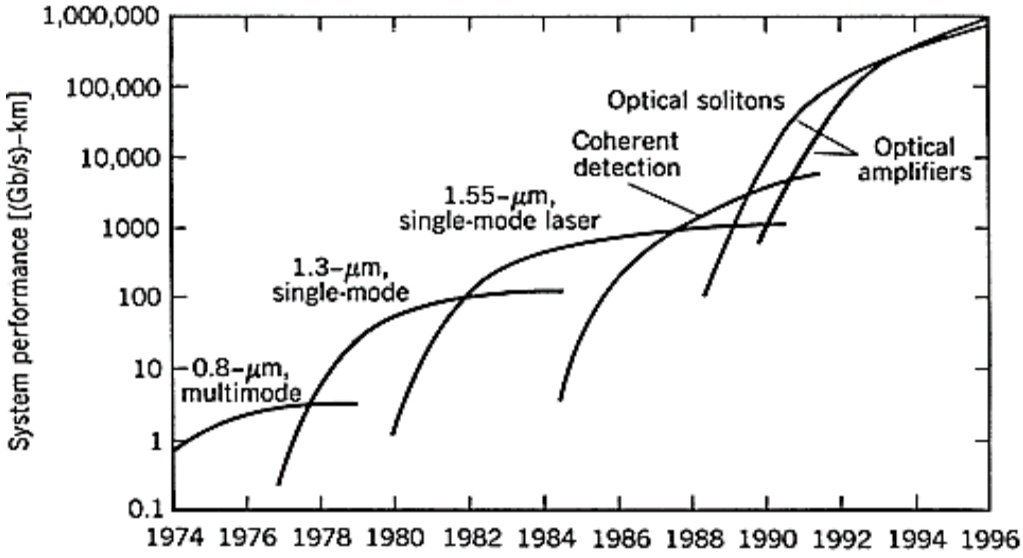

Figure1.2: Progress of fiber optics technology over the period of 1974-1996.

The development of appropriate high power pumps in the mid-1990 [10] exponentially increased the interest of the researchers in Raman Amplifiers .They were quick to show some advantages and features of Raman Amplifiers over EDFAs specially when the transmission fiber itself is used as a Raman amplifier. It was found the Raman amplifiers were suitable for Dense Wavelength Division Multiplexing (DWDM) as they have the possibility of amplification of variable wavelengths over a very broadband operation spectrum.

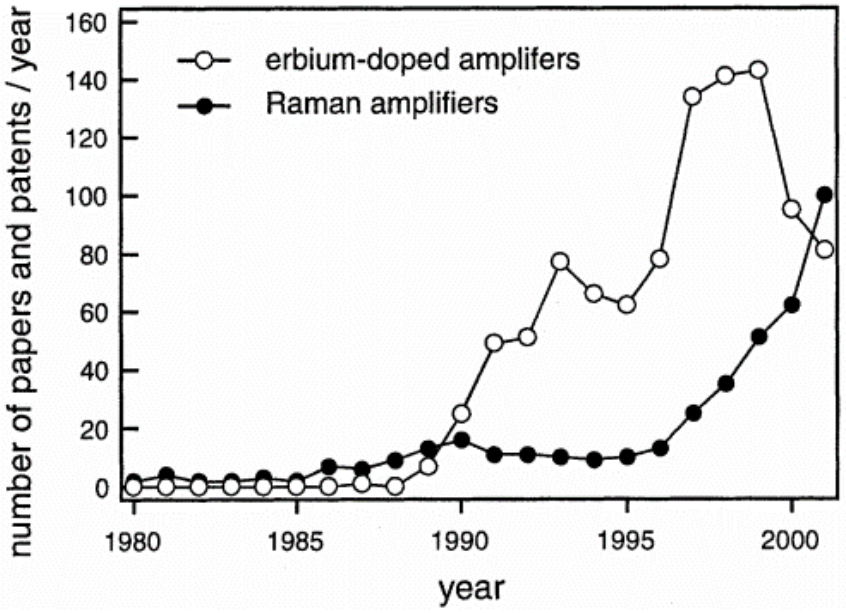

Figure1.3: Published papers in the field of EDFA and Raman amplifiers since 1980.

Over the transmission length of the fiber Raman amplifier a significant double Rayleigh scattering of the signal and amplified spontaneous emission inside the amplifier occurs. These phenomena appear as noises in the transmitted signal and they degrade the amplifier performance. The Raman amplifiers using photonic crystal fibers have a limited gain below 20 dB and poor signal to noise ratio because of these noises. The focus of this thesis is to design a module of photonic crystal fiber Raman amplifier from the knowledge of the fiber cross-sectional characteristics i.e. the geometric parameters and the Germania concentration in the doped area. The module allows to study different air-hole dimension and disposition, with or without a central doped area. In addition the design integrates distributed Raman amplifier and nonlinear optical loop mirror to improve the signal to noise ratio and overall gain by reducing the noise mentioned earlier.

1.3 Modeling Methods

Photonic crystal fibers have a sub-wavelength periodic structure and high refractive index difference. Therefore, the regular modeling methods cannot give accurate results. Instead electromagnetic field modeling methods are applied in Photonic crystal fiber modeling. The finite difference time domain (FDTD) method is commonly used for electromagnetic field calculation and evaluation. This method allows to evaluate the light wave propagation through the PCF structure by integrating Maxwell's equations in the time domain [11]. The FDTD method uses Yee cell and boundary conditions to evaluate the electrical and magnetic field as shown in Figure 1.5. This method allows the observation of the energy flow through the PCF structure for obtaining the transmission and reflection coefficients.

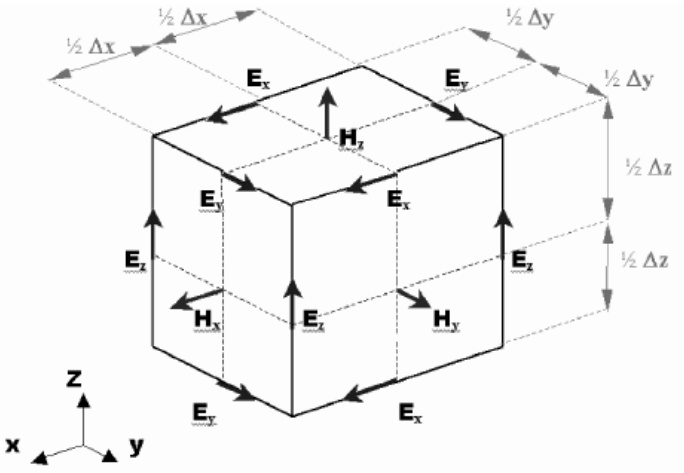

Figure 1.4: Electrical and magnetic fields components described by the Yee cell.

The Optiwave photonics software is to be used throughout this thesis for designing and the simulating the system. In addition it is used to evaluate the overall system performing by using graphical analysis of Optical Signal to Noise Ratio (OSNR), eye diagram and Q-Factor.

Optiwave FDTD uses Uniaxial Perfectly Matched layer (UPML) as the boundary conditions for PCFs. The algorithm uses full vector differential form of Maxwell's coupled curl equations to solve the electrical and magnetic fields in in spatial and temporal domain. This along with Optiwave system automation software contribute in designing, simulating and analysis of the PCF Raman amplifier and the DWDM network amplification system.

1.4 Thesis Overview

This Thesis begins by historical overview of communication system, development of photonic crystal fibers and Raman amplifier in general. Chapter 2 introduces the process of amplification by Raman Scattering in fiber optics. In addition the noise from double Rayleigh scattering and amplified spontaneous emission is analyzed. In Chapter 3 introduces distributed Raman amplifier and nonlinear optical loop mirror as solutions for reducing the noise sources and increasing the system gain. In Chapter 4 light propagation using FDTD is shown. Moreover, a novel design of Raman amplifier based on photonic crystal fiber is implemented, simulated and the results are compared with the previous work. In Chapter5 a high capacity DWDM network amplification system based on the designed PCF amplifier is implemented and compared to a hybrid amplification system based on EDFA. The conclusion of Chapter 6 provides an overview of the finding of this research as well as a summary of future research possibilities.

1.5 References

[1] Brain Bowers "Inventors of the telegraph" in Proceedings of the IEEE, vol 90, no.3 March 2002.

[2] Matthews, Tom L. (1999). Always Inventing: A Photobiography of Alexander Graham Bell. Washington, D.C.: National Geographic Society. pp. 19–21.

[3] R.W. Clifton and B.G. Rich, Senstar Corporation "Advances in Ported Coaxial Cable Technology" in Security Technology, IEEE 10.1109/CCST.1995.524725, 20 Oct. 1995.

[4] Seymour B.Cohn and ralph Levy "History of Microwave Passive Components with Particular Attention to Directional Couplers" in IEEE Transaction on Microwave Theory and Techniques, vol MTT-32,no.9 September 1984.

[5] Steward E.Miller ,Tingye Li and Enrique A.J Marcatili "Research Toward Optical-Fiber Transmission Systems Part I: The Transmission Medium" in Proceedings of The IEEE, vol. 61, no 12, December 1973.

[6] Tingye Li "Advances in Optical Fiber Communications: An Historical Perspective" in IEEE Journal on Selected areas in Communication, Vol. SAC-1, No. 3, April 1983.

[7] P. Yeh, A. Yariv, and E. Marom, "Theory of Bragg fiber*"J. Opt. Soc. Am., Vol. 68, No. 9, September 1978.

[8] J.C. Knight, T.A. Birks, P.St.J. Russell and D.M. Atkin, "All-silica single-mode optical fiber with photonic crystal cladding "Optical Letters.Vol.21, No.19 October 1996.

[9] L. F. Mollenauer, J. P. Gordon, and M. N. Islam, "Soliton propagation in long fibers with periodically compensated loss," IEEE J. Quantum Electron., vol. QE-22, pp. 157–173, 1986.

[10] S. G. Grubb, T. Strasser, W. Y. Cheung, W. A. Reed, V. Mizrachi, T. Erdogan, P. J. Lemaire, A. M. Vengsarkar, and D. J. DiGiovanni, "High power, 1.48 m cascaded Raman laser in germanosilicate fibers," in Proc. Optical Amplifiers and Their Applicat., 1995.

[11] A.tflove,S.Hagness " Computational Electromagantic :The Finite Difference Time-Domain Method" Artech House ,Boston 2000.

Chapter-2
Raman Amplification and Noise Analysis

2.1 Stimulated Raman Scattering

The basic nonlinear process that makes optical fibers work as broadband Raman amplifiers is Stimulated Raman scattering. As mentioned in Chapter 1, Raman amplification phenomena was noticed in the early 1970s. However, as the stimulated Raman scattering extremely limits the performance of multichannel optical fiber communication system, it was mainly observed as a disadvantageous nonlinear effect. The fundamental advantage of Raman amplifiers over EDFA amplifiers is the improved flatness gain over a broadband spectrum. However, The Raman amplifiers have some serious drawbacks as (i) Amplified Spontaneous Emission (ASE) (ii) Double Rayleigh Scattering (DRS) (iii) Multipath-Path interference (MPI) (iv) the multiple reflections caused by ASE.

Raman Effect was discovered by Raman in 1928. He noticed that when spontaneous scattering in any molecular medium occurred, slight amount of power is transferred from a high frequency optical field to a lower frequency field [1]. The fraction of the transferred power depends mainly on the vibrational modes of the molecular medium as shown in Figure 2.1. When a pump photon of energy $h\omega_p$ is boosted to a virtual level a less energy stokes photon ($h\omega_s$) is spontaneously generated. The shift of the molecule in the vibrational modes generates an optical phonon from the energy shift. The Stoke-line and the anti-Stoke line represents the red-shifted and blue shifted components of the radiation respectively [2]. During the calculation, the anti-stoke process is ignored because it doesn't play any role in Raman amplification process. This is due to the fact the

anti-Stoke line has much weaker intensity compared to Stoke –line. In addition it requires the right amount of phonon population and energy in the vibrational modes.

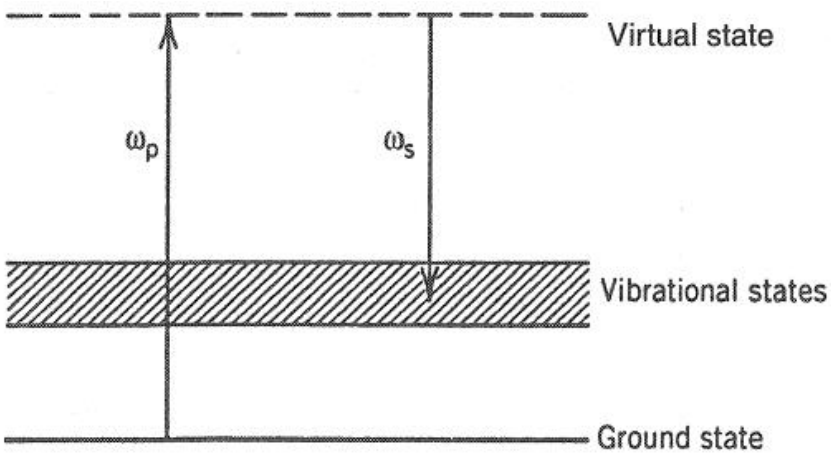

Figure 2.1: Quantum-Mechinal explanation of the Raman Scattering process.

Raman scattering is weak enough to be ignored in low intensity optical fiber propagation. However, in high intensity light wave propagation, Spontaneous Raman scattering (SRS) has observed effect due to the exponential growth of the Stoke line grows in the optical medium nonlinearity. Raman scattering has three important characteristics, (i) stimulated Raman scattering can arise in any type of optical fiber,(ii) Raman gain can happen at any chosen wavelength by selecting the appropriate pump wavelength as the excitation takes place at a virtual level as shown in Figure 2.1,(iii) Raman gain is extremely fast process (order of 10ps)[3]. Figure 2.2 shows an average power model for Raman amplifier with 100 WDM channels to improve the flatness of the gain.

2.2 Raman Gain

Raman gain coefficient g_r is the most influential parameter describing Raman amplifiers. It shows how the Stoke line gains power through SRS from the pump power.

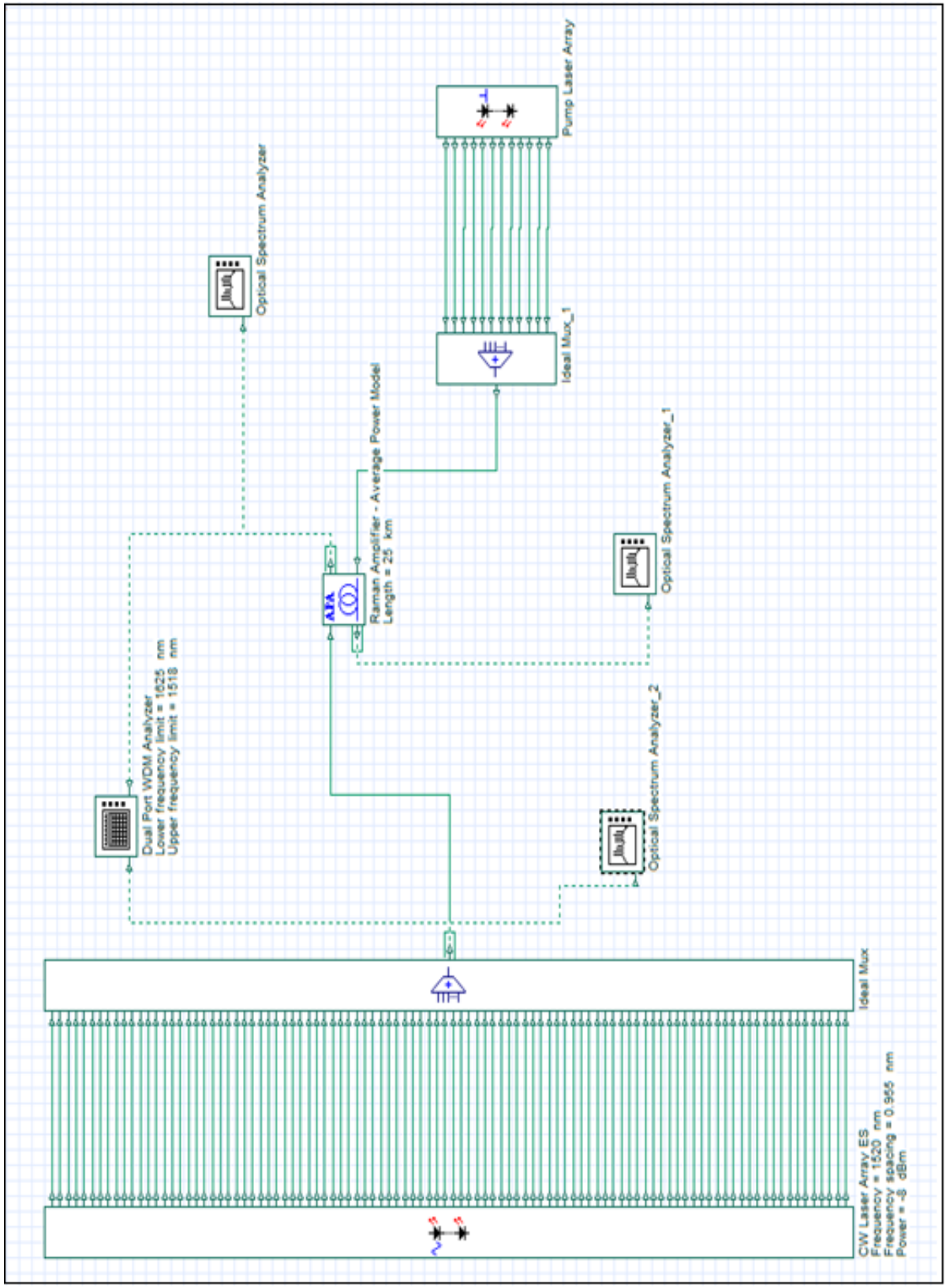

Figure 2.2:100 WDM channels amplified using Raman effects.

It is associated with the imaginary part of the third-order nonlinear susceptibility [4] .However under the Continuous Wave conditions (CW), the basic optical signal power from SRS is controlled by [5]

$$\frac{dI_s}{dz} = \gamma_r(\Omega) I_s I_p \tag{2.1}$$

where $I_s$and I_p are the signal and pump optical fields intensities respectively. γ_r is related to g_r and $\Omega$is the frequency difference between pump and signal frequencies. Equations (2.1) also represents the basic of the Raman amplification as described in Figure 2.3. The pump source is a laser source at 1535 nm and the circulator provides counter propagation for the gain medium.

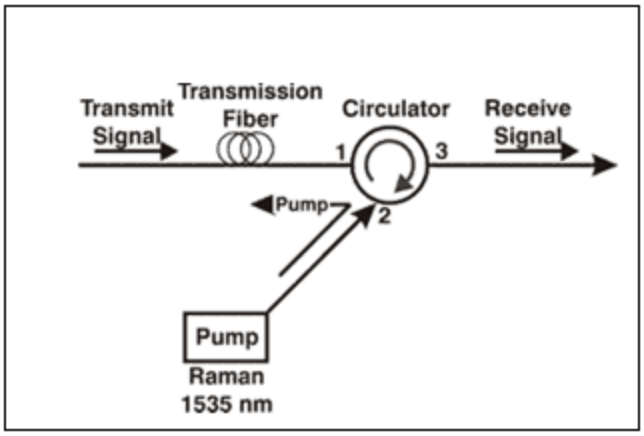

Figure 2.3: Typical Raman amplifier with backward pumping power [5].

As shown in Figure 2.4, the maximum Raman gain is obtained when the difference between the signal and pump frequencies is 13.2 THz. The most important advantage of Raman amplification over EDFA is the constant large gain over a broadband spectrum. This is because the vibrational modes in the silica fiber appear in the bands which make them overlap and creates continuity in the spectrum. The total optical power of the pump and the signal over the fiber length is defined by [6]:

$$P_j(z) = \iint_{-\infty}^{\infty} I_j(x, y, z)\, dxdy \tag{2.2}$$

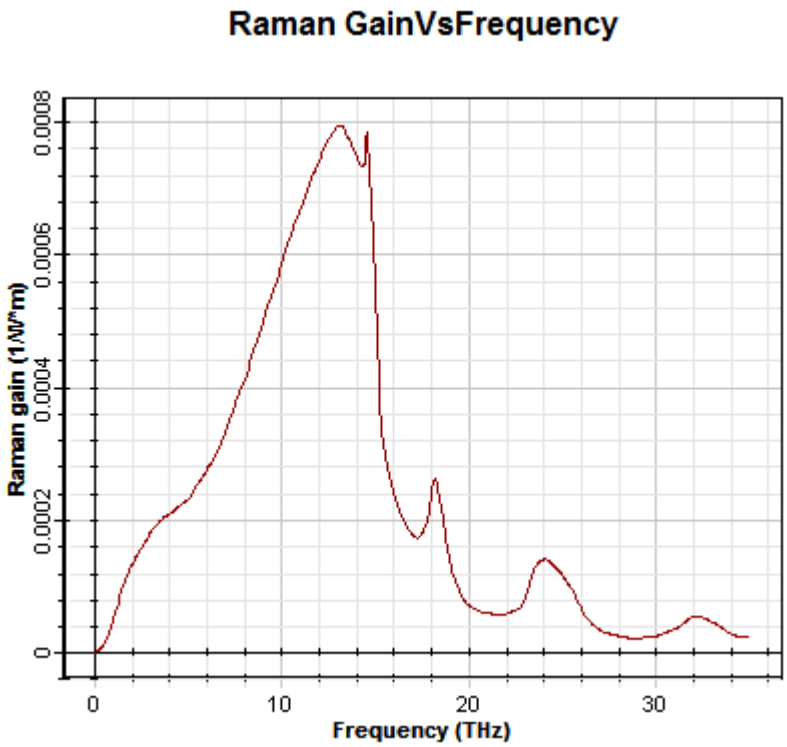

Figure 2.4 Raman gain spectrum as a function of pump -signal frequency difference.

where $= s \; or \; p$, Equation (2.2) can be expressed in differential form as

$$\frac{dP_z}{dz} = (\frac{\gamma_r}{A_{eff}})P_p P_s \tag{2.3}$$

$$\frac{dP_z}{dz} = \; g_r P_p P_s \tag{2.4}$$

where $P_p$is the pump power, P_s is the signal power , and A_{eff} is the effective core area of the fiber described by

$$A_{eff} = \frac{(\iint_{-\infty}^{\infty} I_p(x,y,z)dxdy)(\iint_{-\infty}^{\infty} I_s(x,y,z)dxdy)}{\iint_{-\infty}^{\infty} I_p(x,y,z)I_s(x,y,z)dxdy} \tag{2.5}$$

The importance of the effective area A_{eff} comes from the fact the most of nonlinear effects are described using A_{eff} as shown for Raman scattering. When the optical pump and signal

intensities are considered to have a similar profile for the field intensity $F(x,y)$ [7], equation (2.5) is rewritten as

$$A_{eff} = \frac{\left(\iint_{-\infty}^{\infty}|F(x,y,x)|^2 dxdy\right)^2}{\iint_{-\infty}^{\infty}|F(x,y,x)|^4 dxdy} \tag{2.6}$$

for a Gaussian field intensity with radius r, A_{eff} is defined by

$$A_{eff} = \pi r^2(\lambda) \tag{2.7}$$

The increase in the mode field diameter leads to increase in the effective area. However, for Photonic Crystal fibers, A_{eff} doesn't depend on the core radius, but is changed by manipulating the pitch and hole diameters which plays major role in determining Raman gain as discussed in detail in Chapter 4.

2.3 Signal Amplification by Single- Pump Power

Equation (2.4) assumes that the fiber is lossless and the pump power does not weaken while propagating through the optical fiber [8]. However, in practice, when Stoke and pump wavelengths fiber losses $\alpha_s$and $\alpha_p$respectively are included, equation (2.4) describes the Raman amplification by the following two equations

$$\frac{dP_s}{dz} = g_r P_p P_s - \alpha_s P_p \tag{2.9}$$

$$\kappa\frac{dP_p}{dz} = \frac{\omega_p}{\omega_s} g_r P_p P_s - \alpha_p P_p \tag{2.10}$$

where ω_p is the pump angular frequncy, $\omega_s$is the signal angular frequncy and κ represents the coupling parameter which takes the values between -1 to +1. The minus sign is for the backward pump direction. Equation (2.10) includes the frequency ratio factor ($\frac{\omega_p}{\omega_s}$) to consider the

energy difference between the pump and Stoke photons as the photon energy depends on its frequency. This is verified in lossless fiber medium by

$$\frac{d}{dz}\left(\frac{P_s}{\omega_s}+\kappa\frac{P_s}{\omega_s}\right)=0 \tag{2.11}$$

In this case, Equation (2.11) can be used to represent the conservation of total photon numbers in the SRS process where $\frac{P_s}{\omega_s}$ and $\frac{P_p}{\omega_p}$ are Stoke photons flux and pump photons flux respectively. Equation (2.9) and (2.10) are difficult to solve analytically due to SRS nonlinearity factor. However, in practice, Stoke line power is extremely small and can be neglected compared to the large pump power [9]. By setting $g_r = 0$, Equation (2.9) can be modified as

$$P_p = P_0\exp(-\alpha_p z) \tag{2.12}$$

where P_0 is the input power at $z = 0$ as $P_0 \equiv P_p(0)$. By substituting Equation (2.12) in Equation (2.10) the Stoke power propagating through the fiber is given as

$$P_s(L) = P_s(0)\exp(\, g_r P_0 L_{eff} - \alpha_s L) \tag{2.13}$$

where L is the fiber length .In practice, the amplification fiber length is less that the physical length due to pump absorption and the effective fiber length L_{eff} is defined by

$$L_{eff} = \{[1-\exp(-\alpha_p L\,)]/\,\alpha_p\,\} \tag{2.14}$$

and Equation (2.13) can be simplified by using the net signal gain $G(L)$ as

$$G(L) \equiv \exp(\, g_r P_0 L_{eff} - \alpha_s L) \tag{2.15}$$

$$P_s(L) = P_s(0)G(L) \tag{2.16}$$

The previous mathematical analysis is for the forward pumping, hence, by assuming $\kappa = 1$, $g_r = 0$, $\kappa = -1$ and $P_p(L) = P_0$, the backward pumping is obtained as

$$P_p(z) = P_0\exp[-\alpha_p(L-z)] \tag{2.17}$$

The integration of Equation (2.9) gives the same results for forward and backward pumping, demonstrating that the amplified signal is not affected by the direction of the pump for the same levels. For this reason two pump lasers in opposite fiber ends are used to increase the total pumping power is the summation of the forward and backward pump power P_f and P_b respectively. These powers are described as

$$\frac{dP_s}{dz} = -\alpha_s P_f \tag{2.18}$$

$$\frac{dP_s}{dz} = -\alpha_s P_b \tag{2.19}$$

and the total pumping power at distance z is the solution of Equation (2.17) and Equation (2.18) given as

$$P_p(z) = P_0 \{\mathfrak{r}_r \exp(-\alpha_p z) + (1 - \mathfrak{r}_r) \exp[-\alpha_p (L - z)]\} \tag{2.20}$$

where $\mathfrak{r}_r$ represents the fraction of forward pump power. In this case the signal gain from the total pumping power is given by

$$G(z) = \frac{P_s(z)}{P_s(0)} = \exp(g_r \int_0^z P_z dz - \alpha_s z) \tag{2.21}$$

It is important to state that the best combination for the pumping power is not easily determined because it depends on the system configuration. However for a better Noise figure and SNR the forward pumping is used. But for a long distance system that is limit by the fiber nonlinearity, the backward pumping is used for better performance.

Figure 2.5 shows the power of the signal and the pump with corresponding gains for both forward and backward propagations. For the simulation the following parameters are used, L-25km, $\alpha = 0.2dB/km$,T=300 K ,polarization factor =2, Dispersion =16.75 ps/nm/km , Reference wavelength =1550 nm, Noise bandwidth =120 nm and Noise central wavelength =1570 nm. In Figure 2.5 (a) the interaction between different pump powers and Raman amplification effect is

observed after 25 km. In addition maximum forward gain occurs at shorter wavelengths and larger distance (60km). Figure 2.5 (b) describes the signal power, pump power and the gain in the backward direction along the transmission fiber. Both (a) and (b) show the strong effect of SRS. Due to the nonlinearity associated with Raman amplification, Self-Phase Modulation (SFM) is observed and defined by the parameter

$$\varepsilon = \frac{2\pi n_2}{\lambda_s \ A_{eff}} \tag{2.22}$$

where $\lambda_s$is the Stoke wavelength and n_2 is the nonlinear refractive index[10]. The overall phase shift caused by SFM is obtained from

$$\emptyset_{nl} = \ \varepsilon \int_0^L P_s(z)dz = \ \varepsilon P_s(0) \int_0^L G(z)dz \tag{2.23}$$

the phase shift is evaluated by the ratio

$$R_{nl} = \frac{\emptyset_{nl} with\ pump\ on}{\emptyset_{nl} with\ pump\ off} \quad = L_{eff}^{-1} \int_0^L G(z)dz \tag{2.24}$$

This ratio is helpful to describe On-Off Raman gain by

$$G_A = \frac{P_s(L) with\ pump\ On}{P_s(L) with\ pump\ Off} = = \ \exp(\ g_r P_0) L_{eff} \tag{2.25}$$

2.4 Signal Amplification by Multiple- Pump Powers

With the development of wavelength-division multiplexing (WDM) optical systems operating at 1.55 μm, the multi-pump Raman amplifiers have been developed to provide a large optical broadband for WDM systems [11].

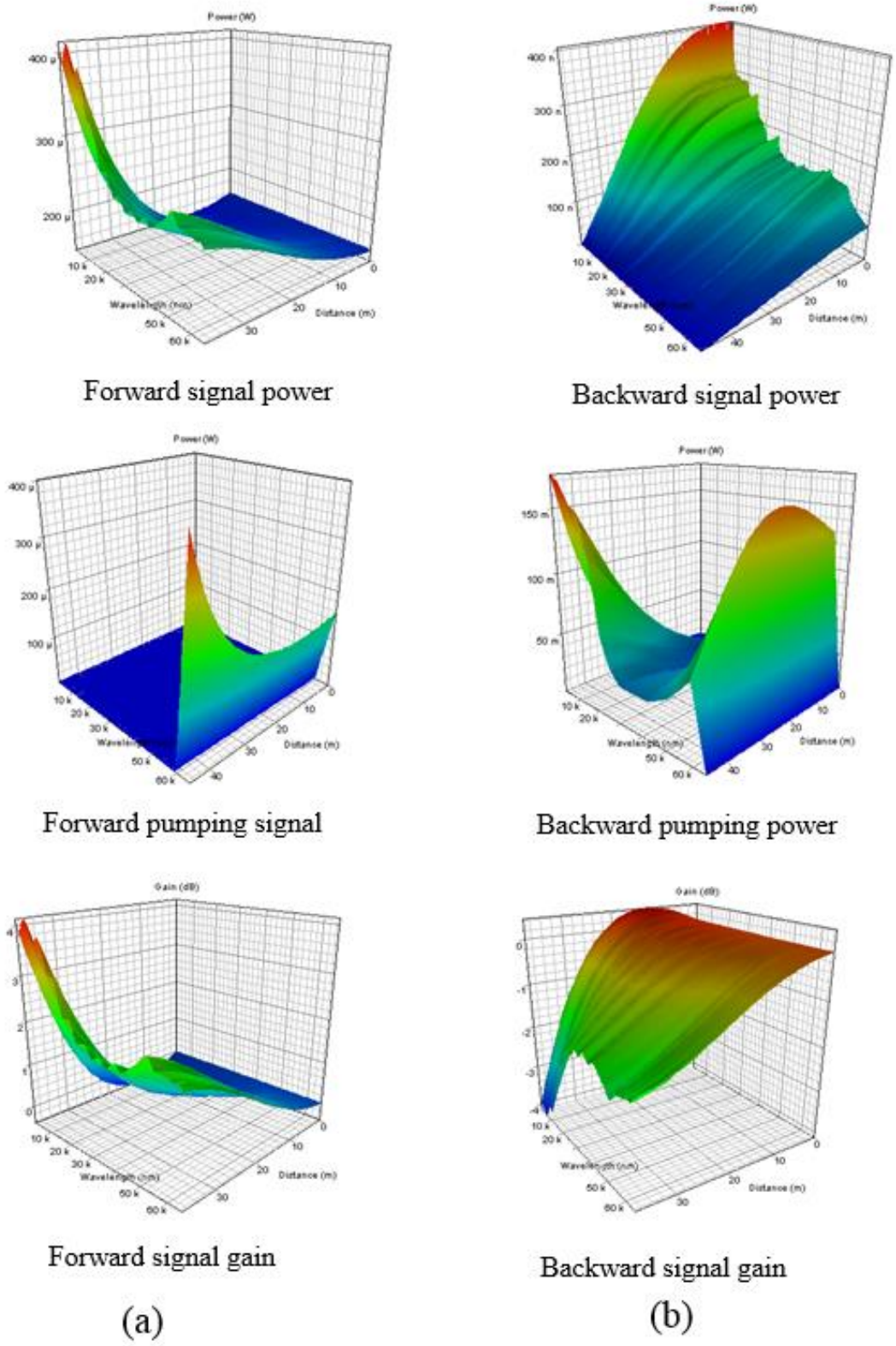

Figure 2.5: (a) Forward gain resulting from forward signal and forward pump. (b) Backward gain resulting from backward signal and backward pump.

Multi-pump Raman amplifiers are based on the flexibility of Raman gain spectrum i.e. Raman gain can be obtained at any wavelength by selecting the appropriate pump wavelengths. Although the gain for a single pump is over a narrower band (few nanometers), but by selecting several pumps at different wavelengths Raman gain can be achieved over broadened and also constant gain over large spectrum is achieved (100 nm)[12].

The design of broadband Raman amplifiers is based on pump-signal interactions. This design is introduced by a numerical model which deals with each frequency separately and needs to be solved for large set of connected equation of the form

$$\frac{dP_s(v)}{dz} = \int_{v'>v} g_r(v', v)\left[P_f(v') + P_b(v')\right] \times \left[P_f(v) + 2hvn_{sp}(v' - v)\right]dv' - \int_{v'>v} g_r(v', v)\left[P_f(v') + P_b(v')\right] \times \left[P_f(v) + 4hvn_{sp}(v' - v)\right]dv' - \alpha(v)P_f(v) + f_r\alpha_r P_b(v) \quad (2.26)$$

where f and b subscripts represents the forward and backward pumps respectively, $v'$and v represents the optical frequencies with a frequency shift Ω between them. In addition the parameter $n_{sp}$is giving by

$$n_{sp} = [1 - \exp(\frac{h\Omega}{k_B T})] \quad (2.27)$$

where k_B is Boltzmann constant, h is Planck constant and T is the amplifier absolute temperature. In this numerical model shows the power caused by Raman scattering by first two terms [13]. Moreover the first factor of 2 accounts for the polarizations modes and the second factor represents the spontaneous emission in both directions. Finally the last two terms include the fiber loss and Rayleigh back scattering, respectively.

2.5 Sources of Noise in Raman Amplifiers

Raman amplifier performance is limited by many factors that need to be compressed. The main two factors are (i) Amplified Spontaneous Emission (ASE) (ii) Double Rayleigh Scattering (DRS). Other sources such as Multi-path interference (MPI) and Polarization-Dependent Gain (PDG) are considered in the final design [14].

2.5.1 Spontaneous Raman scattering

During Raman Amplification, more photons are spontaneously generated with different phases. These random photons cause Amplified Spontaneous Emission (ASE) defined as

$$\frac{dA_s}{dz} = \frac{g_r}{2} P_p(z) A_s - \frac{\alpha_s}{2} A_s + f_n(z,t) \tag{2.28}$$

where A_s represents the signal field as $P_p = |A_s|^2$ and the noise generated by spontaneous Raman scattering is represented by Langevin source $f_n(z,t)$[15]. This noise is random and can be modeled by Markovian stochastic process with $\langle f_n(z,t) \rangle$ =0, Gaussian statistics and a second moment as

$$\langle f_n(z,t) z' f_n(z',t') \rangle = n_{sp} h v_0 \, g_r P_p(z) \delta(z\text{-}z') \, \delta(t\text{-}t') \tag{2.29}$$

where the independency of the scattering events is shown by the Delta function ,each photon has average energy hv_0 and n_{sp} is the spontaneous Raman scattering factor. By integrating (2.28) we get

$$A_s(L) = \sqrt{G(L)} A_s(0) + a_{ASE}(t) \tag{2.30}$$

where $a_{ASE}(t)$ represents the total noise caused by ASE and is giving by

$$a_{ASE}(t) = \sqrt{G(L)} \int_0^L \frac{f_n(z,t)}{\sqrt{G(z)}} \tag{2.31}$$

and

$$G(z) = exp\left(\int_0^z [\, g_r P_p(z' - \alpha_s)]\, dz'\right) \tag{2.32}$$

This noise has $a_{ASE}(t) = 0$ on average and second momentum as

$$\langle\, a_{ASE}(t)\, a_{ASE}(t')\rangle = G(L) \int_0^L dz \int_0^L \frac{\langle f_n(z,t) z' f_n(z',t')\rangle}{\sqrt{G(z)G(z')}}\, dz' \tag{2.33}$$

$$= S_{ASE}\delta(\text{t-}t') \tag{2.34}$$

where

$$S_{ASE} = n_{sp} h v_0\, g_r G(z) \int_0^L \frac{P_p(z)}{G(z)} dz \tag{2.35}$$

$\delta(\text{t-}t')$ shows that S_{ASE} continues to grow and occurs for all frequencies because of the assumption of Markovian [16]. However Raman amplifiers operate on certain bandwidth and ASE noise power is limited by the optical filter bandwidthB_{opt}. Thus ASE power is described by

$$P_{ASE} = 2 \int_{-\infty}^{\infty} S_{ASE}\, H_f(v) \mathrm{d}v$$

$$P_{ASE} = 2\, S_{ASE}\, B_{opt} \tag{2.36}$$

It can be seen from Equation (2.36) that the polarization modes are doubling the effect of P_{ASE}. Figure 2.6 (a) and (b) describe P_{ASE} in both forward and backward directions, respectively.

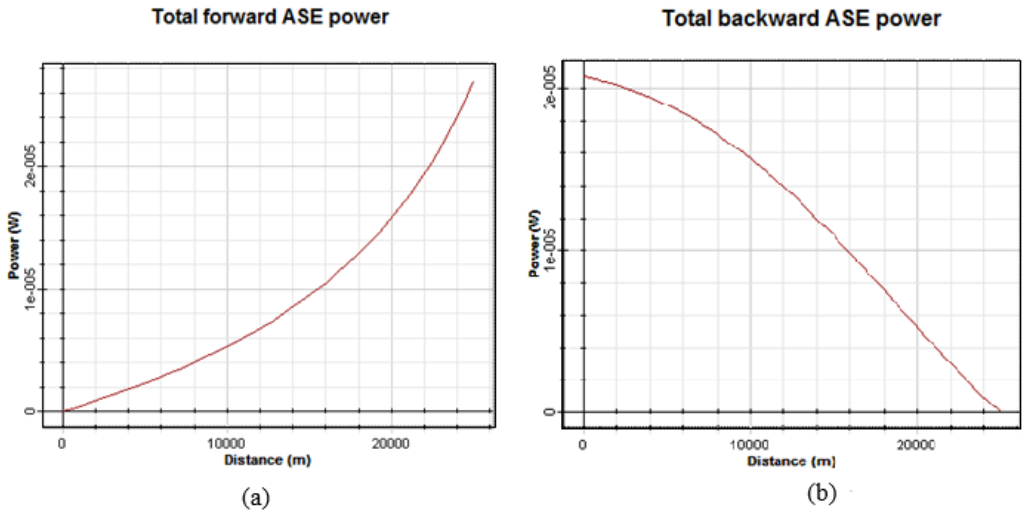

Figure 2.6 :(a) ASE power in forward direction. (b) ASE power in backward direction.

As seen from Figure 2.6 (a) and (b), ASE power occurs in $\pm z$ directions with boundary conditions $P_{ASE}^{+}(0)=0$ and $P_{ASE}^{-}(L)=0$. ASE power is simulated for both polarization components in the optical filter bandwidth. The optical Signal to Noise Ratio (SNR) in this case is given by

$$\mathrm{SNR}_0 = \frac{P_s(L)}{P_{ASE}} = \frac{G(L)P_{in}}{P_{ASE}} \tag{2.37}$$

The degradation in SNR caused by ASE is described by the noise figure F_n as

$$F_n = \frac{\mathrm{SNR_{in}}}{\mathrm{SNR_{out}}} \tag{2.38}$$

where F_n is defined as

$$F_n = 2n_{sp}\, g_r \int_0^L \frac{P_p(z)}{G(z)}\, dz + \frac{1}{G(L)} \tag{2.39}$$

Equations (2.35),(2.37) and (2.39) imply that P_{ASE} , SNR_0 and F_n depend on the pump scheme. Figure 2.7 (a) (b) and(c) is obtained by assuming noise free input signal and ideal photodetector at the receiver port. Figure 2.7 (c) shows that NF has high sensitivity due to the previous assumptions. The kinks in NF spectrum are due to the shot noise and other sources such as multiple-path inference and spontaneous-spontaneous beating [17].

2.5.2 Double Rayleigh Scattering

Rayleigh scattering is one of the basic loss mechanisms in optical fibers and occurs in all types of fibers. When Rayleigh scattering occurs, most of the scattered light does not affect the propagating signal as it escapes through the cladding. However, some of the backscattered light is coupled through the fiber core in the reverse direction. This backscattered light can be negligible compared to the signal power ($\leq 40dB$)[17],but since the Rayleigh scattering is proportional to the fiber length ,for long optical fiber communication, Rayleigh scattering does have sever effect on the signal gain. Double Rayleigh backscattering (DRS) limits Raman amplifiers performance

by generating in-band cross talk component (same spectral range of the signal) in the forward direction. This is the major noise source in Raman amplifier that affects the signal power. Moreover it causes ASE to occur due to part of the backscattered photons increasing the total noise.

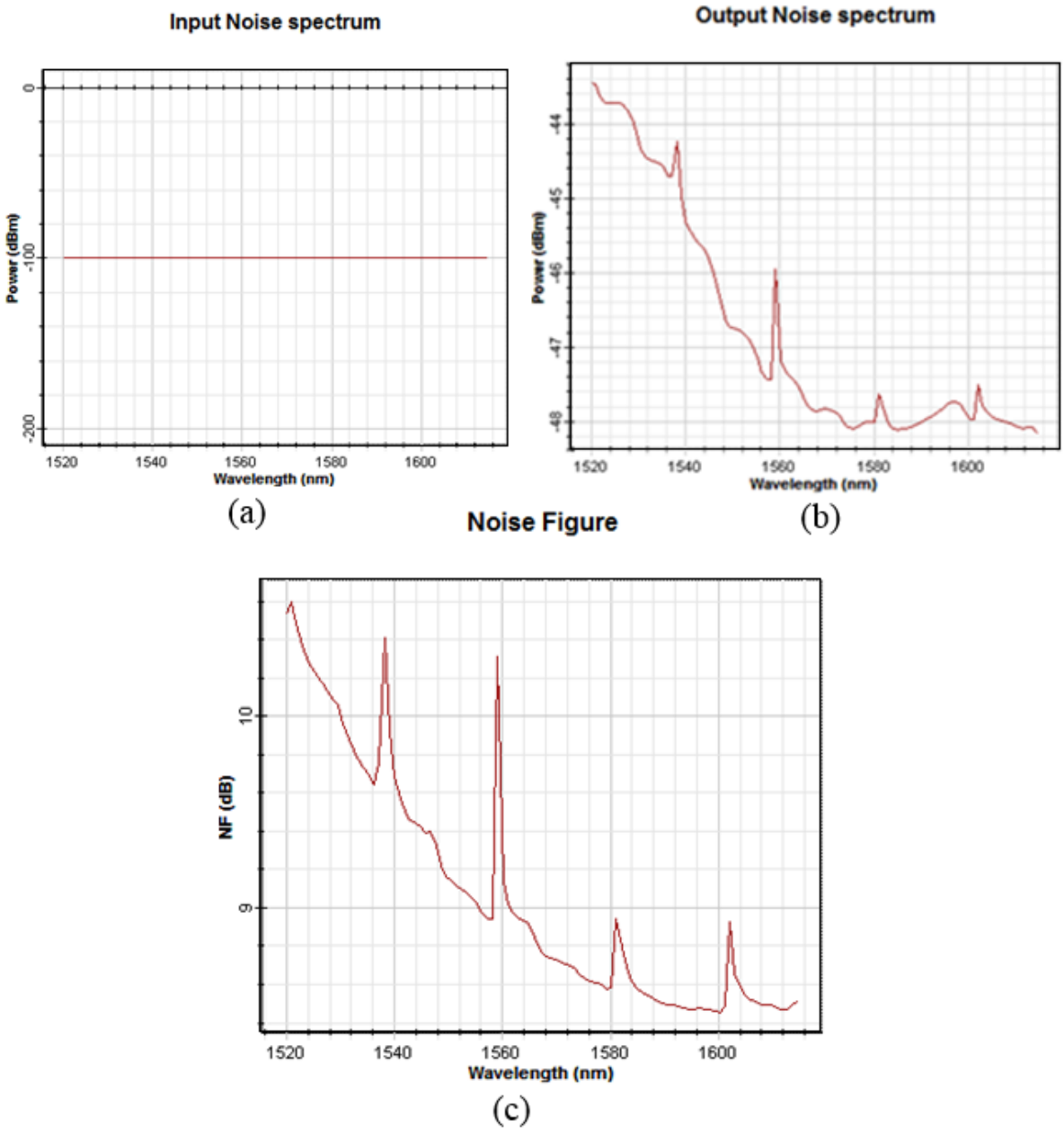

Figure 2.7: (a) Ideal signal with negligible noise power, (b) output noise spectrum (c) the amplifier Noise Figure (NF).

Double backscattered Rayleigh noise depends on the statistical density fluctuations and the depolarizing effect created by birefringence fluctuations. Therefore, calculation of DRS is quite complicated, however by neglecting the depolarizing effect due to its small effect [18], DRS can by defined by

$$f_{DRS} = \frac{P_{DRS}(L)}{P_s(L)} = (f_r \alpha_r)^2 \int_0^L G^{-2}(z)dz \int_z^L G^2(z')dz' \quad (2.40)$$

where P_{DRS} Double backscattered Rayleigh noise. ASE noise is eliminated to increase the accuracy of the measurement. As it was shown, DRS and ASE degrade the Raman amplifier especially at long wavelength or low pumping power .In addition , DRS and ASE have serve effect in limiting the gain.

2.6 Photonic Crystal Fiber (PCF)

The concept of Photonic Crystal fibers (PCFs) was proposed by Yeh et al [7] for the first time in 1978. The first model was reported in 1996 when P.Russell presented the two dimensional photonic crystal fiber with an air core for the first time at the Optical Fiber Conference (OFC) [8]. PCFs are new class of optical fibers with periodically air filled holes forming a hexagonal lattice around its cross section. Light propagates in the solid core of the PCF by total internal reflection between the air hole cladding and solid core in a similar way of classical optical fibers. Nevertheless as shown in Figure 2.8 the light can be guided through totally different mechanism when using Hollow Core Fibers. The air core fibers use photonic bandgap as the guiding mechanism allowing the light to propagate in the hollow core region i.e lower –index region. Detailed simulation and analysis for PCF wave propagation has been presented in Chapter 4.

Unlike Conventional optical fibers, in this case the photonic crystal fibers have high flexibility in the structure design. As shown in Figure 2.8 there are different parameters to manipulate like the distance between the holes (Λ), the hole diameter (d) the structural shape of the air holes and the refractive index of the cladding. The freedom in designing and modeling of PCF has provided many features that are not possible in conventional optical fiber. For example, endless single-mode fibers at large wavelengths, zero dispersion PFCs at visible wavelengths and so on. The flexibility in PCFs design allows to vary different structure parameters like the hole diameter and the lattice period to easily achieve small effective areas.

In the case of classical optical fibers, the small effective area is achieved by heavily doping the fiber core which increases the fiber losses due to increase in the nonlinearity. However, by manipulating the geometrical structure of PCFs, small effective area of pure silica fiber core is obtained which leads to larger Raman gain. Therefore, the best medium for amplification application would be photonic crystal fibers.

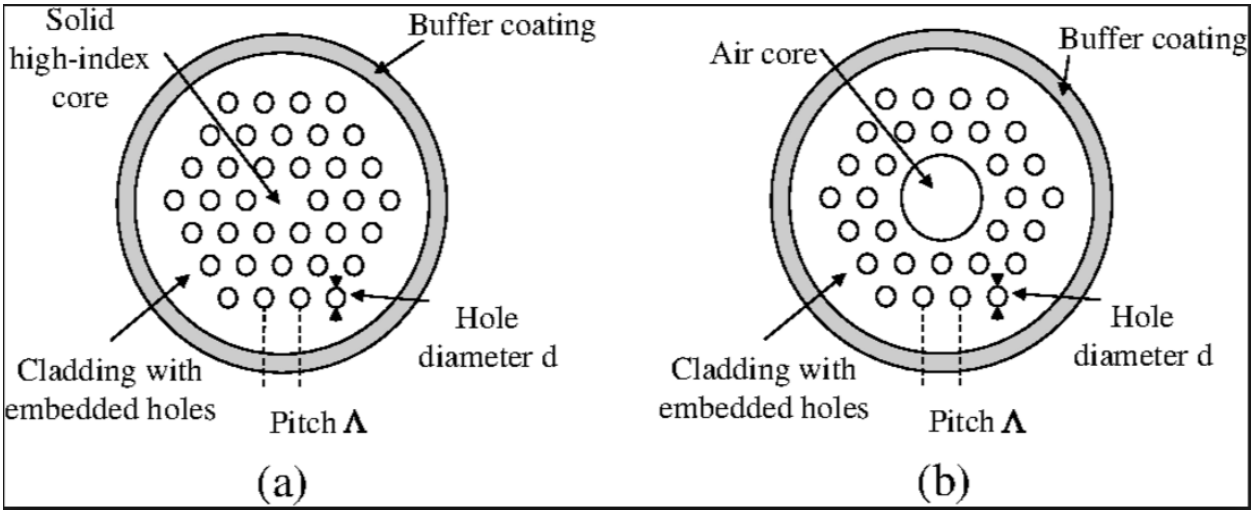

Figure 2.8: (a) Photonic crystal fiber structure. (b) Hollow-core photonic-bandgap fiber structure.

2.7 References

[1] S. P. Singh , R. Gangwar, and N. Singh "Nonlinear Scattering Effects in optical Fibers" Progress In Electromagnetics Research, PIER 74, 379–405, 2007.

[2] Ji-Xin Cheng, Y. Kevin Jia, Gengfeng Zheng, and X. Sunney Xie "Laser-Scanning Coherent Anti-Stokes Raman Scattering Microscopy and Applications to Cell Biology" Biophysical Journal Volume 83 July 2002 502–509.

[3] Wei Wang, Henrik N. Poulsen, Lavanya Rau,Hsu-Feng Chou, John E. Bowers, and Daniel J. Blumenthal "Raman-Enhanced Regenerative Ultrafast All-Optical Fiber XPM Wavelength Converter "Journal of Lightwave Technology ,Vol 23,No.3 March 2005.

[4] Adelbert Owyoung "Coherent Raman Gain Spectroscopy Using CW Laser Sources" IEEE Journal of Quantum Electronics, Vol .QE-14, No.3 March 1987.

[5] Haisheng Rong, Richard Jones , Ansheng Liu , Oded Cohen , Dani Hak , Alexander Fang and Mario Paniccia "A continuous-wave Raman silicon laser" Nature | Vol. 433 | 17 February 2005.

[6] Victor E. Perlin and Herbert G. Winful "Optimal Design of Flat-Gain Wide-Band Fiber Raman Amplifiers" Journal Lightwave Technology, Vol. 20, No. 2, February 2002.

[7] Jake Bromage, Karsten Rottwitt, and M. E. Lines "A Method to Predict the Raman Gain Spectra of Germanosilicate Fibers With Arbitrary Index Profiles" IEEE Photonic Technology Letters.Vol.14, No.1 January 2002.

[8] Amos Hardyand R. Oron, "Signal Amplification in Strongly Pumped Fiber Amplifiers" IEEE Journal of Quantum Electronics, Vol. 33,No.3, March 1997.

[9] S.R. Chinn, "Analysis of counter-pumped small-signal fiber Raman amplifiers "Electronics Letters.Vol.33, No.7 March 1997.

[10] Govind P.Agrawal and Anders Olsson “Self-Phase Modulation and Spectral Broadening of Optical Pulses in Semiconductor Laser Amplifiers” lEEE Journal OF Quantum Electronics, Vol. 25,No.11, November 1989.

[11] Shu Namiki and Yoshihiro Emori “Ultrabroad-Band Raman Amplifiers Pumped and Gain-Equalized by Wavelength-Division-Multiplexed High-Power Laser Diodes” IEEE Journal On selected topics in Quantum Electrons, Vol. 7, No. 1, January/ February 2001.

[12] Y. Emori, K. Tanaka and S. Namiki “100nm bandwidth flat-gain Raman amplifiers pumped and gain-equalised by 12-wavelength-channel WDM laser diode unit” IEEE Electronics Letters Online No. 19990921 May 1999.

[13] M. Achtenhagen,a) T. G. Chang, and B. Nyman “Analysis of a multiple-pump Raman amplifier”Applied Physics Letters Vol.78 No.10 March 2001.

[14] M. Vasilyev, B. Szalabofka, S. Tsuda, J.M. Grochocinski and A.F. Evans, “Reduction of Raman MPI and noise figure in dispersion-managed fibre” Electronics Letters Online No: 20020184 ,Jaunuary2002.

[15] Sazzad M. S. Imran, Minoru Yamada, Fellow, IEEE, and Yuji Kuwamura “Theoretical Analysis of the Optical Feedback Noise Based on Multimode Model of Semiconductor Lasers” IEEE Journal of Quantum Electrons, Vol. 48, No. 4, April 2012.

[16] Howard Kidorf, Karsten Rottwitt, Morten Nissov, Matthew Ma, and Eric Rabarijaona “Pump Interactions in a 100-nm Bandwidth Raman Amplifier” IEEE Photonic Technology Letters, Nol.11.No.5.May 1999.

[17] N.A.Olsson “Light wave systems with optical amplifier” J.Light wave Technol.vol.7,pp 536-545,2001.

[18] P. B. Hansen, L. Eskildsen, A. J. Stentz, T. A. Strasser, J. Judkins, J. J. DeMarco, R. Pedrazzani, and D. J. DiGiovanni "Rayleigh Scattering Limitations in Distributed Raman Pre-Amplifiers" IEEE Photonics Technology Letters, Vol. 10, No. 1, January 1998.

[19] Catherine Martinelli, Laurence Lorcy, Anne Durécu-Legrand, Dominique Mongardien, Sophie Borne, and Dominique Bayart "RIN Transfer in Copumped Raman Amplifiers Using Polarization-Combined Diodes" IEEE Photonics Technology Letters, Vol. 17, No. 9, January 2005.

Chapter-3
Noise Reduction Methods in Raman Amplifiers

3.1 Introduction to Noise Figure

The performance of Raman amplifier is mainly determined by the noise figure (NF). It shows the amount of degradation in the signal and the noise caused by the amplifier. Many definitions have been given for NF, however the IEEE defines it as the ratio between the signal to noise ratio at the input to the signal to noise ratio at the output. NF depends on several amplifier parameters, including noise (ASE, DRS), gain, transmission length, dispersion, and the signal and pump attenuation coefficients. Theoretically, in a lossless transmission fiber with no amplification, NF value is equal to one. However, in practice this is not achievable. In addition, the signal decreases because of losses in the fiber. Therefore, the SNR decreases and the NF increases at the output port. From the previous description, NF can be expressed as:

$$NF = \frac{SNR_{in}}{SNR_{out}} \tag{3.1}$$

where SNR is defined as:

$$SNR = \frac{signal\ power}{noise\ power} \tag{3.2}$$

A Disturbed Raman amplifier (DRA) is an amplifier that uses the transmission fiber in the system as a Raman gain medium by applying a high pump signal with the transmitted signal as shown in Figure 3.1.

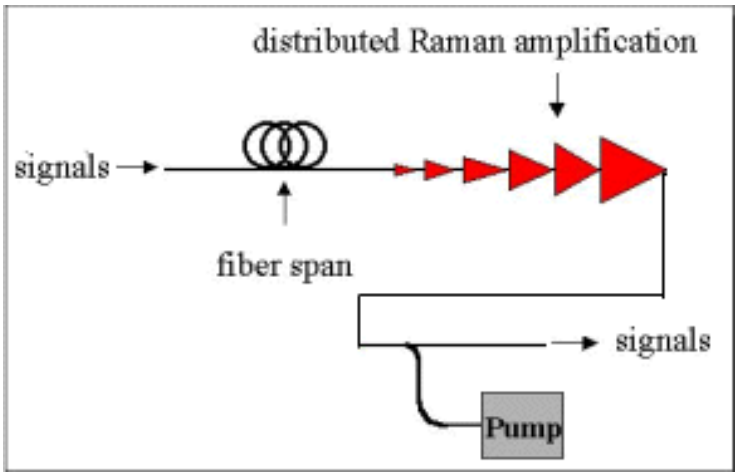

Figure 3.1: DRA uses the fiber span as the Raman amplification medium [1].

The DRA effect is to reduce the nonlinearity penalty, which enhances the total SNR. For several amplifiers in cascade, the total NF is:

$$NF_{total} = NF_1 + \frac{NF_2 - 1}{G_1} + \frac{NF_3 - 1}{G_1 G_2} + \cdots \quad (3.3)$$

where G_i is the net G_{in} for the i^{th} amplifier in the chain. It can be seen from (3.3) that the first stage amplifier has the maximum effect on the total system NF. The effect of the DRA gain for a three channel WDM transmitter is shown in Figure 3.2. From Figure 3.2 it is seen that the Raman gain occurs after approximately 80 km. For different channel wavelengths, the gain varies and results in improvement of 4 to 5 dB.

The propagating signal experiences loss through the transmission fiber. Thus, high gain is required to amplify the signal. To achieve this high gain, high pumping power is required which also produces the amplified spontaneous emission noise (ASE). Figure 3.3 shows the forward and backward noise as a function of the DRA length. It is seen that in the forward pumping case, ASE noise is smaller than the backword pumping. Therefore, the forward pumping scheme is better for

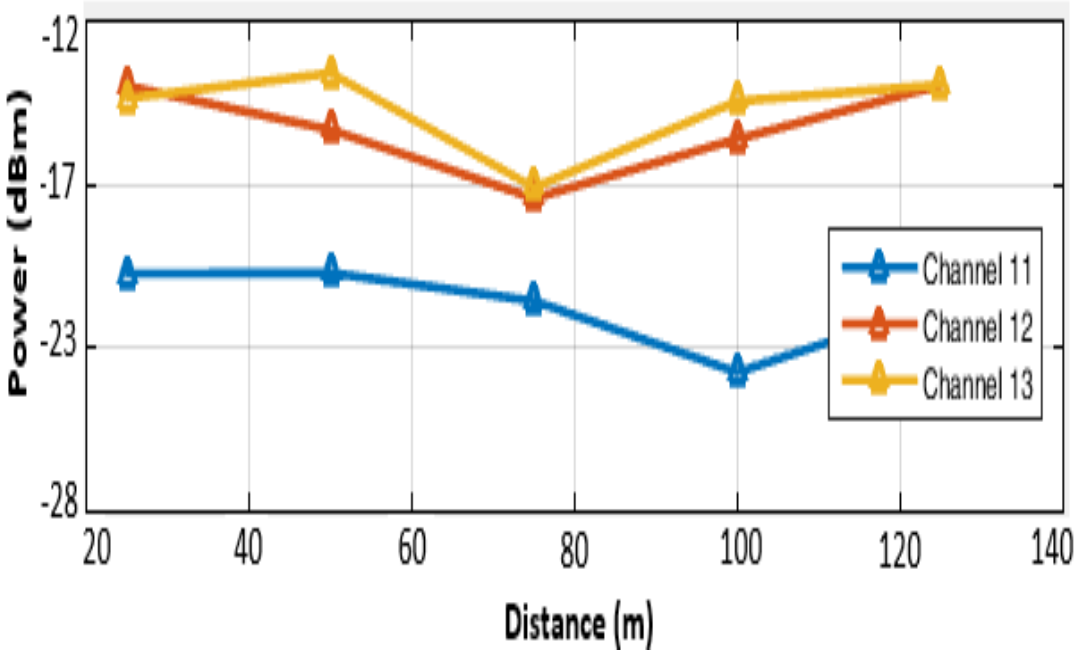

Figure 3.2: Output power as a function of DRA length for wavelengths of Channels 11, 12, and 13 (1550 nm, 1549.6 nm, 1549.2, respectively).

minimizing the noise. If ASE noise is dominant, the NF is approximated by adding the shot noise in the second term linearly as [2]:

$$NF \approx \frac{2P_{ASE}(L)}{hvB_{opt}G_{net}} + \frac{1}{G_{net}}$$

$$NF \approx \frac{P_s(0)}{hvB_{opt}OSNR_{out}} + \frac{1}{G_{net}} \tag{3.4}$$

where $B_{opt}$is the operating bandwidth, v is the signal frequency ,h is Plank's constant ,P_{ASE} is the noise caused by ASE , $G_{net}$is the net gain, $OSNR_{out}$ is the optical signal to noise ratio at the output port and P_s is the signal power. Moreover, in term of spectral noise density N_s , the optical noise at the signal wavelength is defined by [3]:

$$\frac{dN_s}{dz} = -\alpha_s \left[N_s - \frac{hv_s}{2}\right] + C_R P_p [N_s - \frac{hv_s}{2}] \tag{3.5}$$

where C_R is Raman gain efficiency, v_s is the signal frequency and P_p is the pump power. Figure 3.4 shows that increasing the pumping power from 0 to 880 mw decrease NF from 28 to 23.5 dB. This improvement in NF is related to the improvement in signal power shown in Figure 3.2. When vacuum fluctuation limits the input signal (known as shot noise limitation) , N_s is expressed by:

$$N_s = G\frac{hv_s}{2} + (G-1)\frac{hv_s}{2} + 2\alpha_s G D_{inv}\frac{hv_s}{2} \tag{3.6}$$

where α_s is the signal attenuation and D_{inv} is the vacuum fluctuation which is given by:

$$D_{inv} = \int_0^L \left[\frac{1}{G(z)}\right] dz \tag{3.7}$$

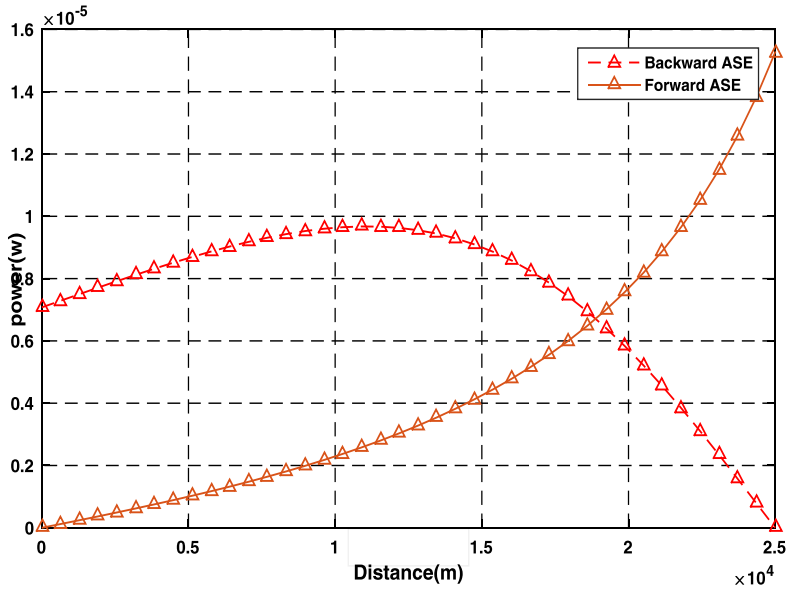

Figure 3.3: ASE noise power versus DRA length with signal power of -10 dBm and pump power of 880 mW.

When D_{inv} is considered as the white Gaussian noise in the optical bandwidth, NF is described by:

$$NF = \frac{N_s}{G\frac{hv_s}{2}} \tag{3.8}$$

$$NF = 1 + \frac{G-1}{G} + 2\alpha_s D_{inv} \tag{3.9}$$

The effect of the DRA pumping power on improving the noise figure is shown in Figure 3.4. Increasing the pumping power from 0 to 1200 mW reduces the total noise figure from 28 to 22 dB.

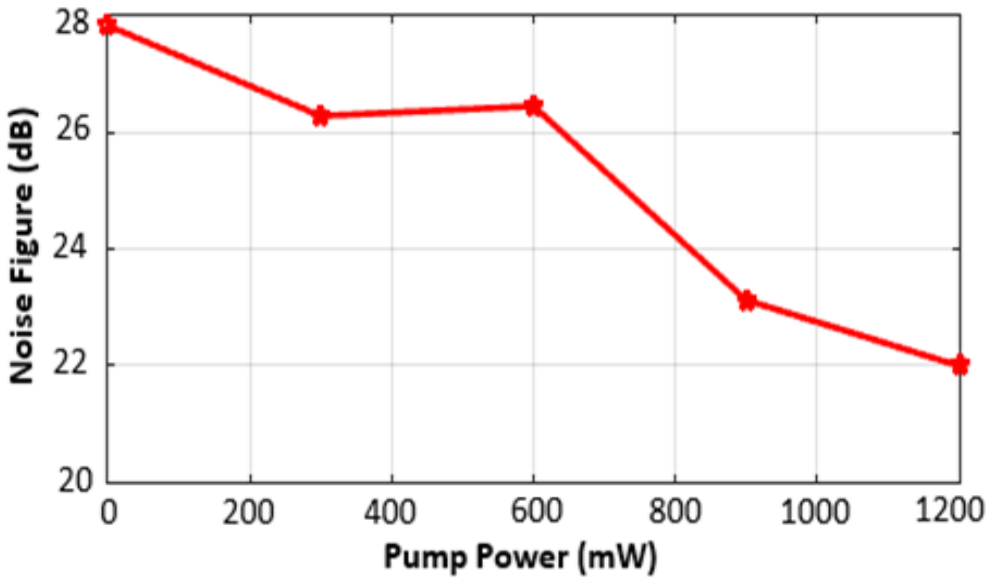

Figure 3.4: Simulated values of NF versus the pump power for a channel.

DRA also has noticeable improvement in BER and Q factor since they are related to SNR and NF. BER can be calculated by

$$BER = \frac{1}{2} erfc(SNR) \tag{3.10}$$

where $erfc$ is the complementary error function. SNR is related to the photocurrent and the total noise. Therefore the effect of DRA on BER and Q factor is observed at the receiver photodetector as shown in Figure 3.5 (a) and (b).

3.2 Simulation Setup and Results

In this Section, DWDM network system using a Distributed Raman Amplifier (DRA) was simulated. In addition, it was compared to a similar system that uses a discrete Raman amplifier (RA).

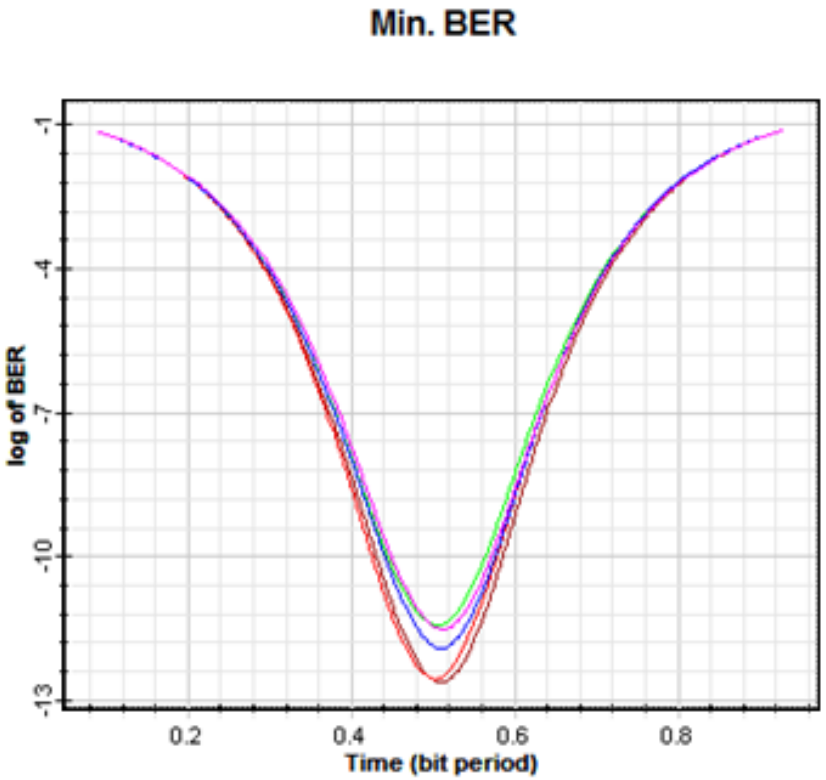

Figure 3.5(a): The effect of different pump power of DRA on BER

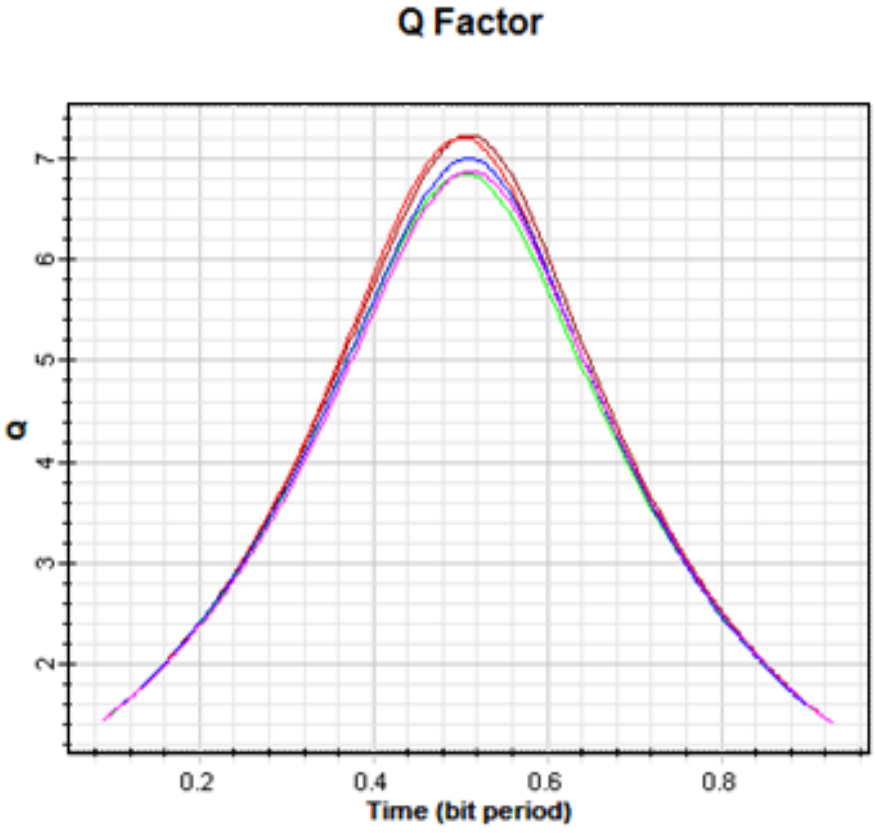

Figure 3.5(b): The effect of different pump power of DRA on Q factor

Different parameters such as BER, Q factor, Eye diagram, Noise Figure, SNR and power gain were compared. All parameters chosen in this simulation were based on simulation and experimental results in [4].

3.2.1 Simulation Setup

A. Discrete Raman Amplifier

Using OptiSystem 14 software, a DWDM network model using a discrete Raman amplifier model was setup. Fig 3.6 shows a 16 channel DWDM system located between 193.85 THz and 19.10 THz .These channels are spaced by 50 GHz and launched with -10dBm power. Network traffic was created using Pseudo Random Bit Sequences (PRBS) at each channel. PRBS generator is also utilized as generate Non-Return –to-Zero (NRZ) signals by controlling the NRZ generators. NRZ signal is applied on the Continuous wave laser (CW) using Mech-Zehnder modulator (MZ) to achieve On/Off keying modulated (OOK). The parameters used in Figure 3.6 are shown in Table 3.1.

Table 3.1: Simulation parameters used for discrete Raman amplifier.

Name	**Symbol**	**Value**
Length	L	25 km
Attenuation	α_s	0.2dB/km
Signal Wavelength	λ_s	1552 nm
Signal Power	P_s	-10 dBm
Effective area	A_{eff}	80 μm^2
Temperature	T	300 K
Pump wavelength	λ_p	1440 nm
Pump Power	P_p	20 dBm

B. Disturbed Raman Amplifier

In addition to the previous model, Distributed Raman Amplifier with forward and backward scheme was added to the design. Forward and backward pump wavelength was setup at 1470 nm.

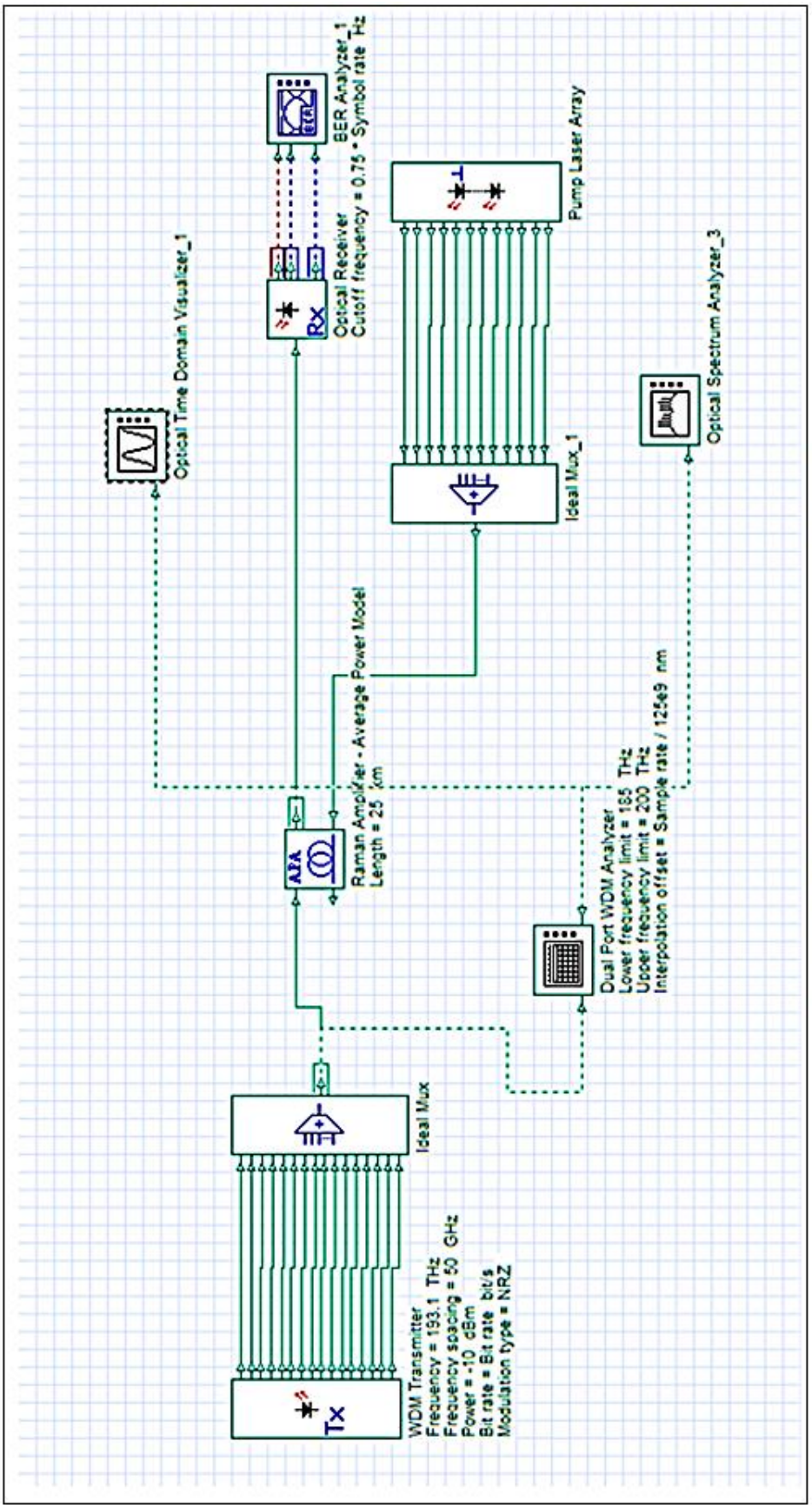

Figure: 3.6 Block Diagram of a DWDM system using discrete Raman amplifier

After the signals are multiplexed by the WDM multiplexer, they are coupled with the pump power coming from the CW laser by the pump coupler and launched through the transmission line in the same direction (Forward scheme). Moreover, anther CW pump laser is located at the end of the bidirectional fiber to launch pump power in the opposite direction (backward scheme). Both schemes use the bidirectional fiber as the Raman gain medium to amplify the signal through it as shown in Figure 3.7. At the receiver, PIN photodetector is used to convert the optical signal to electrical signal and low pass Bessel filter to visualize BER, Q factor and Eye Diagram. The parameter used in the simulation are shown in Table 3.2.

Table 3.2: Simulation parameters for distributed Raman amplifier.

Name	**Symbol**	**Value**
Length of DRA	L	100 km
Attenuation	α_s	0.35 dB/km
Dispersion	D	16.75 ps/nm/km
Nonlinearity	n_2	26e-21 m^2/w
Effective Area	A_{eff}	80 μm^2
Rayleigh Backscattering	α_{scat}	50e-006 1/km
Pump wavelength	λ_p	1470 nm
Pump Power	P_p	880 mW

3.2.2 Simulation Results

In this section, the results from discrete Raman amplifier model and distributed Raman amplifier model described in Figure 3.6 and Figure 3.7 respectively are compared. The Eye Diagram is a practical measurement method to determine the quality of the received signal and the amount of the damage caused by the communication system. Figure 3.8 (a) and (b) illustrate the improvement in the Eye Diagram scheme when DRA is used. Different type of noise sources such as third –order dispersion, Differential group delay and all scattering types were considered in the simulation.

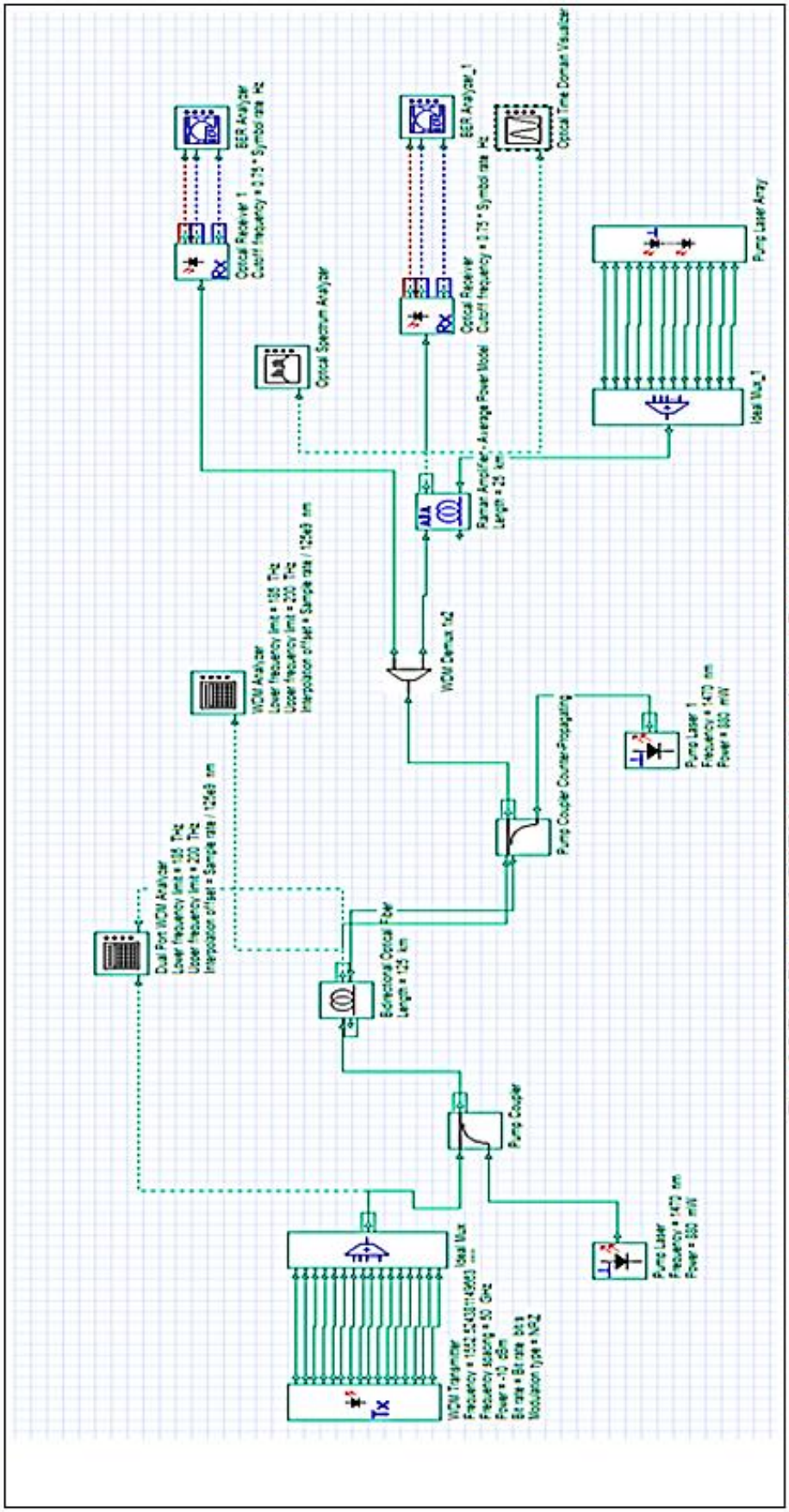

Figure 3.7: Block Diagram of a DWDM system using distributed Raman amplifier

In the discrete model, the eye diagram suffers from high jitter and distortion due to the noise generated in Raman medium. DRA model shows a relaxed eye with proper termination. The DRA system performance was improved by reducing the detective noise and the distortion. Additionally, the jitter was reduced and the total receiver sensitivity was improved. Figure 3.9 and Figure 3.10 describe the enhancement in the Q factor and Bit Rate Error (BER).

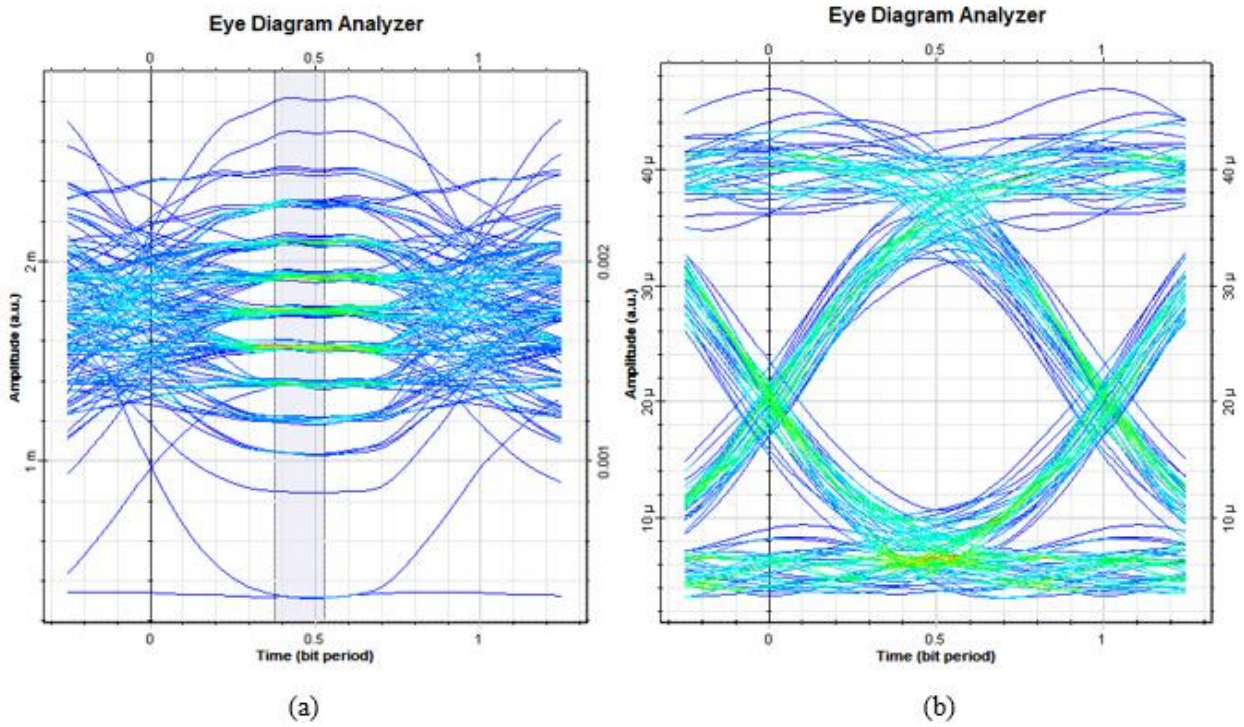

Figure3.8: Eye diagram pattern for (a) discrete Raman amplifier (b) distributed Raman amplifier.

As shown in Figures 3.9 and 3.10. DRA allows higher bit rate at longer distances ≤90 km. In comparison, for a typical 90 km span, DRA effectively improves the Q factor by 3.2 dB for a 16 –channel system with 50 GHz spacing. By using 880 mW pumping power, 10^{-11}BER was achieved. Therefore, WDM system with a NRZ bit rate of 20 GB/s was achieved for a 90 km span [5]. Table 3.3 compares all other parameters.

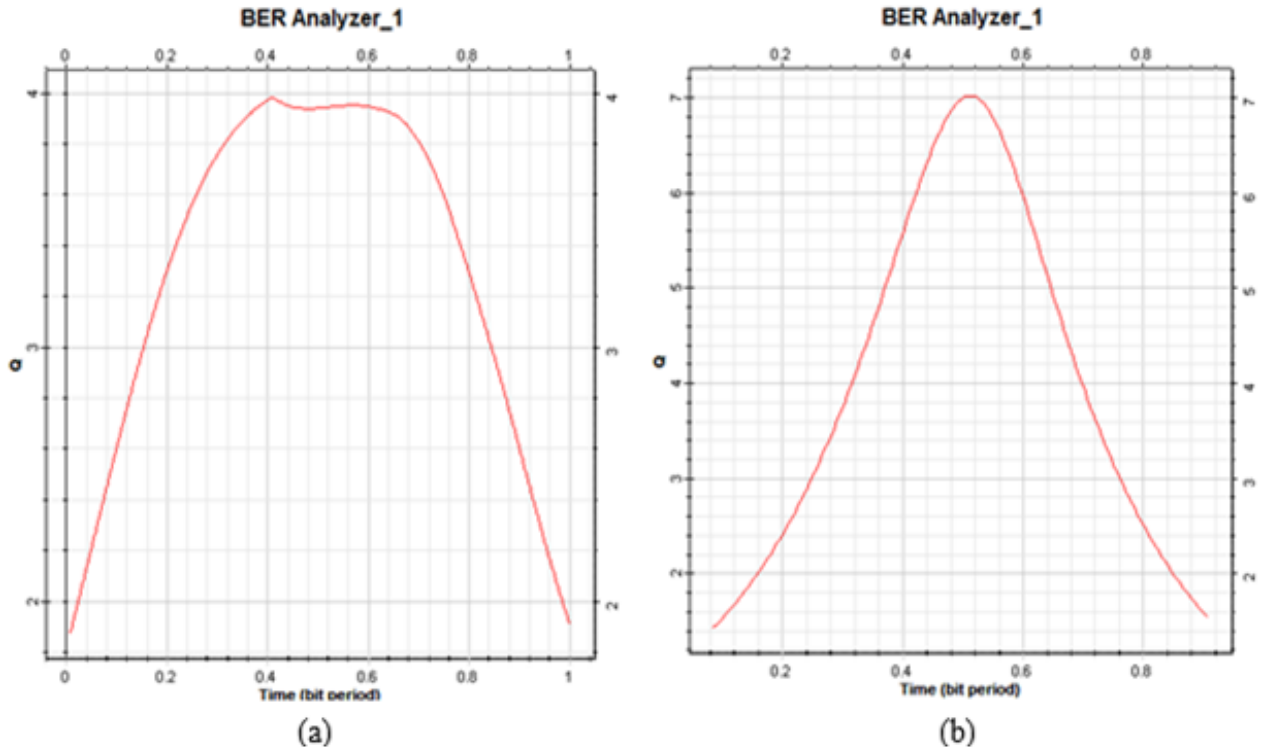

Figure 3.9: Q Factor for (a) discrete Raman amplifier (b) distributed Raman amplifier

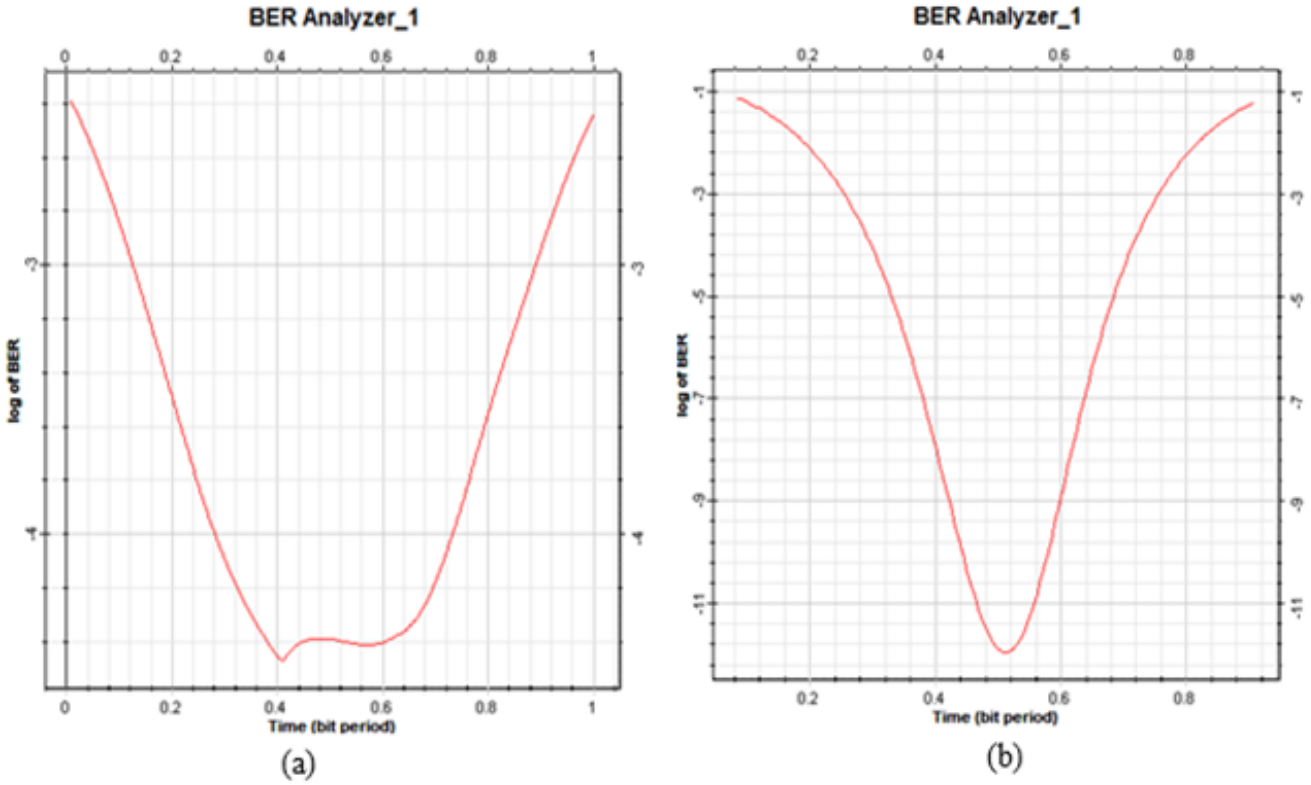

Figure 3.10: BER for (a) discrete Raman amplifier (b) distributed Raman amplifier

Table 3.3: Comparison between DRA and RA parameters obtained by BER analyzer.

	DRA	*RA*
Max. Q Factor	7.01321	3.99872
Min. BER	1.1447e-012	3.14127e-005
Eye Height	1.73047e-005	0.000357448
Threshold	1.93414e-005	0.000326062

As shown in the previous results, there are many important advantage of using DRA. First advantage is improving signal to noise ratio compared with discrete amplifiers. This means lower signal power, higher bit rate and longer transmission distance. Second is flatter gain and less nonlinearity penalty. In addition, DRA is a suitable for WDM networks as low-noise preamplifier. However, DRA amplifiers suffer from several challenges. The main challenge is higher power requirement for optimal noise characterization, in the previous case 880 mW. In addition, the nonlinearity effect requires minimum length of 40 km. Thus, DRA is not efficient for short-distance communication. At the same time, DRA have high sensitivity to any environmental or physical changes.

3.3 Nonlinear-Optical Loop Mirror

Nonlinear-optical loop mirror (NOLM) is a nonlinear switching device that is based on the nonlinear phase difference caused by self-phase modulation (SPM). It offers good switching characteristics with simple construction and with no need for interferometer alignment [6]. Figure 3.11 shows NOLM configuration. The basic concept is for an optical power coupler with a ratio

of $\alpha : 1 - \alpha$ and the two output ports connected with each other. The linearly coupler works as an optical mirror [7].

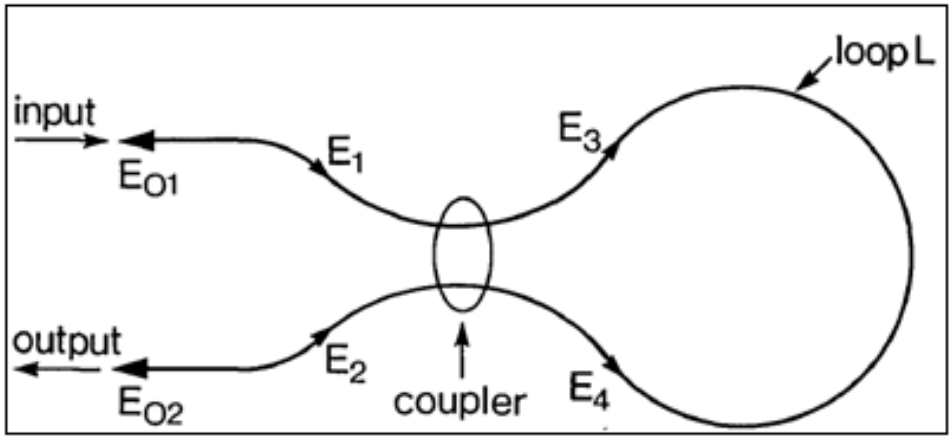

Figure: 3.11 Optical loop mirror configuration [7].

The input power E_{01} is split in to two counter-propagating fields $E_3$and E_4 depending on the coupling ratio. Then it recombines at the coupler output port as E_{02}. The counter-propagating fields have the same optical path length L as they travel the same path but in opposite directions. However, since the phase velocity depends on the intensity, the nonlinear effect of the propagation is not similar for the two paths when $\alpha \neq 0.5$. This optical device responds to the phase difference between the counter-propagating fields. Thus, it has phase sensitivity without interferometer alignment requirement for the optical paths.

By permitting SPM in the optical loop L and using coupling ratio $\alpha \neq 0.5$, the phase shift caused by the propagating field E of the NOLM in Figure 3.11 is described by:

$$\emptyset = \frac{2\pi n_2 |E| L}{\lambda} \tag{3.11}$$

where $n_2$represents Kerr nonlinear effect and λ is the wavelength. The relationship between input and output fields of the coupler are described by:

$$E_3 = \alpha^{1/2} E_1 + i(1-\alpha)^{1/2} E_2 \quad (3.12.a)$$

$$E_4 = i(1-\alpha)^{1/2} E_1 \ + \alpha^{1/2} E_2 \quad (3.12.b)$$

for the NOLM described in Figure.3.11 with single input field at port 1 E_{1N} ,these equations are changed to the phase shift caused by Kerr nonlinearity as

$$E_3 = \alpha^{1/2} E_{1N} \exp(i\alpha - 2\pi n_2 |E_{1N}|^2 L/\lambda) \quad (3.13.a)$$

$$E_4 = i(1-\alpha)^{1/2} E_{1N} \exp(i(1-\alpha)\, 2\pi n_2 |E_{1N}|^2 L/\lambda) \quad (3.13.b)$$

The output fields E_{02} is obtained from Equation (3.12) by setting $E_4 = {E_3}^*$ and $E_3 = {E_4}^*$ as:

$$|E_{02}|^2 = |E_{1N}|^2 (1 - 2\alpha(1-\alpha)\{1 + \cos[(1-2\alpha)|E_{1N}|^2 \times 2\pi n_2 |E_{1N}|^2 L/\lambda]\}) \quad (3.14)$$

from Equation (3.14) it can be seen that for any value of $\alpha \neq 0.5$, 100% of the input power can be obtained in port 2 whenever

$$2\pi n_2 |E_{1N}|^2 L/\lambda = m\frac{\pi}{1-2\alpha} \quad , \ m = odd \quad (3.15)$$

when m is even, minimal power occurs and it is giving by

$$|E_{1N}|^2 = |E_{1N}|^2 [1 - 4\,\alpha(1-\alpha)] \quad (3.16)$$

Figure 3.12 shows the transferred power at port 2 corresponding to Equation (3.13) for $\alpha =$ 95% and $\alpha = 45\%$. The input power is set at 310 mW (25dBm), $n_2 = 34.462 * 10^{-21}$L=10.007 km and $\lambda = 1550\, nm$. As seen when $\alpha = 45\%$ half of the power is coupled. However, the optimum switching ratio happens in Figure 3.12 when α is closest to 0.5. NOLM can be described as intensity–dependent threshold device that operates as fast saturable absorber. Therefore, it can be used to reduce ASE noise. Optical switching characteristics were experimentally observed by Doren in [8]. Those characteristics were used in [9] for passive mode locking lasers. In addition, intensity dependent characteristics were used to obtain pulse compression in [10].

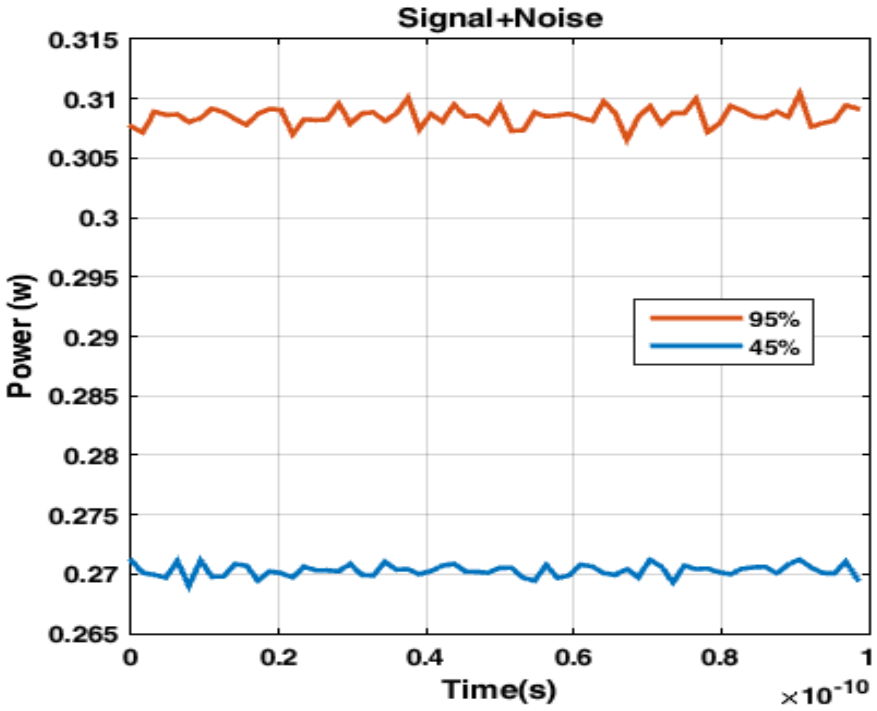

Figure: 3.12 Coupled power at port 2 for $\alpha = 95\%$ and $\alpha = 45\%$.

3.4 Simulation Setup and Results for NOLM

The simulation setup for the NOLM is shown in Figure 3.13. The input signal is the pulse from CW laser with 0.1 MHz line width. The laser power is set to 25dBm at 1552 nm. The pulse is amplified using 25 km Raman amplifier with pump power of 600 mW at 1440 nm. Then the pulse is split between port 3 and port 4 by 3 dB coupler which is part of NOLM. The signal from port 3 propagates clockwise in the optical loop. The signal from port 4 propagates counter-clockwise in the optical loop. A *10 km* Bidirectional fiber with *0.2 dB/km* attenuation was used for the nonlinear loop. The Differential group delay was set to *0.05 ps/km* and the Dispersion is -0.69 ps/nm/km at 1550 nm. The input signal at port 1 and the output signal at port 2 were investigated

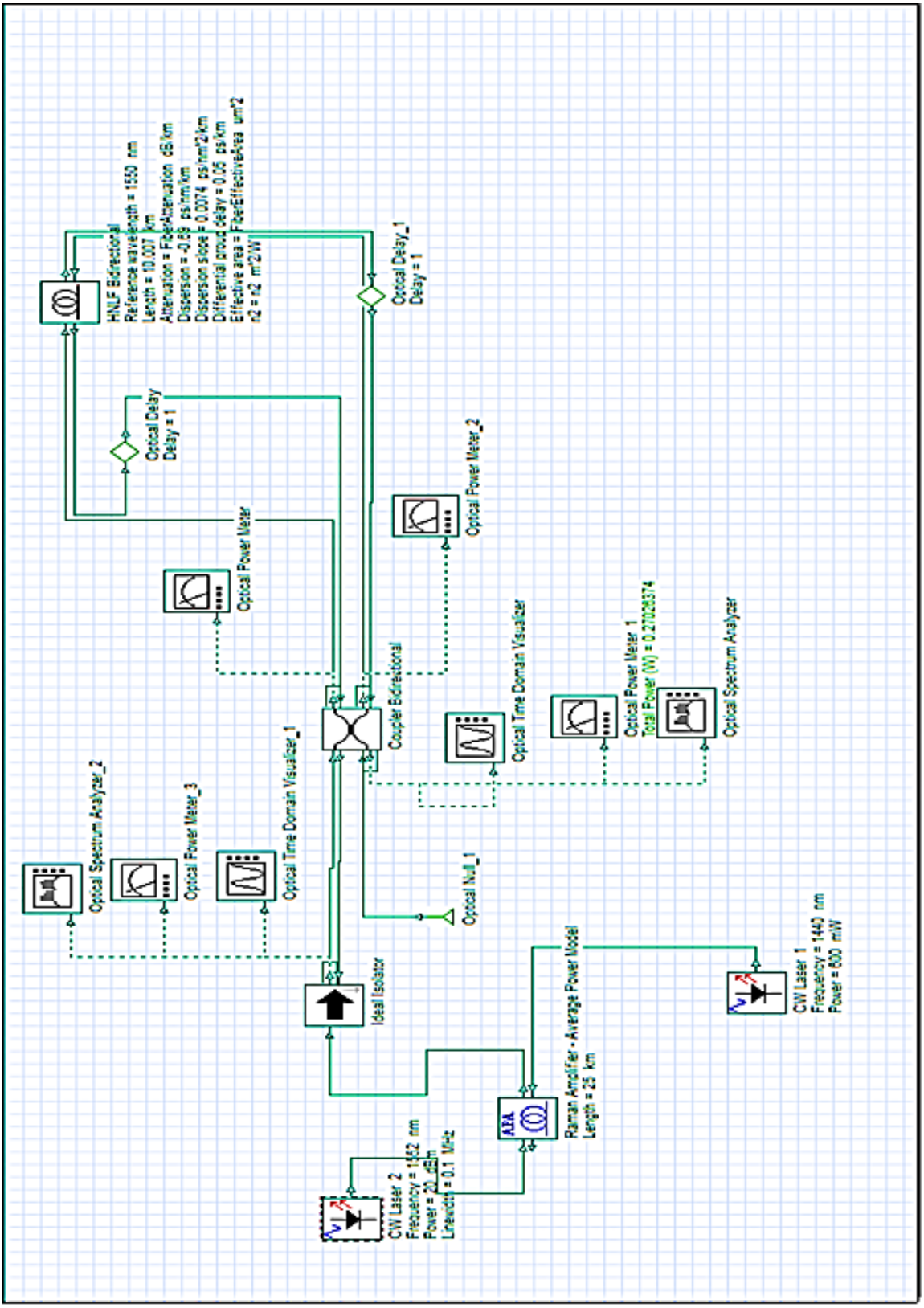

Figure: 3.13 Simulation setup for NOLM nonlinear switching.

using optical visualizers to observe the reduction in the noise. These parameters were chosen according to the experimental parameters in [11].

As mentioned earlier, NOLM operates as a threshold device that passes the strong signals and blocks the weak signals. Thus, it can be used as ASE noise elimination method. Figure 3.14 (a) and (b) show the CW laser input signal before and after NOLM respectively. The Max power was reduced by 1.29 dB due to losses in the loop length. However, the minimum value was increased by 0.06 dB due to the noise reduction. Figure 3.15 (c) and (d) show the reduction in ASE noise through the use of NOLM. The input power to NALM after Raman amplifier was 24.93 dBm. The noise of input power is -27 dBm and the transmitted signal noise is -36 dBm showing a reduction of 9 dB due to eliminating ASE noise. In addition, ASE peak intensity is reduced by 9 dB and ASE minimum intensity is reduced by 10 dB.

The SNR improvement is smaller than expected as shown in Figure 3.16 (e) and (f) .The peak power with ASE noise was 313mW. After NOLM, the peak power without ASE noise was 272mW. However, the ratio between the signal intensity and ASE intensity before and after using NOLM was improved by 2.72 dBm after the noise reduction. As it was show in this section, ASE noise can be reduced using NOLM. However the signal after the reduction is not stable. This is a result of the frequency chirp and phase change generated by the propagation through the loop as shown in Figure 3.17 (g) and (h).

The nonlinear intensity -dependent switching causes frequency chirp. The chirp is disadvantage for long-distance optical transmission fiber. However, by using Externally Modulated Lasers (EMLs) instead of Directly Modulated Lasers (DMLs), frequency chirping is

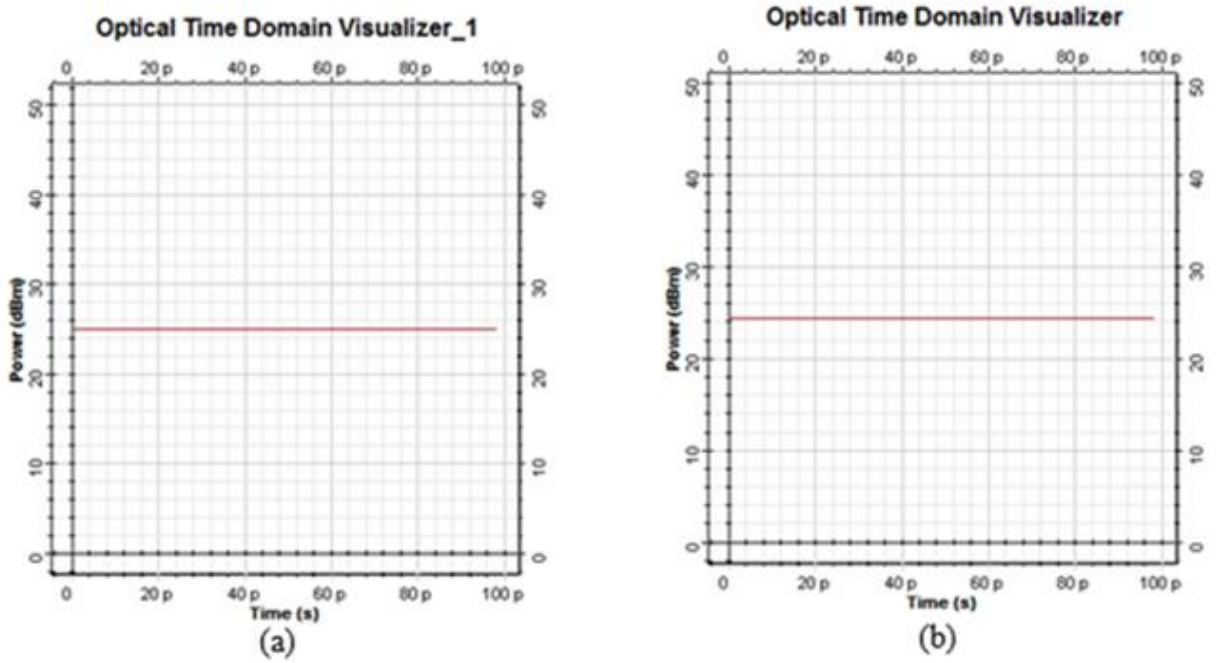

Figure 3.14: (a) Input signal power at port 1 before NOLM (b) Transmitted signal power at port 2 after NOLM.

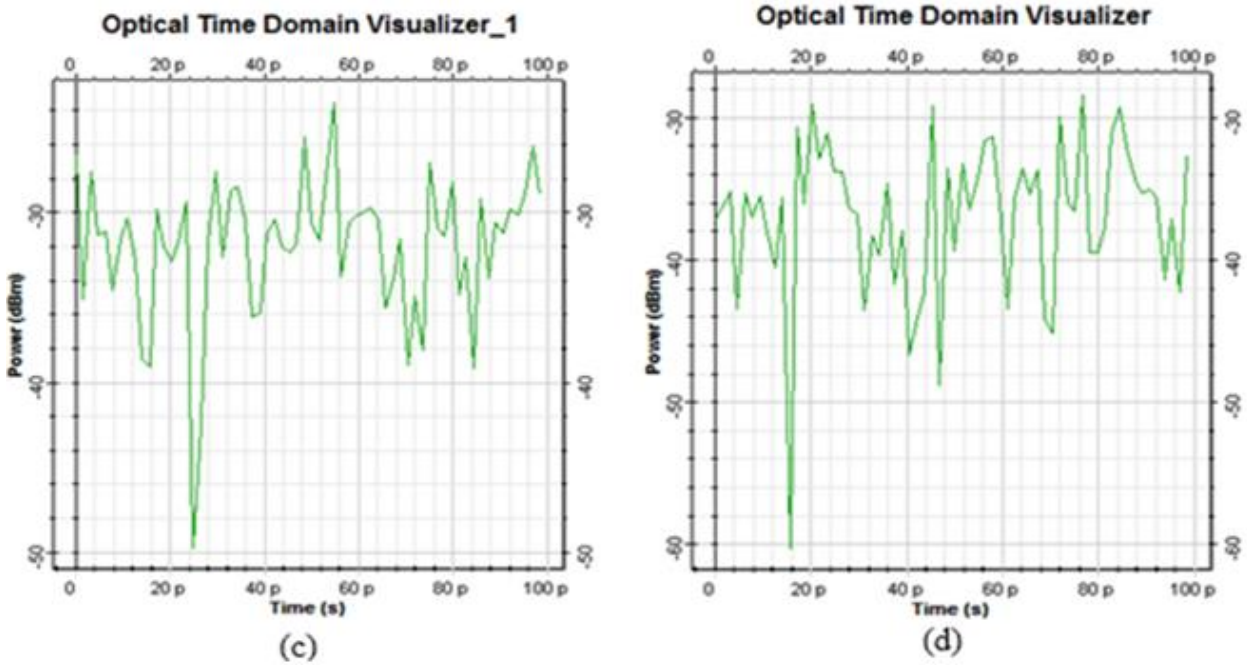

Figure 3.15: (c) Input noise power at port 1 before NOLM, (d) Transmitted noise power at port 2 after NOLM.

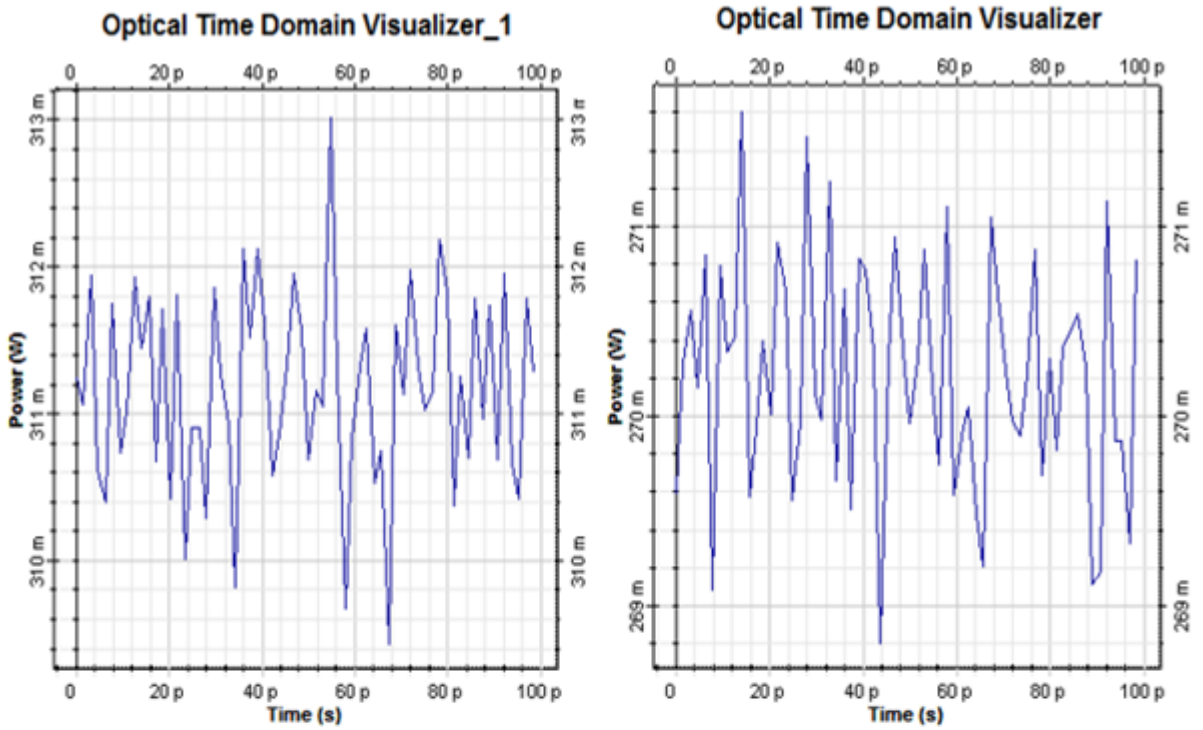

(e) (f)

Figure: 3.16: (e) Input signal and noise power at port 1 before NOLM, (f) Transmitted signal and noise power at port 2 after NOLM.

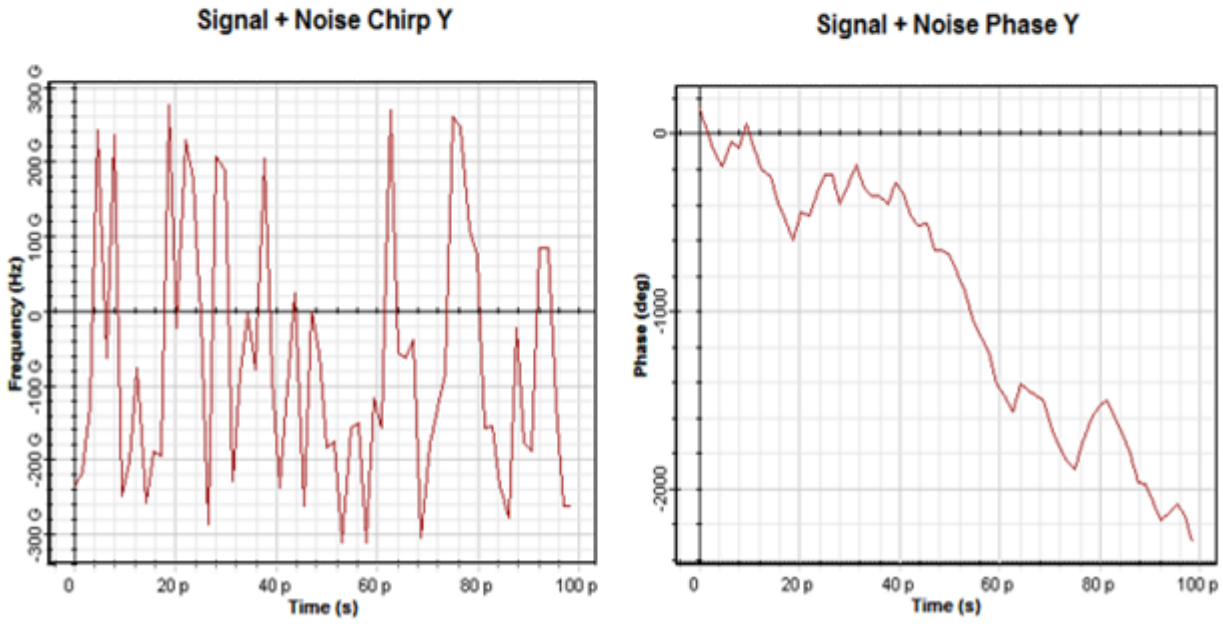

(g) (h)

Figure.3.17: (g) Frequency chirp caused by NOLM, (h) phase change caused by NOLM.

extremely reduced. This is because external modulated lasers overcome the power fluctuation and the high-end chirping by ON-OFF operation.

3.5 References

[1] Andrew Stentz, Torben Nielsen, and Per Hansen "Raman Amplifiers Use Span Fiber to Raise Signal Strength" Lucent Technologies, April 13, 2000.

[2] D.Derickson,Ed., Fiber Optics Test and Measurement. Upper Saddle River,Nj:Prentice-Hall,1998.

[3] B.Bristiel;Shifeng Jiang; P. Gallion; E.Pincemin "New model of noise figure and RIN transfer in fiber Raman amplifiers" Photnoic Technology Letters,IEEE Volume 18,Issue 8 ,pp980-982,April2006.

[4] Ninh T.Bui,Tuan Q.Nguyen and Hoi V.Pham "Effects of ASE Noise and Dispersion Chromatic on Performance of DWDM Networks using Distributed Raman Amplifiers" IJCNIS Vol.6,No.2 August 2014.

[5] T.N.Nielsen , A.J.Stenst and K. Rottwitt "3.28 Tb/s transmission over 3× 100km of nonzero-dispersion fiber using C and l band distributed Raman amplification" IEEE Photon Technol. Lett. Vol12 Aug 2000.

[6] N.J Doran and David Wood "Soltion-processing element for all-optical switching and logic" Vol. 4, No. 11/November 1987/J. Opt. Soc. Am. B

[7]N.J Doran and David Wood "Nonlinear-optical loop mirror"Optics letters .Vol.13, No.1 January 1988.

[8] N.J Doran, D>S.Forrester and B.K.Nayer "Experimental investigation of all optical switching in Fiber loop mirror devices" Electron Lett,Vol.25 ,pp.267-269, 1989.

[9] A.G Bulushev, E.M.Dianov, and O.G Okhotnikov "Passive mode locking of laser with a nonlinear fiber reflector"Opt,Lett Vol.17,pp 968-970,1990.

[10] K.Smith,N.J Doran, and P.G.J. Wigley "Pulse sharping compression and pedestal suppression employing a nonlinear optical loop mirror"Opt.Lett Vol15 .pp1294-1296,1990.

[11] Eiichi Yamada and Masataka Nakazawa "Reduction of Amplified Spontaneous Emission from a Transmitted Soliton Signal Using a Nonlinear Amplifying Loop Mirror and a Nonlinear Optical Loop Mirror" IEEE Journal of Quantum Electronics, Vol. 30, No. 8, August 1994.

Chapter -4

Photonic Crystal Fiber (PCF) Raman Amplifier

Recently, Photonic Crystal Fiber (PCF) have gained significant attention due to their capability of controlling the light wave inside the fiber by using tiny air holes through the fiber. The refractive index of PCF is periodically changed due to the air holes created in the PCF region which is made from pure silica. The PCF structure analyzed in this Chapter is Hexagonal Photonic Crystal Fiber (HPCF), i.e the air holes around the core are arranged in Hexagonal shape. Thus the hole diameter (d) and the pitch Λ offer better flexibility to demonstrate the propagation mechanism in PCF and analyze the design parameters. The azimuth view of the basic two dimensional hexagonal lattice photonic crystal is shown in Figure 4.1. The waveguide propogation mechanism for this PCF can be understood by the effective refrctive index model shown in Figure 4.2. As seen the central area with no holes has higher refractive index, similar to the core in the conevntional fibers.

4.1 Modeling

There are various numerical techniques and algorithms to measure light wave prorogation in photonic crystal fibers such as Finite Element Method (FEM), Finite-Difference Time-Domain (FDTD), Plane Wave Expansion (PWE), etc. For optical wave propagation, FDTD is suitable numerical tool to investigate these integrated and diffractive optic devices. This is due to FDTD

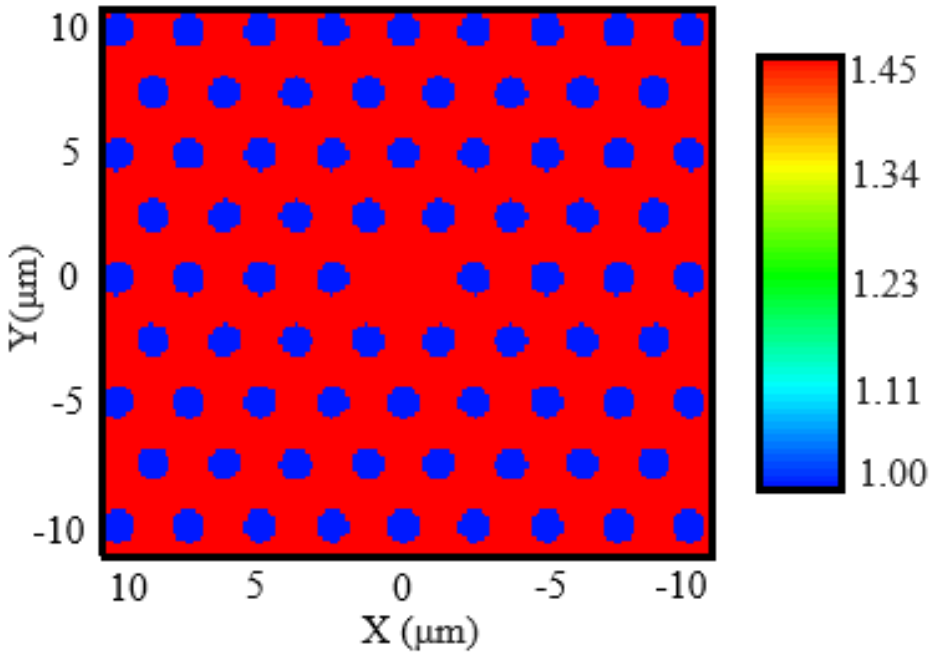

Figure 4.1: Structure of photonic crystal fiber with air fraction ratio (d /Λ) = 0.45.

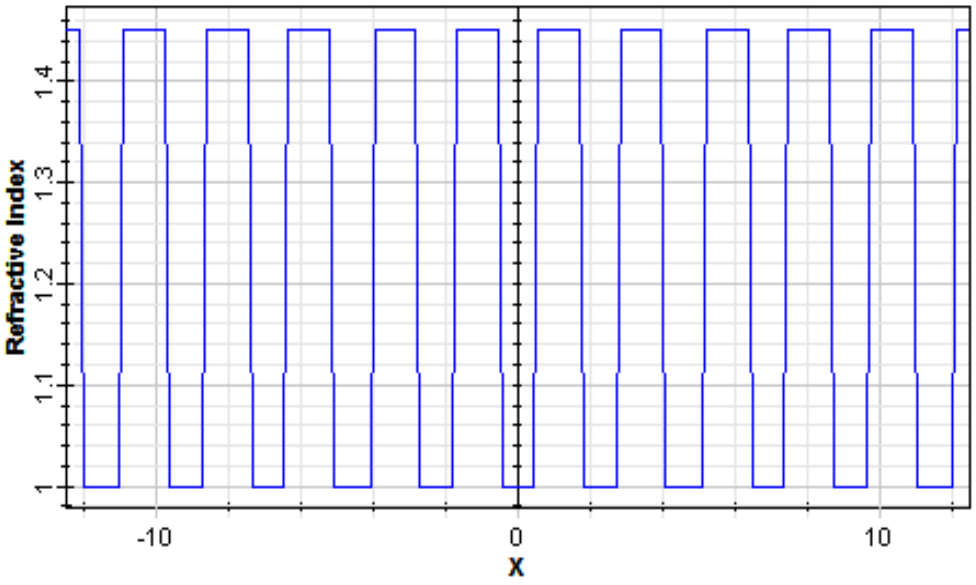

Figure 4.2: PCF refractive index profile.

ability to compute different light parameters like scattering, reflection, propagation, diffraction and polarization accurately. Moreover, without need to any pre-assumptions or approximations FDTD can model material dispersion and anisotropy easily. For submicron devices with small particle structure, FDTD is practical and effective method for simulation and analysis [1]. In addition, components such as Complex Poynting vector, transmission and reflection coefficients can be included due to the frequency solutions offered by FDTD by exploiting Fourier transforms.

4.2 Finite-Difference Time Domain (FDTD) Basics

FDTD is a geometrical and direct temporal solution for Maxwell's equations, thus, it solves all types of electromagnetic and photonics problems. It is based on three main elements, Yee's finite elements, Boundary conditions and initial field. FDTD algorithm for non-magnetic materials solution is based on the following Maxwell's curl equations

$$\varepsilon_r(\omega, x, y, z) = \varepsilon_r(x, y, z) \tag{4.1}$$

$$\frac{\partial \vec{E}}{\partial z} = \frac{\partial \vec{H}}{\partial z} = 0 \tag{4.2}$$

$$\frac{\partial D_z}{\partial z} = \frac{\partial H_y}{\partial z} - \frac{\partial H_x}{\partial z} \tag{4.3}$$

$$D_z(\omega) = \varepsilon_0 \varepsilon_r(\omega) E_z(\omega) \tag{4.4}$$

$$\frac{\partial H_x}{\partial t} = -\frac{1}{\mu_0}\frac{\partial E_z}{\partial y} \tag{4.5}$$

$$\frac{\partial H_y}{\partial t} = -\frac{1}{\mu_0}\frac{\partial E_z}{\partial x} \tag{4.6}$$

where D,E and H are the Displacement , electrical and magnetic fields , respectively., ε_r is the complex relative dielectric constant which depends on the angular frequency and is equal to the

square of the refractive index. As seen from these equations, Maxwell's equations are presented by six electromagnetic quantities E_x, E_y, E_z, H_x, H_y and H_z . Different locations on Yee cell (grind cell) represent solutions for each field components as shown in Figure 4.3 [3].

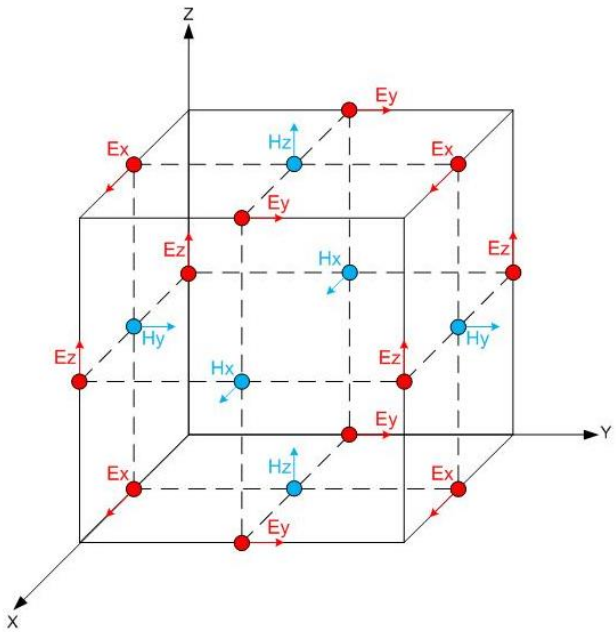

Figure 4.3: Yee's cell model.

When assuming an infinite structure in *z* direction and the other fields are independent of *z*, Maxwell's equations can be categorized in two sets with three vector components each. These two sets can be solved in x-y plane only and represent the transverse electric (TE) and the transverse magnetic (TM) field equations. FDTD uses discrete space and time grid to solve these equations. Wave propagation in PCF is directly related to Photonic band gab (PBG) structure. Thus, PBG calculation is done first using FDTD for both TE and TM polarization [2].

OptiFDTD is used in this chapter to run 2D- FDTD numerical simulation for the PCF structure described in Figure 4.1. The excitation of the field pattern in the first step cause the steady state

oscillation occurs in the periodic cell. Figure 4.4 is used to do FDTD simulation and analysis for a pure silica fiber with Hexagonal air hole shape along the fiber axis.

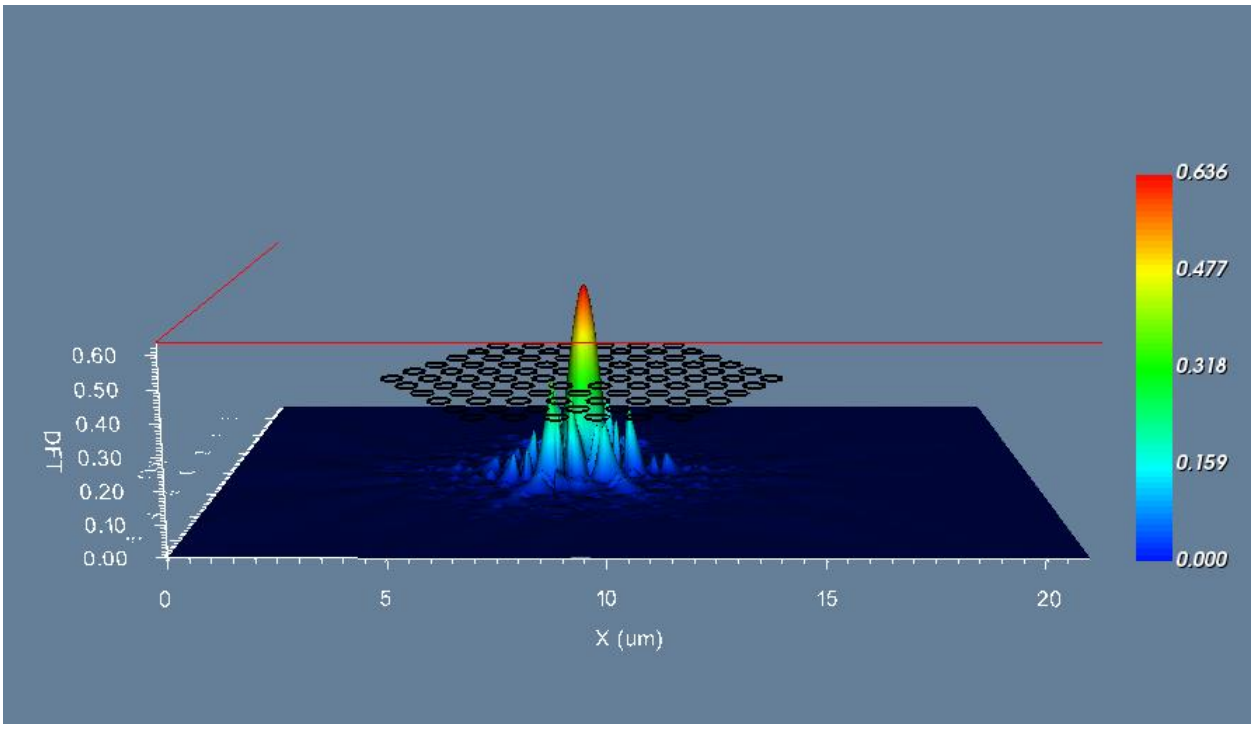

Figure 4.4: Propagation of modes through Hexagonal PCF at λ=1.5 μm.

As seen in Figure 4.4, the confinement of the light wave in the core is possible for the modes that satisfy Maxwell's equations. Each mode has a different refractive index and different corresponding speed. These modes show that the light is adapted to the constrains enforced by the guide.

4.3 Wave propagation in 2-D PCF

For 2-D PCF analysis, the two dimensions represent (x-y plane) and the light wave is assumed to be moving in z direction. Thus, all $\frac{\partial}{\partial z}$ components of both a TE and TM modes in z-direction

are neglected [4]. In the 2-D calculation domain, Δx , Δy and Δz represent space steps in x, y and z directions, receptivity. Meshes have different refractive indices, dispersion parameters and different type of material information in general [5] [6]. The minimum space steps are defined by

$$(\Delta x\ , \Delta y\ \ \Delta z) \leq \frac{\lambda_{min}}{10 n_{max}} \tag{4.7}$$

and the corresponding time step is given as

$$\Delta t \leq \frac{1}{v\sqrt{\frac{1}{(\Delta x)^2}+\frac{1}{(\Delta y)^2}+\frac{1}{(\Delta z)^2}}} \tag{4.8}$$

were v is the speed of light. For 2-D structure from Equation (4.8) is rewritten as

$$\Delta t \leq \frac{1}{v\sqrt{\frac{1}{(\Delta x)^2}+\frac{1}{(\Delta y)^2}}} \tag{4.9}$$

The electrical field propagation shown in Figure.4.5 is based on the temporal and spatial discretization of Maxwell's equations in the time domain. Light propagation through fiber is made by total internal reflections phenomena. This light is treated as electromagnetic wave, so that it can be analyzed by solving the Maxwell's equations. These equations are solved by verifying the propagation constant between maximum core value and minimum cladding value [7][8].The effective refractive index of the cladding is calculated as [9]:

$$n_{eff} = \frac{\iint n^2|E|^2 ds}{\iint |E|^2 ds} - \frac{1}{k^2}\frac{\iint n^2\left|\frac{dE}{dr}\right|^2 ds}{\iint E^2 ds} \tag{4.10}$$

where n is core refractive index, E is the propagating electrical field, k is the propagation constant , r is the distance between the hole and the fiber center and s is the surface area unit. E is described by Equations (4.5) and (4.6). The confinement loss occurs when the modes propagate in a smaller space resulting in partial propagation outside the fiber center as shown in Figure 4.6(a) and (b).

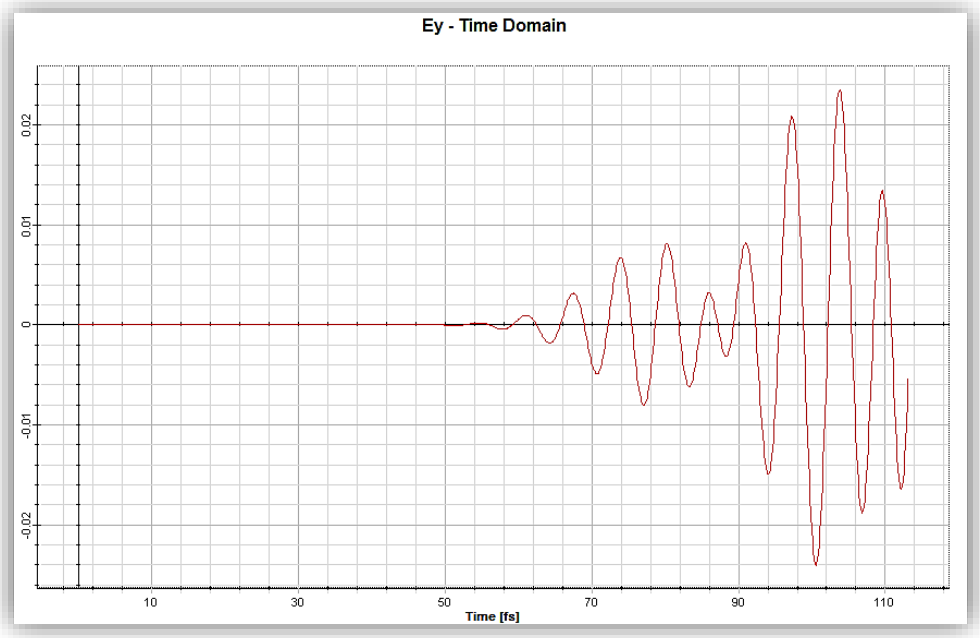

Figure 4.5: Electrical field propagation as function of time.

The input field used is Sine-Modulated Gaussian Pulse that has 2.262 (μm) full width at $1/e^2$ and amplitude of 1 (V/m).The corresponding propagating mode has power of 0.634 (V/m) and confinement loss of 0.289 (V/m). These losses are due to the leaky nature of modes and the PCF non-perfect structure. However, by controlling the geometrical structure parameters (hole and pitch diameters) and the operating wavelength, these losses can be minimized and the modes are guided inside the core.

4.4 PCF Raman Amplification Model

In this section, parameters such as the ratio of hole to pitch diameter, the pitch, GeO2 concentration, the effective doped core area are chosen to obtain maximum Raman amplification.

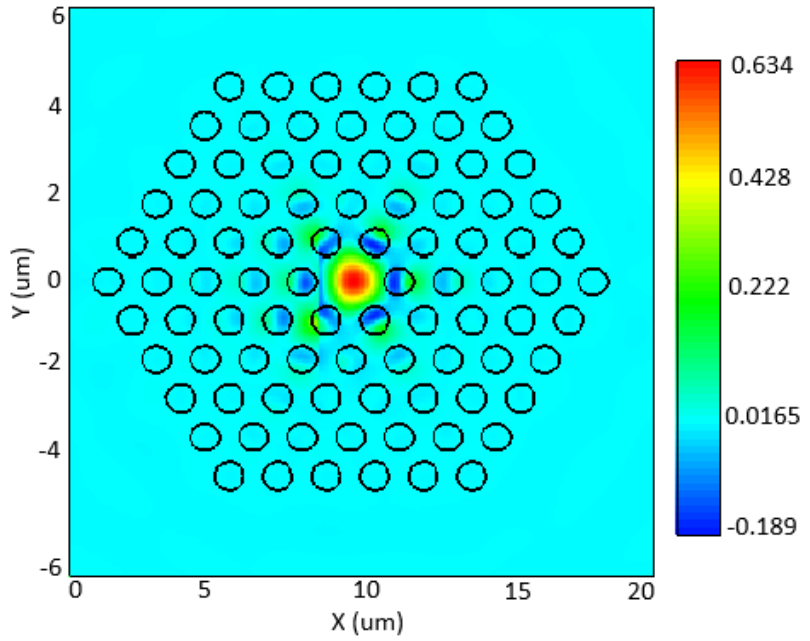

Figure 4.6: (a) Optical filed Distribution (Real part).

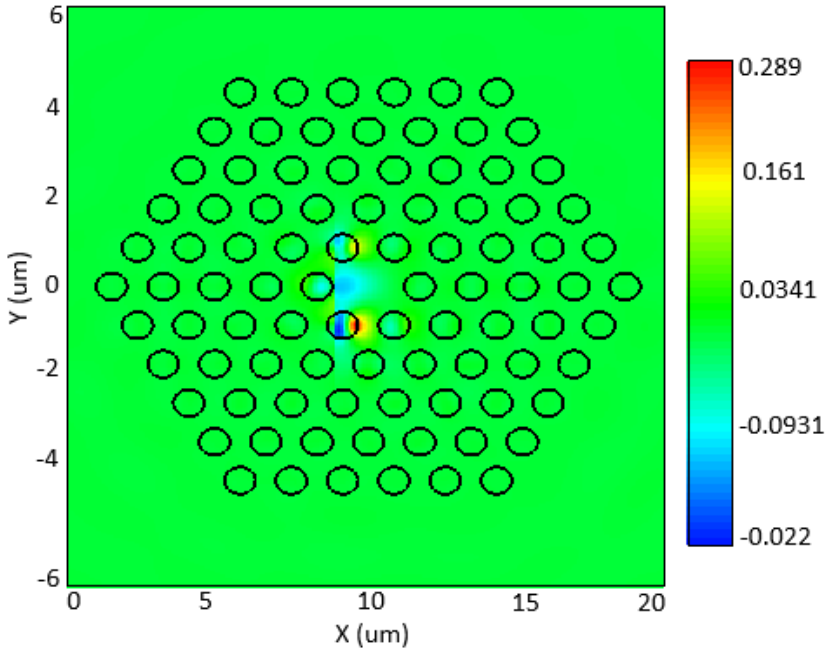

Figure 4.6: (b) Optical filed Distribution (Imaginary part).

In Chapter 2, Raman amplification was simulated and analyzed in details. In addition, in the previous sections of Chapter 4, PCF structure and mode propagation was simulated using FDTD. Here Raman amplification properties for Hexagonal PCF are investigated by manipulating the geometrical parameters (*d*, *Λ*). As a consequence, the cladding effective index is changed. Thus, the propagating field distribution, effective area and Raman gain coefficient are modified according to the relationships described in Chapter 2. The PCF is considered a silica bulk fiber with *Λ* between 0.4 and 4.8 μm and *d/Λ*= 0.45, 0.6, 0.75, 0.9 [10]. The profile of Raman effective area and Raman gain coefficients as a function of the pitch is reported in Figure 4.7(a) and 4.7(b), respectively. The fixed (*d/Λ*) ratio represents air to silica ratio in the cross section area [11].

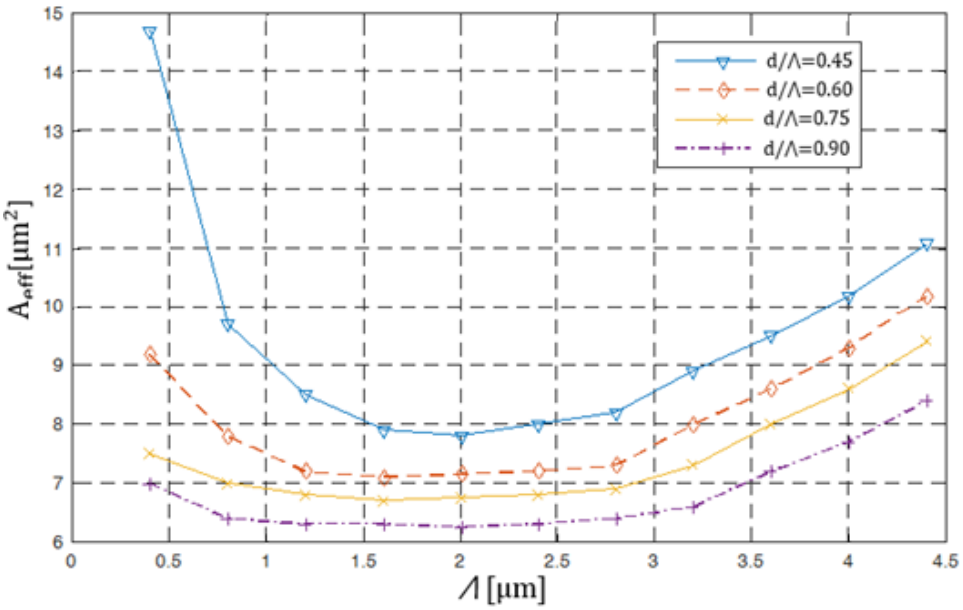

Figure 4.7: (a) Raman effective area for different PCFs structures as function of the pitch Λ.

As shown in Figure 4.7 (a) and 4.7(b), Raman gain coefficient is inversely proportional to the effective area .Thus for fixed (*d/Λ*) PCF and the optimum value of *Λ* (≈ 1.5 μm in this

case), the effective cross section area is minimized . Thus, Raman gain coefficient is maximized. This situation is obtained by applying a very narrow high field in a small core radius PCF with large difference between the core and the cladding refractive indices. Moreover, by increasing the pitch value the core radius is increases. However, the refractive index does not vary as it only depends on the air fraction ratio.

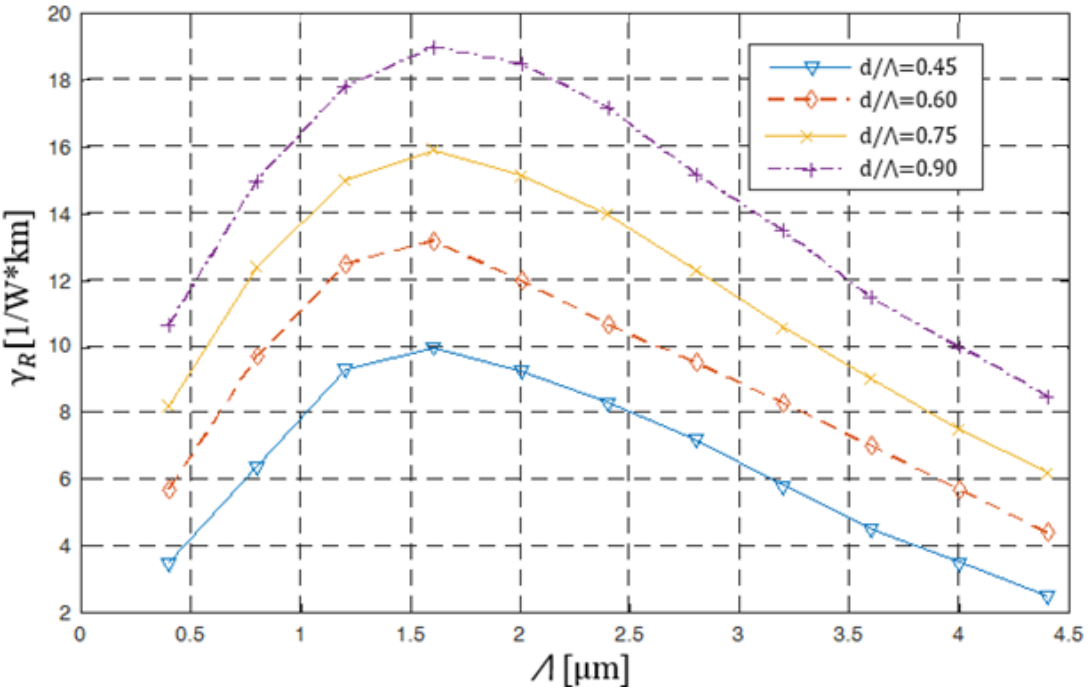

Figure 4.7: (b) Raman gain coefficient for different PCFs structures as function of the pitch Λ.

In addition, the smallest effective area occurs in PCF with $d/\Lambda=0.9$ and results the largest Raman amplification coefficient. However, in spite of high Raman coefficient, high Raman amplification is not achieved due to high attenuation losses and high nonlinearity in the fiber [12][13]. The effect of adding Germania dopants on PCF core is shown in Figure 4.8. GeO_2 concentration has been increased from 0% to 20 % for PCFs with fixed air fraction ratio,

d/Λ=*0.45, 0.60, 0.75* and *0.90* with Λ=*3.5 μm.* The effect of increasing the doping level (GeO_2) on the effective mode index is given in Table 4.1 [13].

Table 4.1: Effective Refractive Index for different doping level.

Refractive Index *(n)*	Effective Refractive Index $Re(n_{eff})$	Effective Refractive Index $Im(n_{eff})$
1.46 (pure silica)	1.44037166	0.000000102
1.48	1.46048416	0.000000123
1.49	1.47054253	0.000000132
1.60	1.58124464	0.000000197

Raman gain coefficient is calculated for each PCF structure. As shown, Raman gain coefficient is linearly proportional to the doping concentration similar to conventional fibers [14]. However, in this case, Raman gain coefficient γ_R is not inversely proportional to A_{eff} like silica bulk PCF shown in Figure 4.8. This is because it depends on the amount of the field that lies in the Germania- doped region. Hence, maximum value of γ_R doesn't necessarily occur at minimum A_{eff}[15]. It is Important to mention that the PCF core radius R_c is calculated using $R_c = \Lambda - d/2$ to obtain the minimum A_{eff} .This is according to optimal combination between the core dimension and core-cladding refractive index difference [16]. Doped PFCs have shown great improvement in γ_R so that values as high as 20 $[W^{-1}km^{-1}]$ is calculated for 20% GeO_2 concentration. Table 4.2 compares peak γ_R obtained here with other commercially available fibers to show the large enhancement achieved using doped PCFs [17] [18][19].

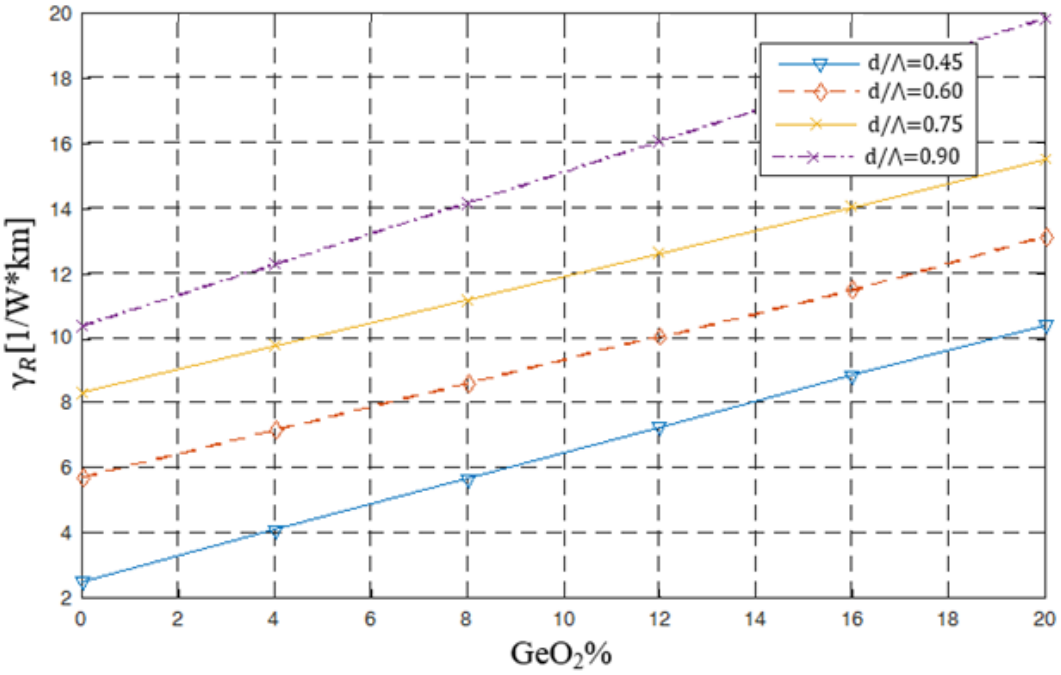

Figure 4.8: Raman gain coefficient as function of Germania concentration with Λ=3.5 μm.

Table 4.2: Comparison between Raman gain coefficients for different fibers.

Fiber type	γ_R
Single Mode Fiber (SMF)	$0.50[W^{-1}km^{-1}]$
Nonzero Dispersion-Shifted Fiber (NZ-DSF)	$0.75[W^{-1}km^{-1}]$
Dispersion-Shifted Fiber (DSF)	$0.75[W^{-1}km^{-1}]$
Dispersion-Compensation Fiber (DCF)	$3[W^{-1}km^{-1}]$
Raman Amplifier Fiber (RA)	$5[W^{-1}km^{-1}]$

4.5 PCF Attenuation and Dispersion Analysis

Attenuation and Dispersion in PCF are caused by almost the same mechanisms found in conventional fibers such as: confinement loss, bending losses, local imperfections, polarization loss and Rayleigh scattering. However, the effects of these mechanisms on the overall loss, the level of each of them and their dependence on wavelength are different from conventional fibers. The minimum level of attenuation of$\approx 0.15\ dB/km$ achieved in conventional fibers is limited by material absorption and fundamental scattering in bulk silica glass. In PCFs most of the light propagates in air, and in Hollow Core Photonic Crystal Fibers (HC-PCF) 99% of the light propagates in air. Thus, decreasing the bulk attenuation below 0.002 dB/km is achievable [20].

4.5.1 Dispersion and Confinement loss Analysis

Effective mode refractive index (n_{eff}) at given wavelength is calculated using FDTD method to solve Maxwell's equation for any guided mode and given by:

$$n_{eff} = \frac{\beta}{k_0} \tag{4.11}$$

where β is the propagation constant and the free space number k_0 is

$$k_0 = \frac{2\pi}{\lambda} \tag{4.12}$$

The n_{eff} is described by both real and imaginary parts. Hence, chromatic dispersion *D(λ)* and confinement loss *(L_c)* are obtained by [20] :

$$D(\lambda) = -\frac{\lambda}{c}\frac{d^2 Re[n_{eff}]}{d\lambda^2} \tag{4.13}$$

$$L_c = 8.868 \times k_0 \times Im[n_{eff}] \tag{4.14}$$

$D(\lambda)$ is calculated using Sellmeier equation. Thus, it represents the total dispersion of the PCF which include both material and waveguide dispersion. The chromatic dispersion is shown in Figure 4.9 for different PCFs structure. In Figure 4.9, the chromatic dispersion for four different PCFs structures are compared. As seen, the change obtained in the dispersion is small, which be

seen that increasing the air fraction ratio increases the dispersion. For d/Λ=0.9 at $\lambda = 1.55\mu m$, the positive dispersion is 2.345ps/(nm-km). Thus, in order to reduce the dispersion, the hole diameter need to be reduced.

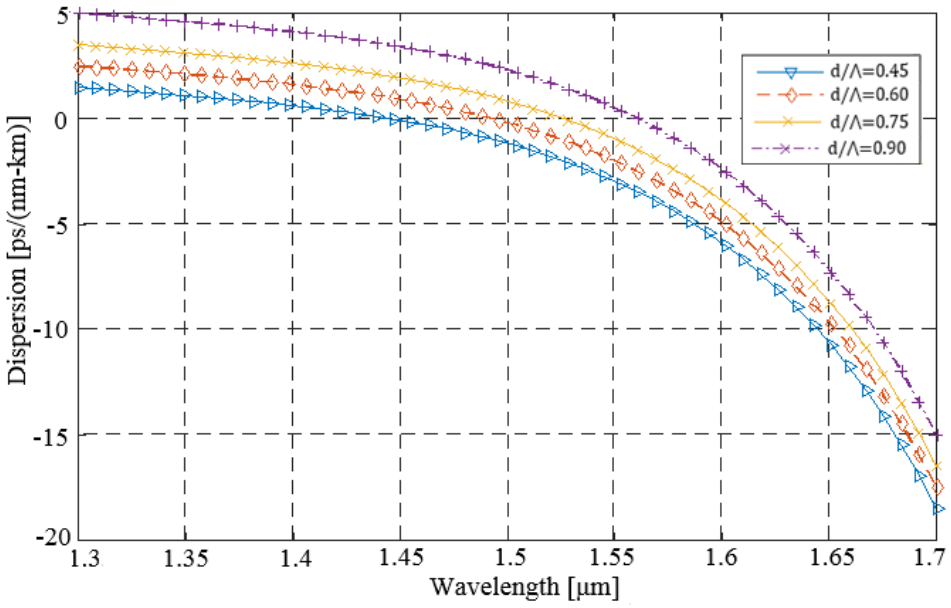

Figure 4.9: Chromatic dispersion curve as function of wavelength.

On the other hand, as shown in Figure 4.10, the confinement loss decreases as the hole diameter increases. At 1.55μm wavelength, the confinement loss is 0.352 dB/km for d/Λ=0.45 and 0.189 dB/km for d/Λ=0.45.

4.5.2 Scattering Loss Analysis

In addition to Dispersion and Confinement losses, PCFs are limited by scattering losses which depend on the wavelength, effective index and surface roughness.

A) Surface Roughness

Surface roughness occurs due to surface capillary waves (SCWs) existing during PCF fabrication. As glass solidifies, the SCWs freeze, creating a surface roughness given by the Spectral Density $\delta(\kappa)$ as [21] :

$$\delta(\kappa) = \frac{k_B T_g}{4\pi\gamma\kappa} \coth\left(\frac{\kappa W}{2}\right) \tag{4.15}$$

where κ is the spatial frequencies between κ and κ+dκ, γ is the surface tension ,T_g is the glass transition temperature and W is hole perimeter.

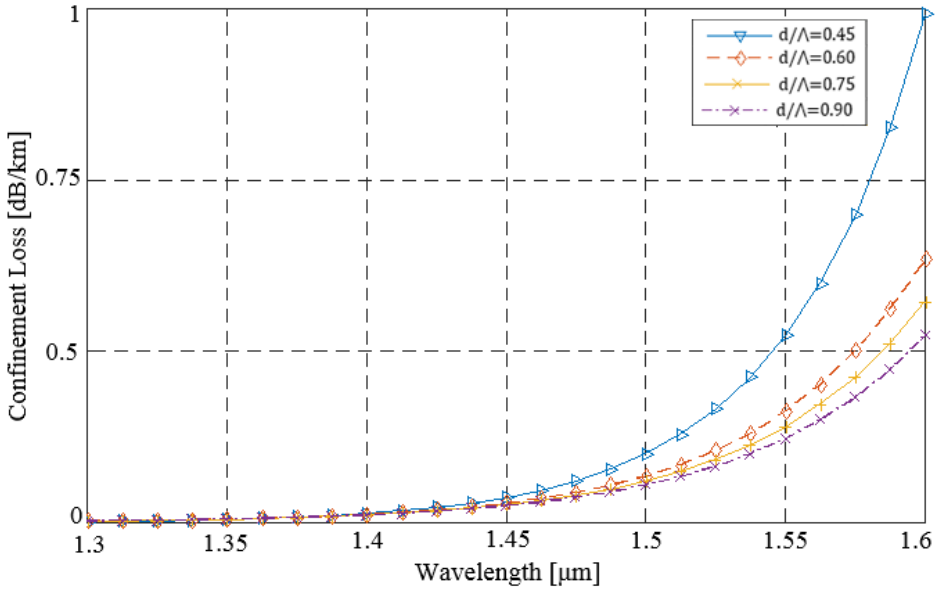

Figure 4.10: Confinement Loss curve as function of wavelength.

B) Dependence on Effective Index

The surface roughness causes some of the light energy to scatter from the fundamental mode with refractive index n_0 to other scattered mode with refractive index n. The overlapping between the fundamental mode and the surface mode F is approximated by:

$$F = \left(\frac{\varepsilon_0}{\mu_0}\right) \frac{\oint_{hole\ perimeter} |\boldsymbol{E}|^2 dl}{\oint_{cross\ section} \boldsymbol{E} \times \boldsymbol{H}^* dA} \tag{4.16}$$

where **E** and **H** are the electric and magnetic field distributions of the fundamental mode, respectively. The fraction of power $\alpha_n(n)$ scattered from those modes is:

$$\alpha_n(n) \propto \frac{F}{|n-n_0|} \tag{4.17}$$

This equation represents the intensity of the scattered modes by effective index and thus, the direction of scattering [22].

C) Dependence on wavelength

From the two previous sections, the attenuation is proportional to the intensity of roughness component between *n* and $n+\delta_n$ given by:

$$u^2 = \frac{4k_BT}{4\pi\gamma(n-n_0)} coth\left(\frac{(n-n_0)kW}{2}\right)\delta_n \tag{4.18}$$

where $k_B$is Boltzmann constant and T is the temperature. The attenuation to these modes is proportional to u^2 Attenuation unit is inverse length, hence it is inversely proportional to the cube of the minimum attenuation wavelength (λ_c) [23]. So that the net attenuation α is given by:

$$\alpha(\lambda_c) \propto \frac{1}{\lambda_c{}^3} \tag{4.19}$$

This equation can be used to predict attenuation level for different wavelengths. As seen this type of scattering attenuation is different from Rayleigh scattering that is proportional to $1/\lambda^4$. When PCFs were invited, they had high attenuation ($> 20d\ dB/km$). However, the attention level was reduced dramatically to reach few dB/km by the early 2000s. As seen, PCF attenuation need to be measured experimentally. For the PCF amplifier design, the experimental values of attenuation reported by *Katsusuke Tajima and Jian Zhoue* in [24] are used as the attenuation reference for the PCF amplifier. Table 4.3 shows recent years experimental works in achieving minimum PCF attenuation and Effective Area at $\lambda = 1.55$ μm presented in [25][26][27].

Table 4.3 Attenuation levels for different PCFs designs.

Reference	Attenuation (α)	Effective Area (A_{eff})
[24]	0.37 dB/km	20 μm^2
[25]	0.48 dB/km	130 μm^2
[26]	0.28 dB/km	80 μm^2
[27]	0.58 dB/km	25 μm^2

4.6 PCF Raman Amplifier Design

In conventional PCFs, 20 rings of the same hole size are used to achieve a structure with acceptable attenuation levels. Recently, researchers have found that using a multi-layer structure with different hole diameters can achieve zero-dispersion and very low confinement loss. In that case, the PCF is a two air holes design to achieve zero dispersion and low confinement loss at *1.55μm.* The design is based on *Saeed Olyaee* work in [28] using FDTD. The PCF design is based on the simple equal air-hole structure shown in Figure 4.1. Reducing the air fraction ratio decreases the dispersion but at the same time it increases the confinement loss. Therefore, the structure has a small d/Λ rate and the low confinement loss is achieved by changing the outer air holes diameter. The design is shown in Figure 4.11(a) and 4.11(b). The structure parameters are described in Table 4.4. A PCF Raman amplifiers with a smaller effective area and higher Raman coefficient compared to the described in Figure 4.11 and Table 4.4 are achievable. However, there is no experimental results reported for attenuation losses and scattering losses.

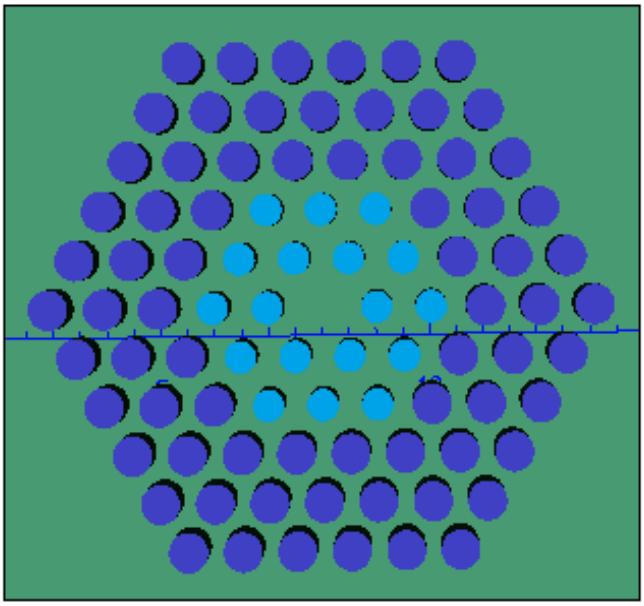

Figure 4.11: (a) PCF structure with Λ=3.46, d_1=0.95 and d_2=0.95.

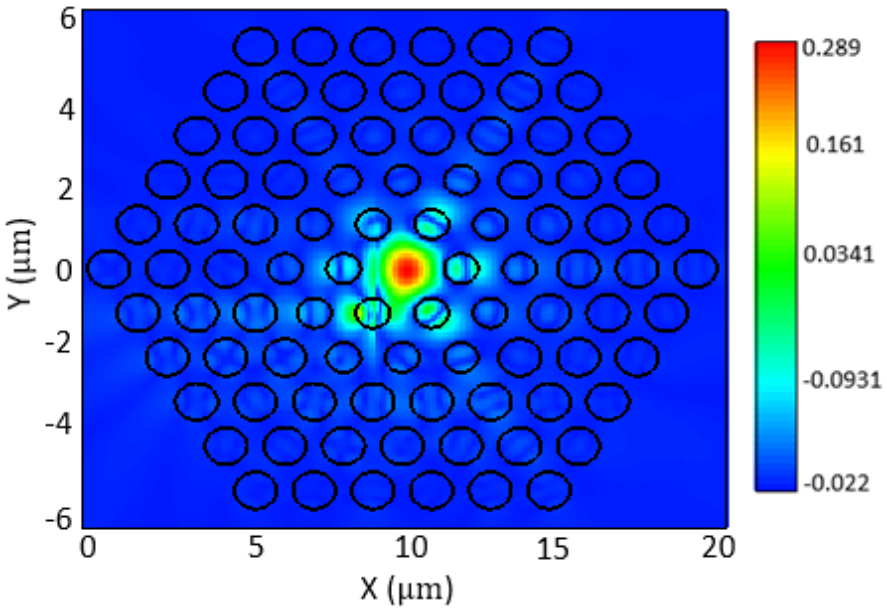

Figure 4.11: (b) PCF mode field distribution.

Table 4.4: Proposed PCF Parameters.

Parameter	Sample	Value	Unit
Wavelength	λ	1.55	μm
Effective Area	A_{eff}	20	μm^2
Raman Gain Coefficient	γ_R	9.25	$W^{-1}km^{-1}$
Attenuation losses	$\alpha(\lambda)$	0.37	*dB/km*
Doping Level	GeO_2	*20%*	-
Inner hole diameter	d_1	1.44	μm
Outer hole diameter	d_2	1.*74*	μm
Pitch	Λ	3.2	μm
Air fraction ratio	d/Λ	0.45	-
Core Radius	R_c	*2.48*	μm
Dispersion	$D(\lambda)$	2.5×10^{-4}	*Ps/(nm.km)*
Confinement loss	L_c	15.34×10^{-4}	*dB/km*

4.7 References

[1] Stanislav Kraus and Michal Lucki "Dispersion Compensating Photonic Crystal Fiber With Enhanced Achieved By Modified Core Geometry" Optics and Optoelectronics, Vol.10 No.2 June 2012.

[2] P. I. Borel, L. H. Frandsen, M. Thorhauge, A. Harpøth, Y. X. Zhuang, M. Kristensen "Efficient propagation of TM polarized light in photonic crystal components exhibiting band gaps for TE polarized light" Optical Society of America Vol.11,No.15 July 2003.

[3] Michael W. Chevalier, Raymond J. Luebbers and Vaughn P. Cable "FDTD Local Grid with Material Traverse" IEEE Transactions on Antenna and propagation, Vol. 45, No. 3, March 1997.

[4] Jack H.Winters and Richard .D. Gitlin "Electrical Signal Processing Techniques in Long-Haul Fiber-optic Systems" IEEE Transactions on Communication Vol.38,No.9 September 1990.

[5] L. P. Shen, W.-P. Huang, G. X. Chen, and S. S. Jian 'Design and Optimization of Photonic Crystal Fibers for Broad-Band Dispersion Compensation' IEEE PHOTONICS TECHNOLOGY LETTERS, VOL. 15, NO. 4, APRIL 2003.

[6] Jian Ju, Wei Jin, Senior Member, IEEE, and M. Suleyman Demokan "Design of Single-Polarization Single-Mode Photonic Crystal Fiber at 1.30 and 1.55 m", " Journal Of Lightwave Techonolgy, Vol. 24, No. 2, February 2006 825.

[7] M.Midrio, M. Singh, and C. Someda, "The space filling mode of holey fibers: an analytical vectorial solution". Lightwave Tech. 18 (7), pp 1031-1037 (2000).

[8] Z. Zhueun T. G. Brown, ―Analysis of the space filling modes of photonic crystal fibers, Opt. Express 8 (10), pp 547-554 (2001).

[9] L. LABONTE, ―Analyse théorique et expérimentale des principales caractéristiques du mode fondamental dans les fibres optiques microstructurées air silice,‖PhD Thesis, Université de Limoges (2005).

[10] Sagor Biswas, Ragib Shakil Rafi, Md. Abdullah Al-Amin, Sabbir Alam "Analysis of the Effect of Air Hole Diameter and Lattice Pitch in Optical Properties for Hexagonal Photonic Crystal Fiber" Optics and Photonics Journal, 2015, 5, 227-233 July 2015.

[11] A. Ferrando, E. Silvestre, P. Andrés, J. J. Miret, and M. V. Andrés, "Designing the properties of dispersion-flattened photonic crystal fibers," Optics Express, vol. 9, pp. 687–697, Dec. 2001.

[12] P. Petropoulos, T. M. Monro, W. Belardi, K. Furusawa, J. H. Lee, and D. J. Richardson, "2R-regenerative all-optical switch based on a highly nonlinear holey fiber," Opt. Lett., vol. 26, pp. 1233–1235, Aug. 2001. [13] J. H. Lee, Z. Yusoff, W. Belardi, M. Ibsen, T. M. Monro, and D. J. Richardson, "Investigation of Brillouin effects in small-core holey optical fiber: lasing and scattering," Opt. Lett., vol. 27, pp. 927–929, June 2002.

[13] Md. Mahbub Hossain and Md. Maniruzzaman "Analysis of Dispersion and Confinement Loss in

Photonic Crystal Fiber" International Conference on Electrical Engineering and Information & Communication Technology (ICEEICT) 2014.

[14] M. Fuochi, F. Poli, S. Selleri, A. Cucinotta, and L. Vincetti "Study of Raman Amplification Properties in Triangular Photonic Crystal Fibers" Journal Of Lightwave Techonolgy, Vol. 21, No. 10, October 2003.

[15] Blaze Photonics Ltd., Photonic Crystal Fibers, Tutorial, University of Bath, Claverton Down, Bath.

[16] Z. Yusoff, J. H. Lee, W. Belardi, T. M. Monro, P. C. Teh, and D. J. Richardson, "Raman effects in a highly nonlinear holey fiber: Amplification and modulation," Opt. Lett., vol. 27, pp. 424–426, Mar. 2002.

[17] A. Cucinotta, S. Selleri, L. Vincetti, and M. Zoboli, "Holey fiber analysis through the finite-element method," IEEE Photon. Technol. Lett., vol. 14, pp. 1530–1532, Nov 2002.

[18] Sumitomo Electric, Highly Non-Liner Fiber for Discrete Raman Amplification Amplifier (Data Sheet), Sumitomo Electric Lightwave Corp., Research Triangle Park, NC.

[19] F. L. Galeener, J. C. Mikkelsen, R. H. Geils, and W. H. Mosby, "The relative Raman cross sections of vitreous SiO , GeO , B O and P O ," Appl. Phys. Lett., vol. 32, pp. 34–36, Jan. 1978.

[20] B. J. Mangan, L. Farr, A. Langford, P.J. Roberts, D. P. Williams, F. Couny, M. Lawman, M. Mason, S.Coupland, R. Flea, H. Sabert, T. A. Birks, J. C. Knight and P. St.J. Russell, "Low loss (1.7 dB/km) hollow core photonic bandgap fiber," in Proc. Opt. Fiber. Commun. Conf. (2004), paper PDP24.

[21] J. Jäckle and K. Kawasaki, "Intrinsic roughness of glass surfaces," J. Phys.: Condens. Matter 7, 4351-4358 (1995).

[22] J. A. West, C. M. Smith, N. F. Borrelli, D. C. Allan and K. W. Koch, "Surface modes in air-core photonic band-gap fibers," Opt. Express 12, 1485-1496 (2004),

[23] F. P. Payne and J. P. R. Lacey, "A theoretical analysis of scattering loss from planar optical waveguides," Opt. Quantum Electron. 26, 977-986 (1994).

[24] Katsuske Tajima, jain Zhou , Kazuhide Nakajima, and kiminori Sato " Ultralow Loss and Long Length Photonic Crystal Fiber " Journal of Wavelength Technology ,Vol,22 No.1 January 2004.

[25] M.D. Nielsen, C. Jacobsen , N.A. Mortensen , J.R. Folkenberg , and H.R. Simonsen "Low-loss photonic crystal fibers for transmission systems and their dispersion properties" (060.2400) Fiber Properties, (060.2430) fibers, Single-mode. Optical Society of America 2004.

[26] K. Tajima, J. Zhou, K. Kurokawa, and K. Nakajima "Low water peak photonic crystal fibers," 29th European conference on optical communication ECOC'03 (Rimini, Italy), pp. 42-43 (2003).

[27] Michele Bottacini, Federica Poli, Annamaria Cucinotta, and Stefano Selleri "Modeling of Photonic Crystal Fiber Raman Amplifiers" Journal of Wavelength Technology ,Vol,22 No.7 July 2004.

[28] Saeed Olyaee , Fahimeh Taghipour, Mahdieh Izadpana "Nearly zero-dispersion, low confinement loss, and small effective mode area index-guiding PCF at 1.55 μm wavelength" DOI 10.1007/s12200-011-0172-7.

Chapter-5

Development of the PCF Amplification System

In Chapter 3, a pre amplification system using Distributed Raman Amplifier (DRA) was introduced to reduce the nonlinearity penalty and keep the signal level above the noise level which

enhances the total SNR. In addition, Nonlinear Optical Loop Mirror (NOLM) was tested successfully as a methodology to eliminate the noise generated inside the amplification medium. In Chapter 4, a PCF Raman amplifier with zero dispersion, low confinement loss, small effective area and high Raman gain coefficient was successfully proposed and designed. Here, The PCF Raman amplifier deigned in Chapter 4 is simulated, and analyzed. Moreover, all the previously described optical components are integrated as Hybrid amplification system based on EDFA.

5.1 PCF Raman Amplifier Gain

To investigate the performance of the designed PCF amplifier, a DWDM network is used to obtain broadband flat gain as shown in Figure 5.1. Total 24 channels between *1620 nm* and *1528 nm* with *4 nm* separation are transmitted by the proposed WDM transmitter. Each channel has average power of *-10 dBm*. The pumping signal is obtained using a 12 channels CW laser array. The WDM analyzer with wavelength span between *1470 nm* and *1570 nm* is used to get the PCF amplifier gain. Figure 5.2 (a) and (b) show the designed PCF amplifier attenuation as a function of wavelength and Raman gain coefficient as function of the frequency difference between the signal and the pump frequencies, respectively.

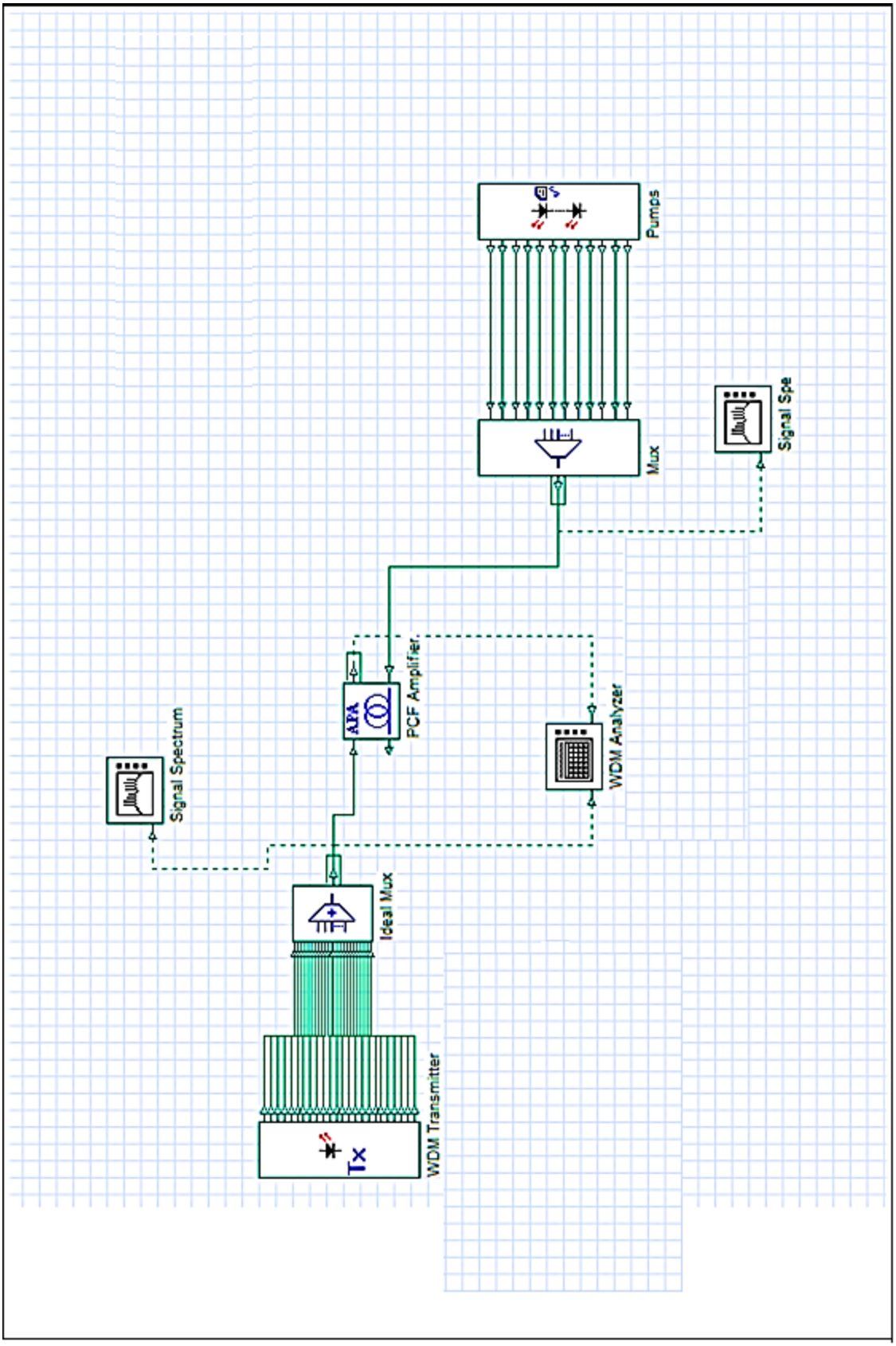

Figure 5.1: PCF amplifier for WDM network.

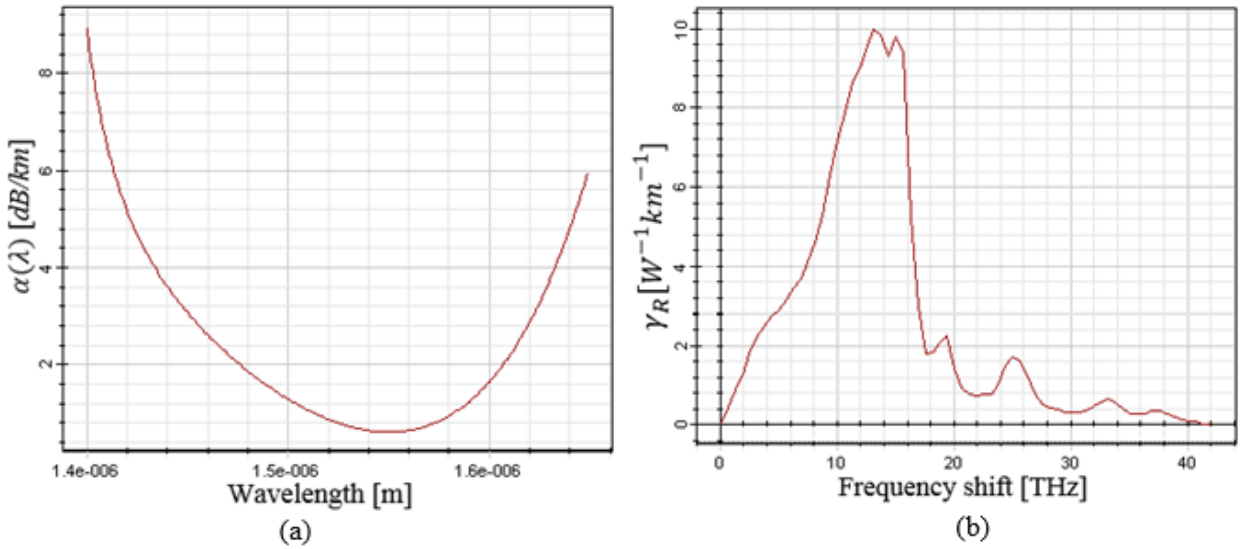

Figure 5.2: (a) attenuation spectrum of the designed PCF. (b) Raman gain coefficient of the designed PCF.

As seen, the ultra-loss fiber used as a medium has attenuation of 0.37dB/km at 1.55 μm. Although it was not specially designed for nonlinear application in [1], by manipulating the geometrical characterized of the PCF amplifier (Λ, d_1, d_2, d/Λ, R_c) and the doping concentration levels (GeO_2), it was able to achieve Raman gain coefficient of 9.25[$W^{-1}km^{-1}$]. The effect of adding the GeO_2 on the Raman Gain is shown in Figure 5.3. In general, Raman amplifiers require high pumping power for short length. For example 5 W for 1-km, when $g_r = 6 \times 10^{-14} m/W$, λ= 1.55 μm and $A_{eff} = 50\mu m$. Average Raman amplifiers require $L \geq 20$ *km* to achieve $G \geq 20$ dB at $P_p = 0.3W$. Moreover, $P_p = 1.0W$ is required to obtain $G \geq 10$ for $L \geq 40$ [2]. Raman Gain is not achieved for short length without doping. After running simulation for different PCF lengths based on [2], it was found that for high doping PCF-Raman Amplifier (RA) the optimal length is *7.5 km* for high doping concentration. Raman Gain *(G)* has maximum value of *G= 17.2 dB* when using the highest concentration (GeO_2 =20%) at λ= 1.55 μm . However increasing the concentration

level above this value generates high scattering losses and hence, increases the NF as shown in Figure 5.4. As seen in Figure 5.4, by increasing GeO_2 concentration from *5%* to *20 %* increases NF from 5 to *10 dB*.

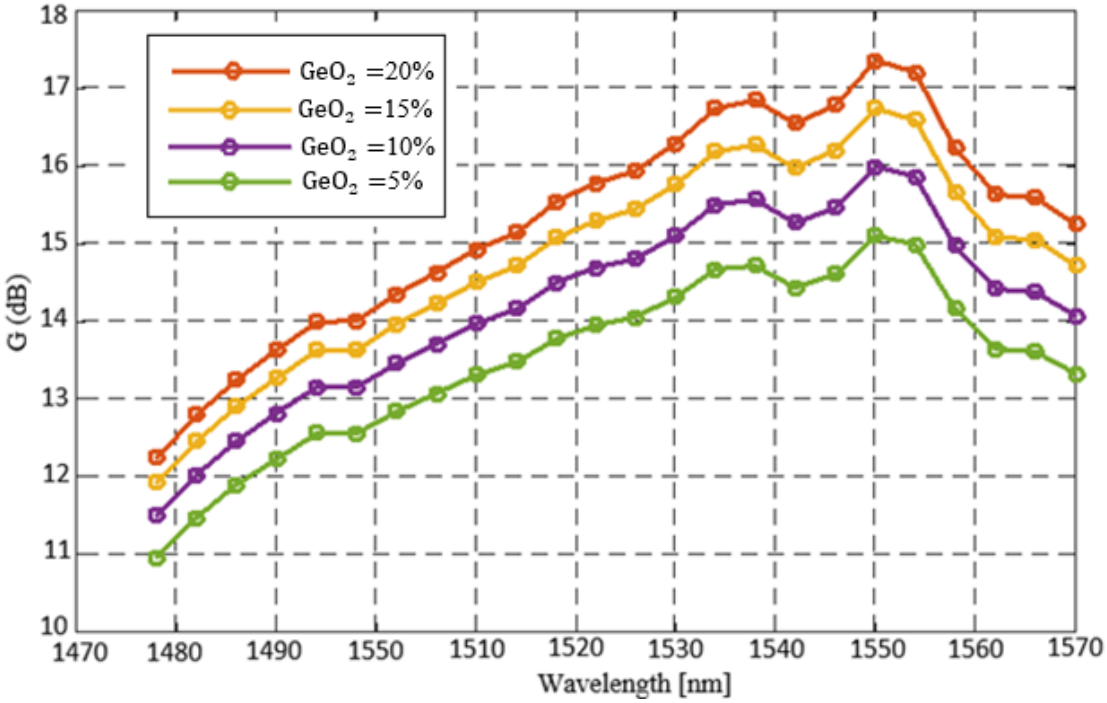

Figure 5.3: Raman Gain for GeO_2 = 5%, 10%, 15% and 20%.

In addition, Raman gain has been simulated for four different pumping schemes. Each scheme has different number of pumps with different wavelengths and associated power from each pump. The total pumping power is set to *1.2 W*. Number of channels was *6,8,10* and *12* pumps for schemes 1, 2, 3 and 4 respectively. The pumping wavelength is between *1405 nm* and *1510 nm*. The gain spectrum is shown in Figure5.5 for the four schemes. It is noticed that increasing the number of pumps, reduces the gain peak but flattens the gain spectrum. Which is the main advantage of Raman amplifier *(RA)* over Erbium-Doped Fiber amplifier (*EDFA*). It can be seen form Figure 5.5 that the gain peaks at 1550 nm with maximum value of +19.3dB and the minimum

value of gain is*10.8 dB* at *1478 nm*. However, the optimum scheme with broadband flatter gain and a gain value of 18.8 dB at 1550 nm was scheme 4.

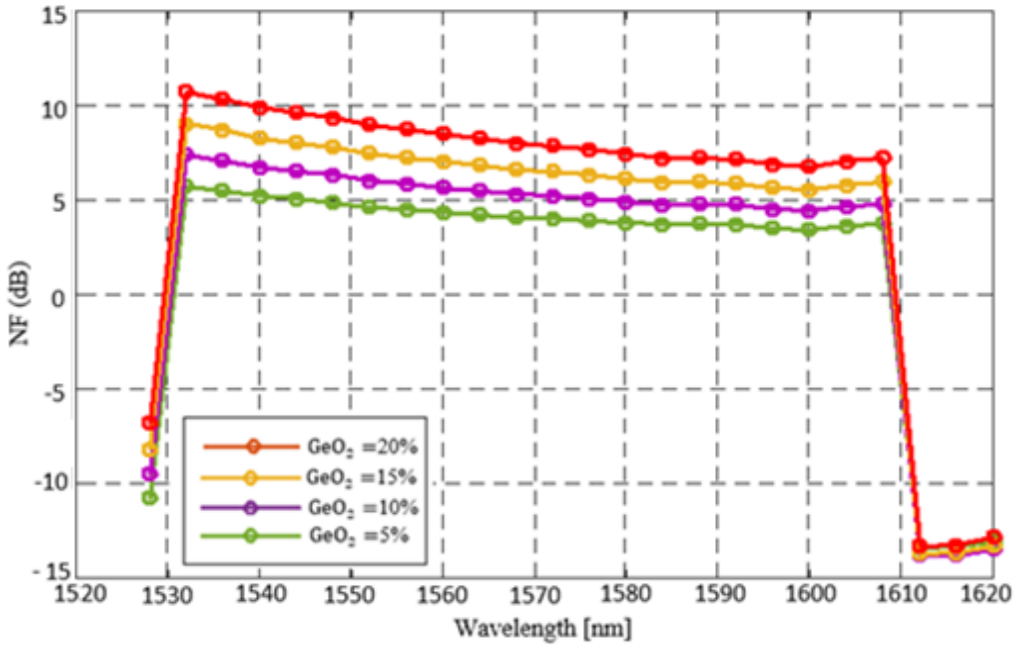

Figure 5.4: Noise Figure for GeO_2 = 5%, 10%, 15% and 20%.

Scheme 4 has 12 pumps between *1405nm* and *1510 nm* with average power of *0 dBm*. Two pumping powers are used. Pump 1 is *140 mW* for the 4 short wavelengths (*1405nm-1457.5nm*) separated by *7.5 nm (~1Thz)*. Pump 2 is *80 mW* for the 8 long wavelengths (*1465nm-1510nm*) separated by *15nm (~2Thz)*. This scheme is quite suitable for DWDM systems for their large bandwidth.

5.2 DWDM Amplification System Description

The proposed DWDM network amplification system shown in Figure 5.8 has three stages, Pre-Amplification, Amplification and Noise elimination system. The amplification system is simulated using Optisystem 14.2. The DWDM network with total capacity of 1.92 *THz (30 GHz* × *64)* with *0.8 nm* separation between the channels has been analyzed.

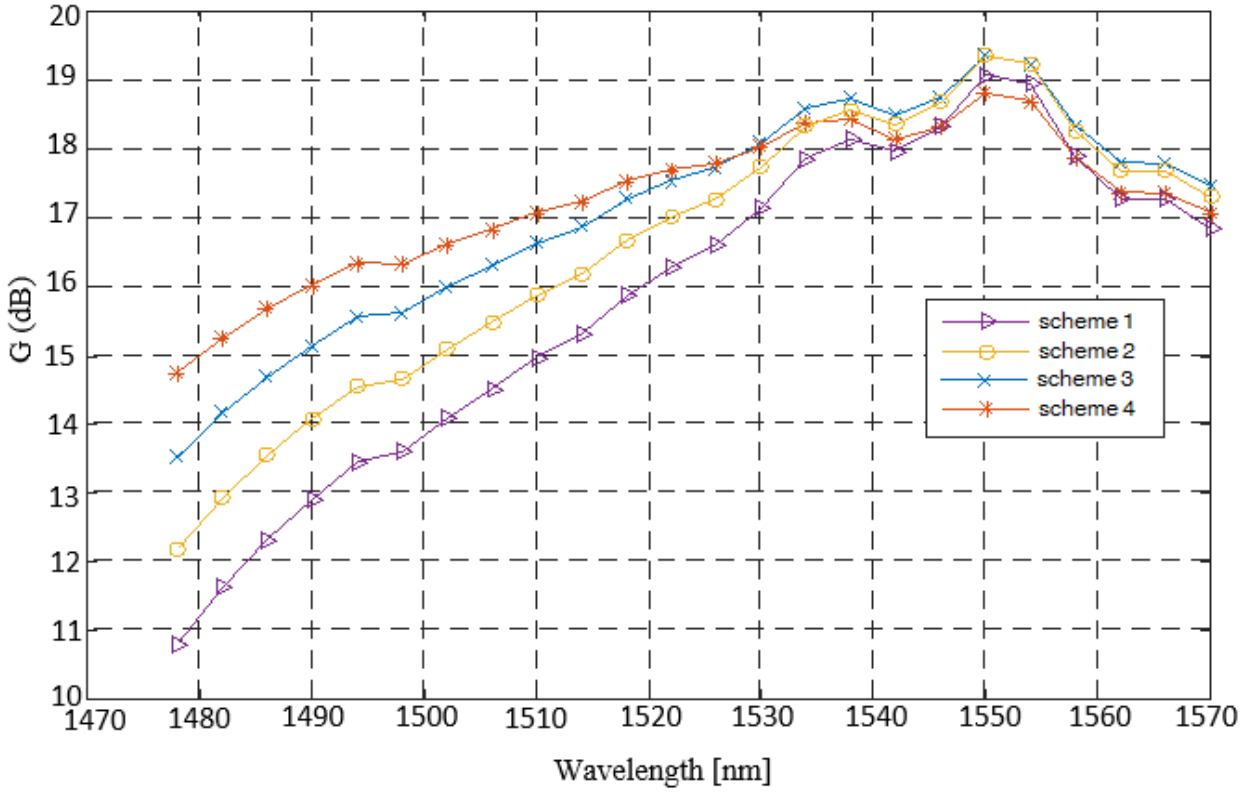

Figure 5.5: Gain spectra for pumping scheme 1, 2, 3, and 4.

Each channel has average power of *-20dBm*. Network traffic has been created using Pseudo Random Bit Sequences (PRBS) at each channel. NRZ signal is applied on the continuous wave laser (CW) using Mech-Zehnder modulator (MZ) to achieve On/Off Keying modulated (OOK). However, in high bit DWDM network, Differential Phase-shift keying (DPSK) is more practical than OOK due to the easier requirements for laser frequency stability and the demodulation sensitivity. Figure 5.6 and Figure 5.7 show comparison of BER and OSNR between DPSK and OOK systems . Almost 3-dB advantage in the receiver sensitivity is obtained when DPSK is used.

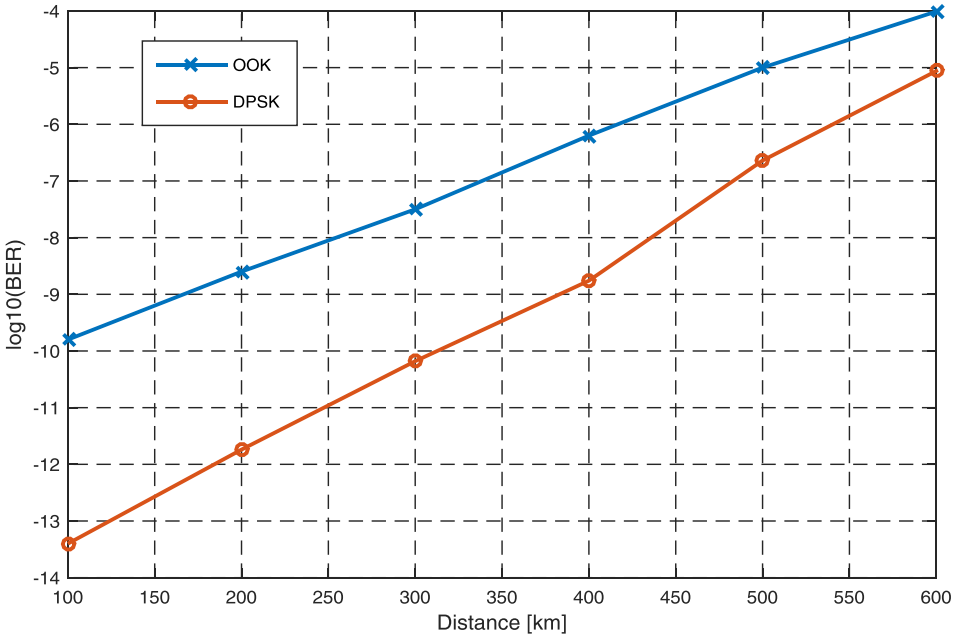

Figure: 5.6: BER for Single channel using RZ-OOK and RZ-DPSK

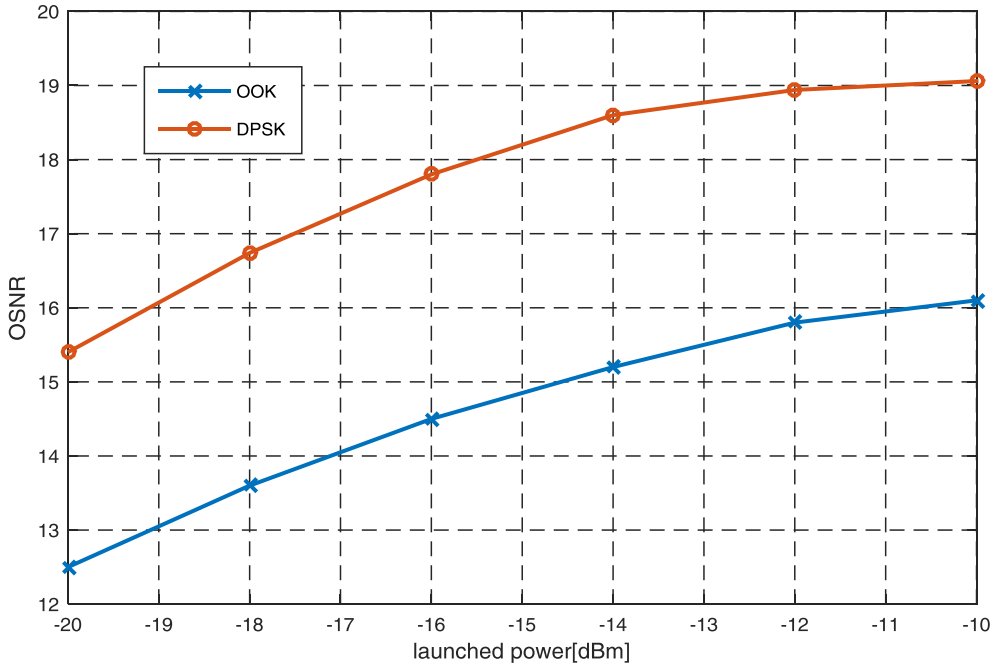

Figure5.7: OSNR for single channel using RZ-OOK and RZ-DPSK

The pre-amplification stage is Distributed Raman Amplifier (DRA) with forward and backward scheme. Forward and backward pump wavelength was setup at *1470 nm*. After the signals are multiplexed by the WDM multiplexer, they are coupled with the pump transmitted from the CW laser by the pump coupler and launched through the transmission line in the same direction (Forward scheme). Moreover, anther CW pump laser is located at the end of the bidirectional fiber to launch pump over the opposite direction (backward scheme). The parameter used for DRA are shown in Table 3.2.

The second stage is the PCF Raman amplifier. Here, The PCF is a two air holes design to achieve zero dispersion and low confinement loss at $1.55\mu m$ using FDTD. The structure has a small d/Λ rate and the low confinement loss is achieved by changing the outer air holes diameter. The design is shown in Figure 4.12 and the structure parameters are described in Table 4.4. The optimum pumping scheme for the designed PCF with broadband flatter gain and a gain value of 18.8 dB at *1550 nm* is implemented by 12 pumps with average power of *0 dBm* as it discussed before.

The final stage is implemented by Nonlinear Optical Loop Mirror (NOLM) as shown in Figure 5.8. The output signal of the PCF amplifier is split between port 3 and port 4 by 3 dB coupler which is part of NOLM. The signal from port 3 propagates clockwise in the optical loop. The signal from port 4 propagates counter-clockwise in the optical loop. A *10 km* Bidirectional fiber with *0.2 dB/km* attenuation was used for the nonlinear loop. The Differential group delay was set to *0.05 ps/km* and the Dispersion is *-0.69 ps/nm/km* at *1550 nm*. At port 2, PIN photodetector is used to convert the optical signal to electrical signal and low pass Bessel filter to visualize BER, Q factor. Eye Diagram and the reduction in Noise.

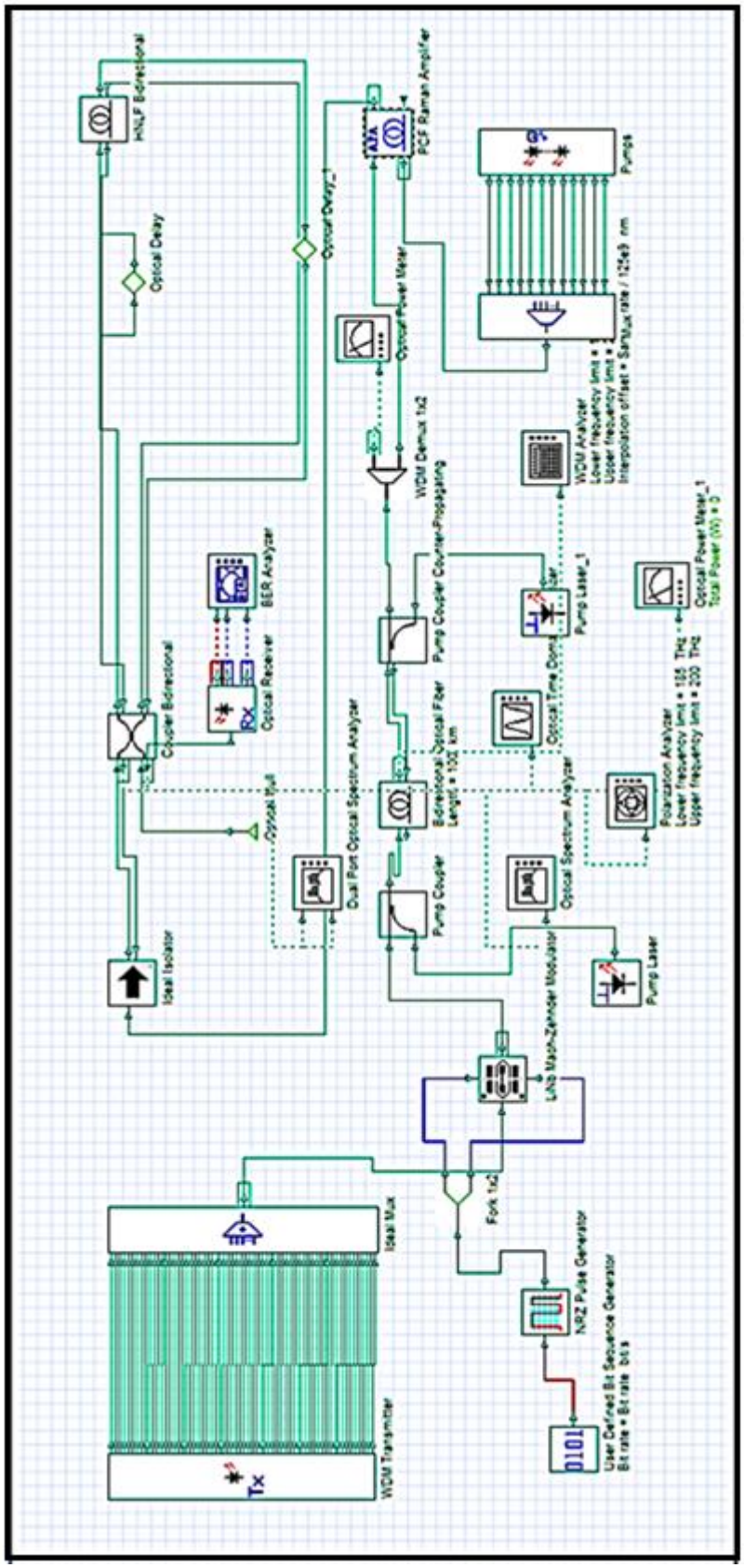

Figure 5.8: DWDM network with amplification system based on PCF-RA.

5.3 Simulation Results

A 64-channel DWDM CW with *0.8 nm* separations between channels boosted by *-20 dBm/ch* was simulated. Figure 5.10 (a) (b) (c) and (d) show the 64 transmitted signal spectrum, DRA pump signal, 12 pumping array of the PCF amplifier , the received signal spectrum and the total noise spectrum. As seen in Figure 5.5, the gain peaks at 1550 nm due to the fact that the PCF amplifier is designed to have zero dispersion and minimum losses at $\lambda=1.55\mu m$. Intensity noise in broadband DWDM communication system enforces strong limits on the network performance [3]. Two techniques for reducing the noise intensity were proposed and demonstrated in Chapter 3. The signal and noise intensities as function of time are shown in Figure 5.9. As it can be seen, the noise is on *-45 dBm* power level for *-20 dBm* input signal.

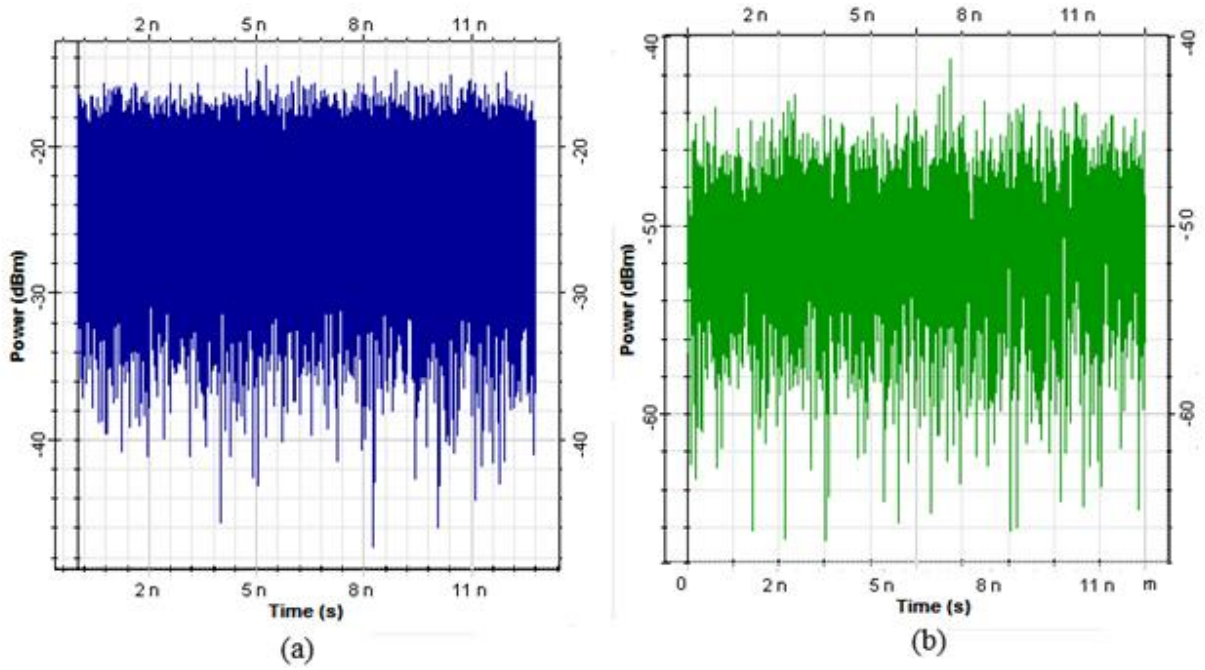

Figure 5.9: (a) Signal power as a function of time. (b) Noise power as function of time.

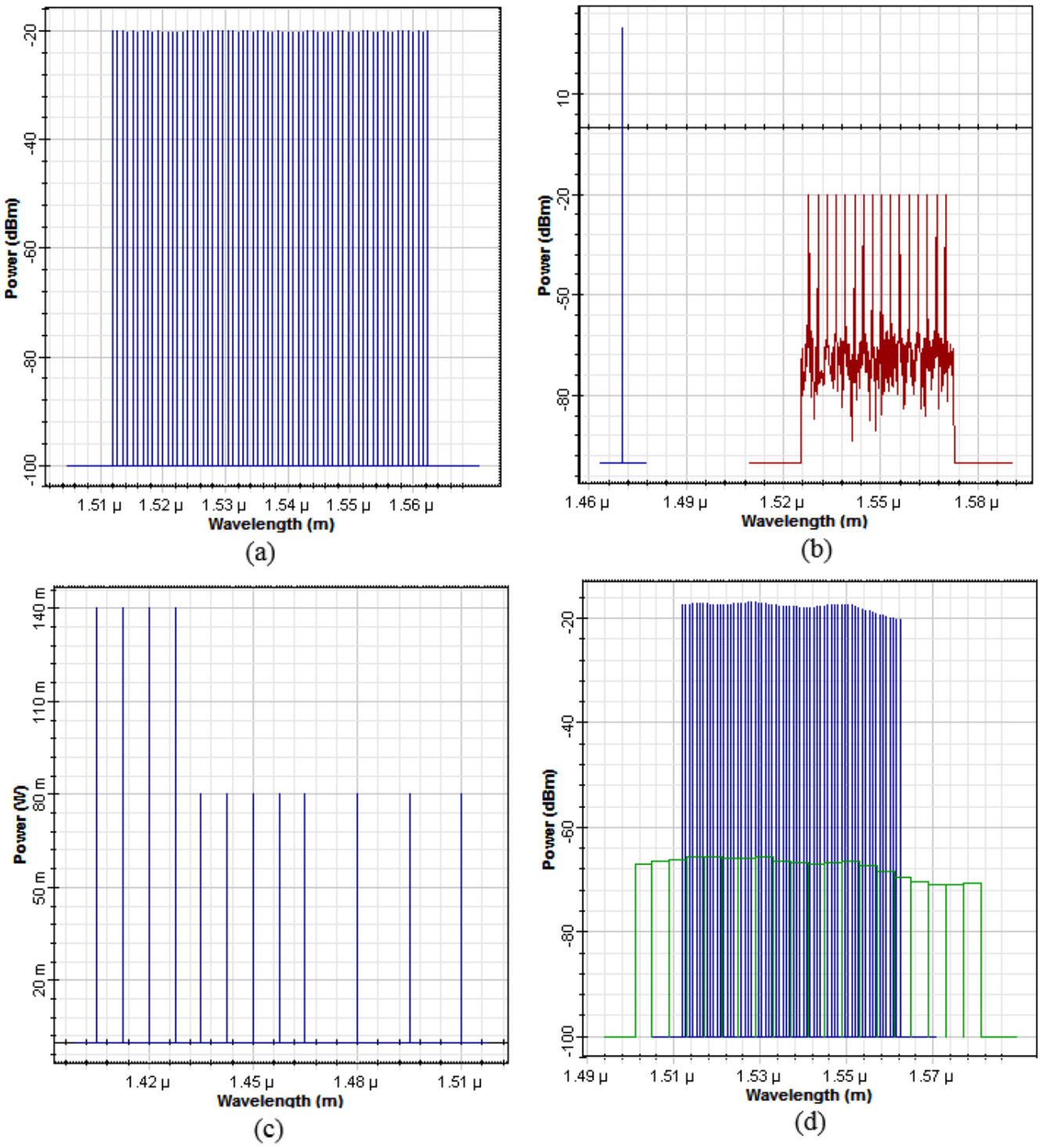

Figure 5.10: (a) the 64 transmitted signal spectrum, (b) DRA pump signal, (c) 12 pumping array of the PCF amplifier, (d) the received signal spectrum and the total noise spectrum.

In addition, Q factor and BER are important parameters in limiting the bit rate, bandwidth and the distance in transmission system. In long distance communication systems, low BER and high Q factor values are required. The main advantage of optical amplifier is the optical signal is amplified without being converted to electrical signal .Thus, high Q factor and low BER values are achievable.

As was found from NOLM simulation in Chapter 3, the output signal is not stable due to the frequency chirp and phase change generated by the propagation through the loop .The nonlinear intensity -dependent switching causes frequency chirp. Thus, Externally Modulated Lasers (EMLs) instead of Directly Modulated Lasers (DMLs) is used by applying NRZ signal on the Continuous Wave laser (CW) using Mech-Zehnder modulator (MZ) to achieve On /Off Keying External modulated (OOK) as shown in Figure 5.8. The stability of the signal is shown in Figure 5.11. The frequency chirping is extremely reduced. This is due to the use external modulated lasers that overcome the power fluctuation and the high-end chirp by ON-OFF operation. Here BER, Q factor and eye diagram for long distance DWDM network ($> 100km$) based on PCF optical amplifier for bit rate of *20GHz* and *25 GHz* and *30 GHz* are shown in Figure 5.12 (a), 5.12 (b) and 5.12 (c),respectively [4]. From the analysis of the Q-factor, BER and eye diagram in Figure 5.12. it is observed that at *30 GHz* a High Q-factor and low BER are obtained. At *25 GHz* bandwidth maximum Q-factor of *13.8445* and minimum BER of *2.0089* e^{-33} is achieved for *100km* network length. For bandwidth larger than 25 GHz, Q- factor decreases and BER increases. As a result, eye diagram suffers from high jitter and distortion [5].

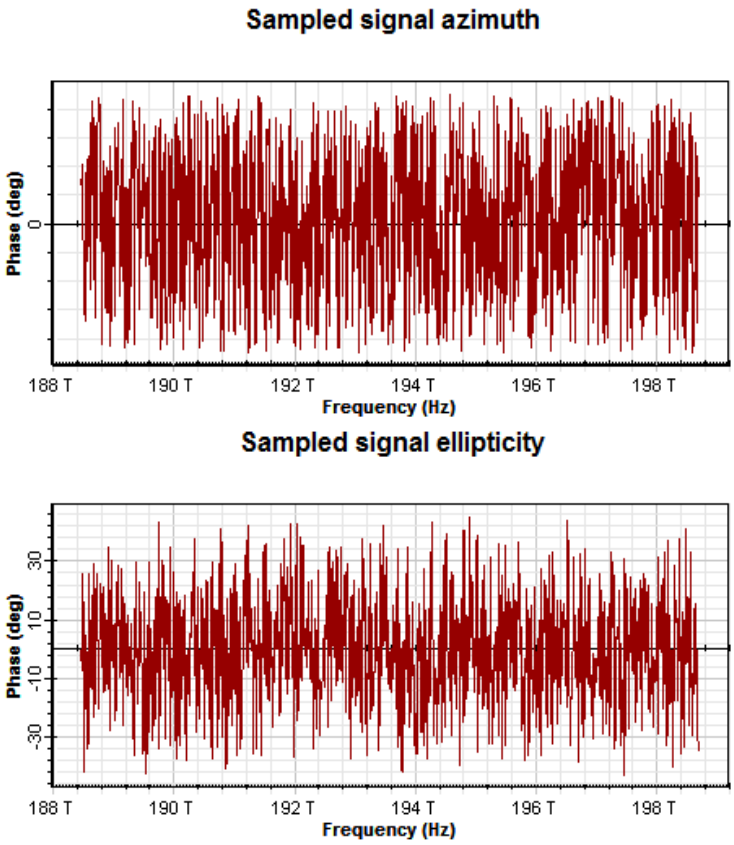

Figure 5.11: Sampled signal phase as function of frequency.

The corresponding OSNR is shown in Figure 5.13. The noise intensity limits for OSNR can be enhanced significantly by increasing the input power. For low bit rate and high optical power OSNR is improved by *20dB*. For a fiber–to-fiber amplification over *20dB*, input power of *-20 dBm* and *25GHz* bit rate, OSNR value is *36.2 dB*.

5.4 Hybrid Amplifier

The increasing demand for larger Bandwidth and higher bit rate DWDM network systems requires upgrading the number of channels, channel speed and spectral efficiency [4].

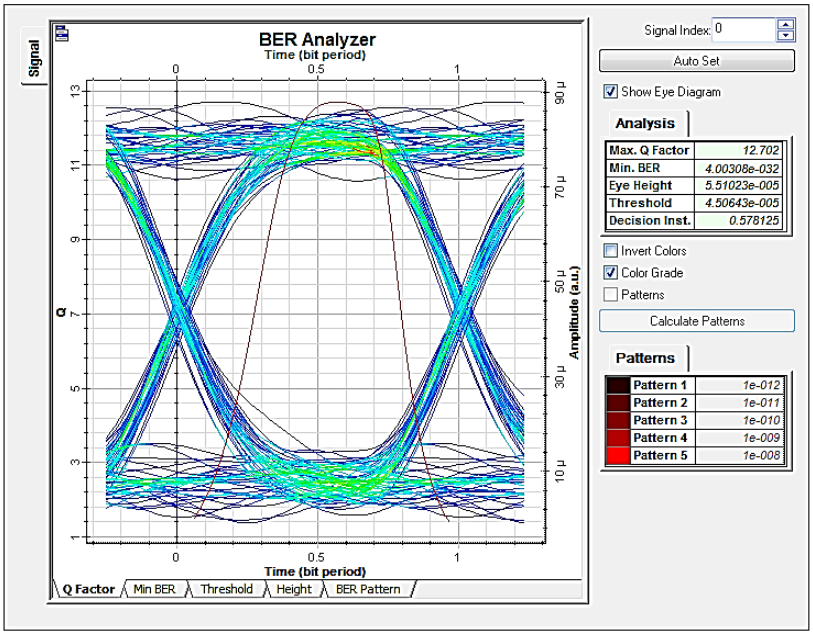

Figure 5.12: (a) Q factor, BER and eye diagram for 20 GHz.

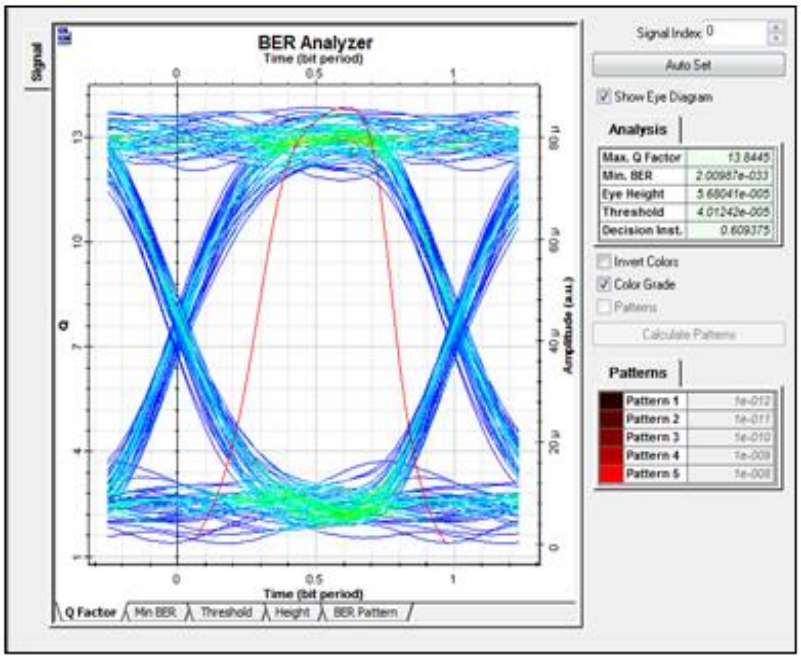

Figure 5.12: (b) Q factor, BER and eye diagram for 25 GHz.

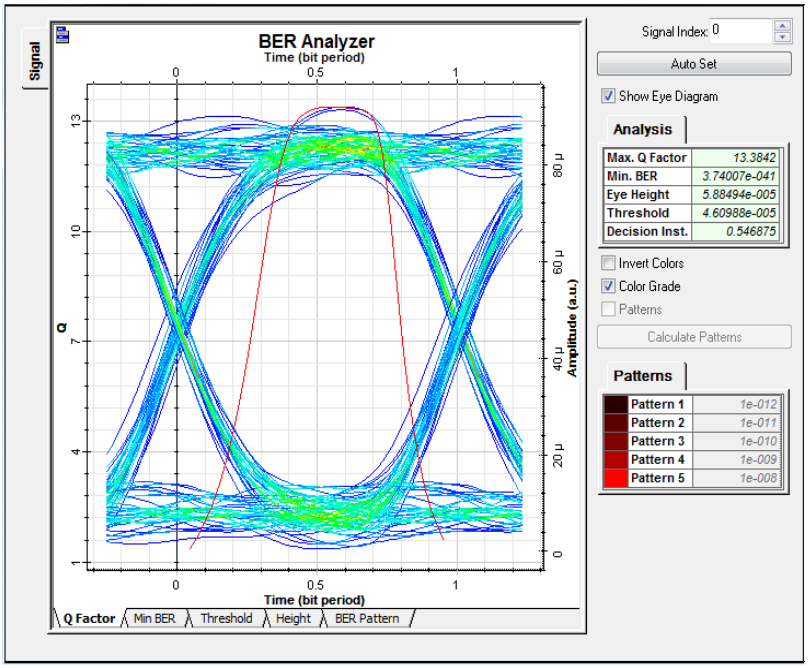

Figure 5.12: (c) Q factor, BER and eye diagram for 30 GHz.

Raman+ EDFA hybrid amplifier offers significant improvement in overcoming those problems. Here, EDFA amplifier is used instead on PCF-RA to achieve high bit rate DWDM network.

5.4.1 Erbium Doped Fiber Amplifier (EDFA)

An EDFA is a silica fiber doped that achieves amplification by simulated emission of photon from Erbium ions. EDFA gain occurs at 1550 nm region and requires pumping laser at wavelength of *980 nm* or *1480 nm*. Thus, EDFA is a C-band optical amplifier [6]. The gain of EFDA is giving by:

$$G_{EDFA} = \frac{\sigma.n_t(W_p - \Gamma)}{2.\sigma.c.p + \Gamma + W_p} \tag{5.1}$$

where $\sigma, n_t, \Gamma, c, p,$ and W_p are the emission cross section, total population density of E_r ions, reciprocal carrier charge life time , light velocity, photon density and particles pump rate,

respectively [7]. EDFA cross section for induced emission as function of wavelength is shown in Figure 5.14.

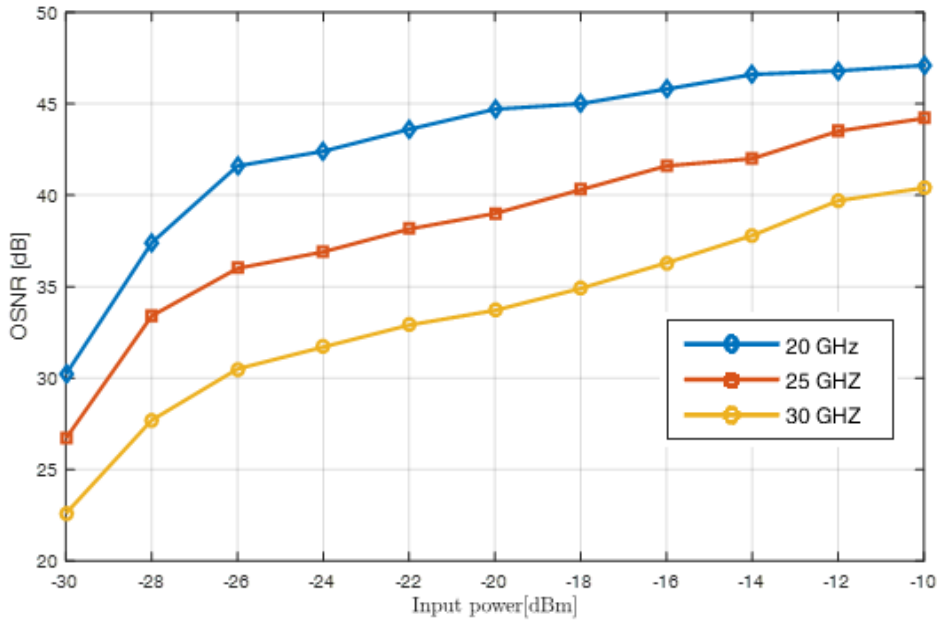

Figure 5.13: OSNR as function of input power for 20GHz, 30 GHz, and 35 GHz.

EDFA gain shape depends on the absorption and emission shape shown in Figure 5.12. Thus, the maximum gain typically occurs between *1530nm* and *1570 nm*. The noise figure (NF) for EDFA is defined by:

$$NF = \frac{P_{ASE}}{h.v.\Delta v.G} + \frac{1}{G} \tag{5.2}$$

Where P_{ASE} is the amplified spontaneous emission power described in Chapter 3, h is Planck's constant, G is EDFA gain, v is the frequency and Δv is the bandwidth. Figure 5.15 shows EDFA gain and NF as function of wavelength with optimal pumping power of *13mW* (*11.14dBm*) [8].

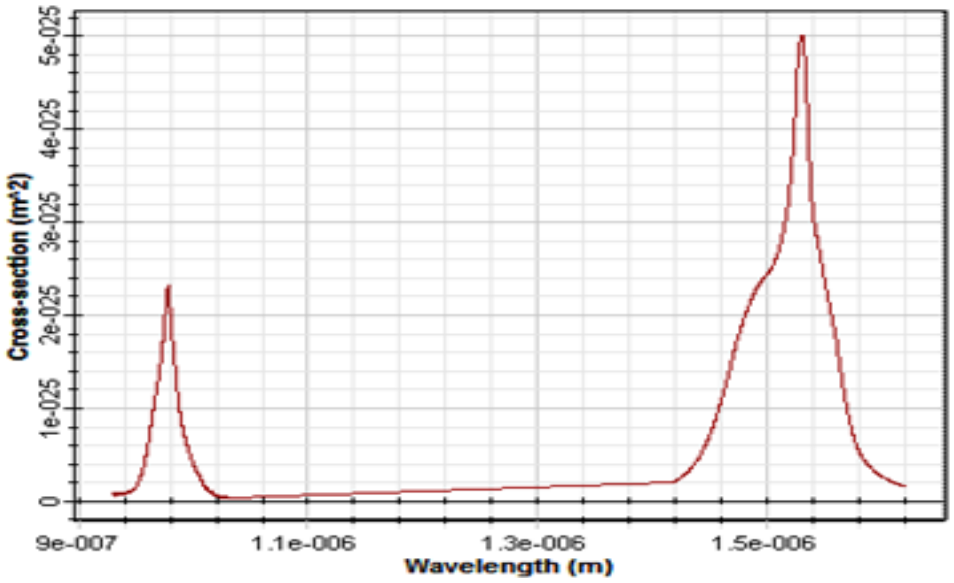

Figure 5.14: EDFA cross section as function of wavelength.

5.4.2 Hybrid Amplifier Configuration

Figure 5.16 shows C-band EDFA and L-band DRA integrated to achieve high gain and large bandwidth amplification system for high speed DWDM network system. EDFA uses pump source at wavelength of *1480 nm* and a power of *13 mW*. Figure 5.17 shows the overall Gain and NF for the hybrid amplifier in the C+L band. The hybrid amplifier has better gain and NF than EDFA or RA [9]. In the C+L band, the gain average value is *45 dB* and the NF average value is *-7 dB*. Hence, this hybrid amplifier has wider, flatter and higher gain bandwidth (*100nm*) with *45dB* gain value.

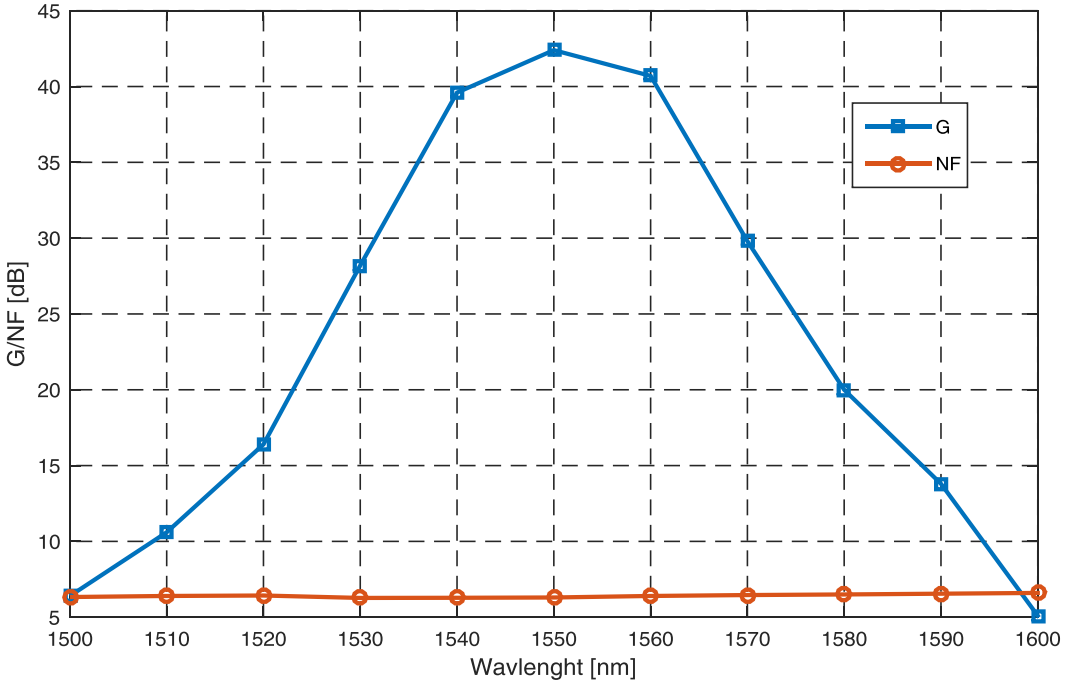

Figure 5.15: C-band EDFA Gain and NF.

It was able to achieve high capacity DWDM network ($40\ GHz \times 64\ channel$) in C+L band (between *1530nm* and *1630 nm*) based on hybrid amplification system integrated with NOLM .Lesser noise is produced and better signal quality is obtained at high bit rate. Moreover, EDFA pumping power is lower that PCF-RA. Thus, the system cost is reduced [10]. The DWDM system is testes successfully results into high bit rate (*40 GHz)* as shown in Figure 5.18. The hybrid amplifier offers low power requirement, low noise, high gain and wider bandwidth. Hence, it represents a potential solution for long –haul DWDM network [11]. This DWDW network with high bit rate and wide bandwidth is optimal for high internet traffic, large number of user and long distance transmission system.

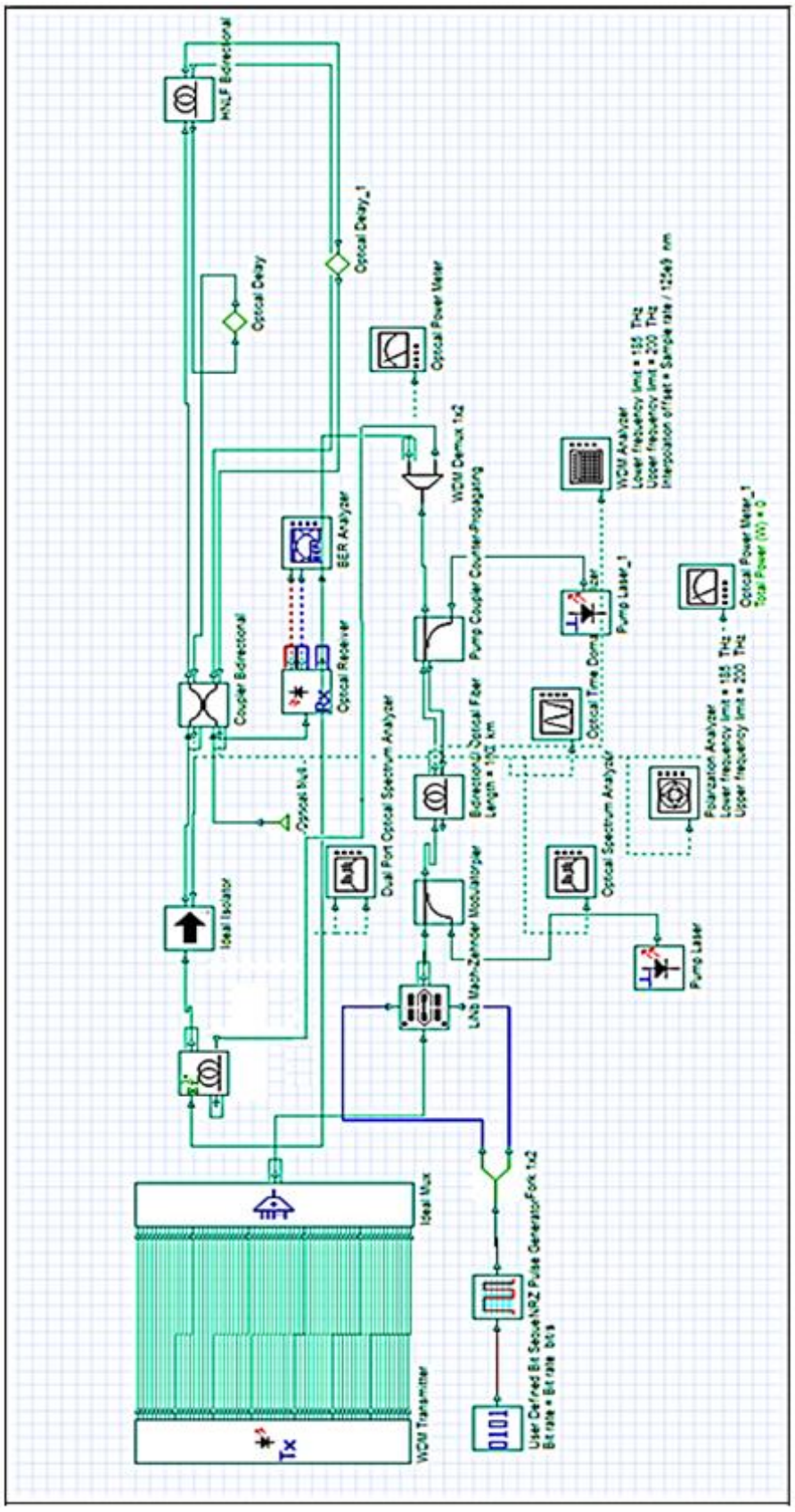

Figure 5.16: DWDM network based on hybrid amplification system.

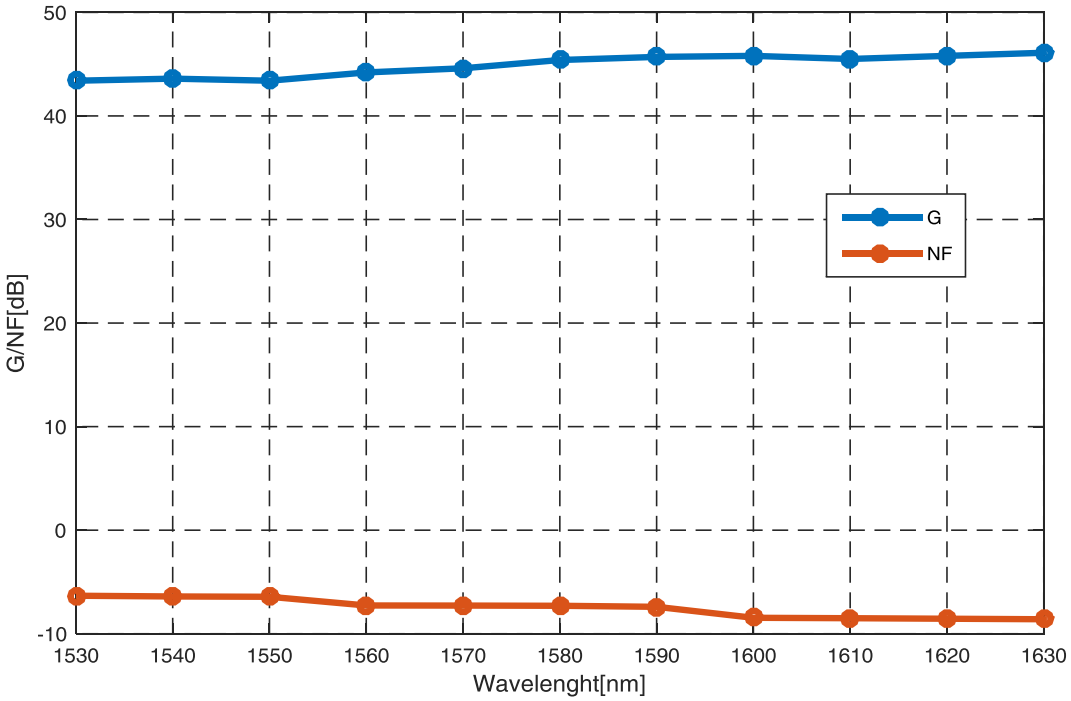

Figure 5.17: Hybrid amplifier gain and NF.

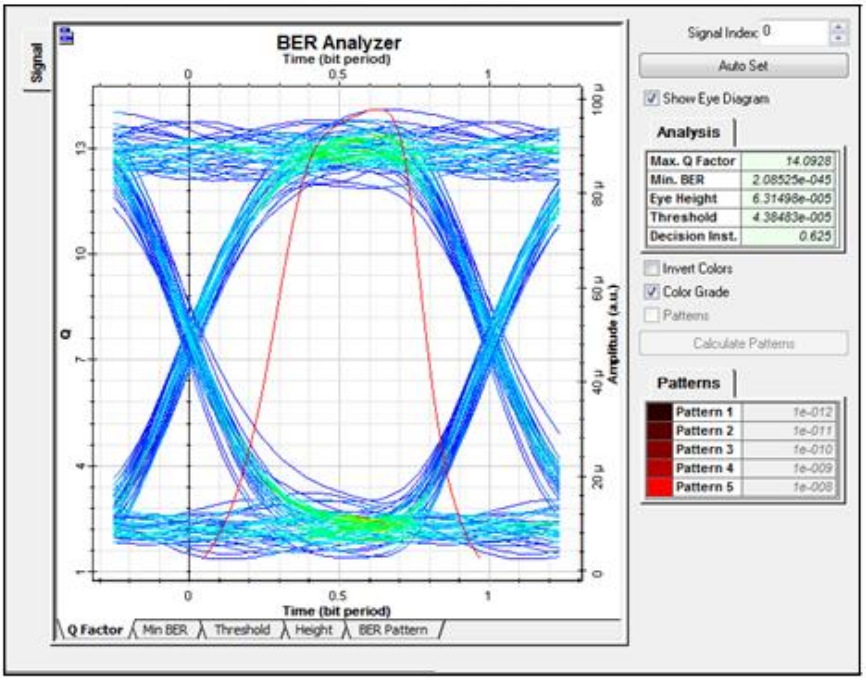

Figure 5.18: Q factor, BER and eye diagram for 40 GHz.

5.5. References

[1] Katsuske Tajima, jain Zhou, Kazuhide Nakajima, and kiminori Sato “Ultralow Loss and Long Length Photonic Crystal Fiber” Journal of Wavelength Technology, Vol, 22 No.1 January 2004.

[2] H. Kidorf, K. Rottwitt, M. Nissov, M. Ma and E. Rabarijanaona, “Pump Interactions in a 100-nm Bandwidth Raman Mmplifier,” IEEE Photon. Technol. Lett., Vol. 11, No. 5, pp. 530-532, May 1999.

[2] Daniel Mahgerefteh, Douglas L. Butler, and Julius Goldhar “Technique for measurement of the Raman gain coefficient in optical fibers” Optics Letter ,Vol. 21, No. 24 ,December 15, 1996.

[3] G. J. Pendock and D. D. Sampson, “Transmission performance of high bit rate spectrum-sliced WDM systems,” J. Lightwave Technol., vol. 14, pp. 2141–2148, Oct. 1996.

[4] Ashwin Gumaste, Tony Antony, "DWDM Network Designs and Engineering Solutions", Cisco Press, December 13, 2002. ISBN: 1- 58705-074-9.

[5] G. Ivanovs, V. Bobrovs, O. Ozolins and J. Porins," Realization of HDWDM transmission system", International Journal of the Physical Sciences Vol. 5(5), pp. 452-458, May 2010, ISSN 1992 - 1950 © 2010 Academic Journals.

[6] P. C. Becker, N.A. Olsson and J.R.Simpson, “Erbium-doped fiber amplifiers fundamentals and technology”, Academic Press.1999.

[7] Dr. W. Luhs , “Experiment 14, Erbium doped fiber amplifier”, MEOS GmbH 79427 Eschbach - August 1998/ July 2003.

[8] Ahmet Altuncu, Arif Basgumus, Burcin Uzunca Ekim Haznedaroglu, “Design and Characterization of High Performance C and L Band Erbium Doped Fiber Amplifiers (C,L-EDFAs),” Dumlupınar University, Kutahya, Turkey.

[9] Arwa H. Beshr, Moustafa H. Aly and A.K. AboulSeoud "Amplified Spontaneous Emission Noise Power in Distributed Raman Amplifiers," International Journal of Scientific & Engineering Research Volume 3, Issue 5, May-2012, ISSN 2229-5518.

[10] J. Hansryd, P. A. Andrekson, J. Li, and P. O. Hedekvist, "Fiber Based Optical Parametric Amplifiers and Their Applications, " IEEE J. of Selected Topics in Quantum Electronics, Vol. 8, No. 3, pp. 506-520, May/June 2002.

[11] S. M. Kobtsev and A. A. Pustovkikh, "Improvement of Raman Gain Flatness by Broadband Pumping Sources," Laser Physics, Vol. 14, No. 12, pp. 1488- 1491, 2004.

Chapter- 6

Conclusion and Future Research Direction

6.1 Conclusion

A novel design to low noise optical amplification system based on a photonic crystal fiber (PCF) Raman amplifier has been thoroughly investigated in this research and applied on a Dense Wavelength Division Multiplexing network (DWDM). It has been shown that using a Distributed Raman amplifier (DRA) in DWDM network plays a significant role in improving the network performance since it reduces the noise figure (NF) and improves bit error rate (BER) of the system. Thus, DRA with low pump power presents a promising technology in long-distance DWDM networks. Furthermore, it has been shown that the generated amplified spontaneous emission (ASE) noise from Raman amplifier is heavily reduced by using nonlinear optical loop mirror (NOLM). Externally modulated lasers (EMLs) have been used instead of directly modulated lasers (DMLs) in DWDM network transmitter to stabilize the output signal by reducing the frequency chirp caused by NOLM.

A 2-D hexagonal photonic crystal fiber (PCF) and wave propagation have been modeled successfully using finite-difference time domain (FDTD) method. In addition, PCF dispersion and confinement losses are analyzed for a chosen wavelength, a low confinement loss, almost zero dispersion, and small effective area PCF was designed using small inner-holes rings and big outer-holes rings. This design has been developed for proposed PCF Raman amplifier because of the small effective area and the compatibility with low loss fiber optics. The properties of the proposed PCF Raman amplifier for different air-hole fraction ratios have been thoroughly described. Moreover, the influence of the geometrical parameters and Germania dopant concentration level

on the PCF cross section have been investigated for the gain and noise performance. It was found that PCF suffers from high background loss for small effective areas. Thus, a tradeoff between loss and PCF effective area has to be made to obtain high Raman gain.

Finally, a hybrid amplification system based on Erbium doped fiber amplifier (EDFA) and distributed Raman amplifier (DRA) has been investigated successfully for high bit rates in DWDM networks. It has been shown that this system has significantly low noise spectrum, high optical signal to noise ratio (OSNR) and low noise figure (NF) compared to discrete amplifiers. In addition, it has much flatter gain profile so that more channels have been accommodated. The hybrid amplifier support high data traffic in C+L band. Features such as wide bandwidth, low NF, flat gain, low noise spectrum and high gain have been achieved. Thus, the proposed model may find many applications in high capacity DWDM networks and can result into high growth in internet traffic for high number of users in long distance DWDM networks.

6.2 Future Research Direction and Improvements

Photonic crystal fibers (PCF) is one of the most sophisticated and specialized waveguide in telecommunication systems so far. The applications of PCF are just beginning to be realized. The following related topics require further investigation for future research:

- The gain and attenuation of the designed PCF-RA can be significantly improved by using Vapour-phase Axial Deposition (VAD) fabrication technique to prepare extremely pure optical glass fiber with very low attenuation and optimal optical properties. Moreover, eliminating the presence of OH contamination improves the gain and reduces the attenuation to a larger exert in small effective area PCF.

- More energy efficient Raman amplification can be achieved by applying monitoring and managing power consumption. Power reduction in Raman amplification is obtained when monitoring and managed power consumption is high and OSNR requirements are high. In addition, using different modulation methods such as polarization-multiplexed Quadrature-phase-shift-keyed (PM-QPSK) and polarization-multiplexed rectangular 16-array quadrature amplitude modulation (PM-16-QAM) leads to lower power consummation per bit due to the higher spectral efficiency.

- Design and simulation of a Hollow-Core Photonic Crystal Fiber (HC-PCF) Raman amplifier. HC-PCF allows the possibilities of using liquid or gas in the core section of the fiber. In addition, since the light propagation in HC-PCF is based on the Photonic bandgap, it gives new opportunities in the realization of optical waveguides with cladding refractive index below the core refractive index. These features are not possible in the proposed PCF Raman amplifier because the light propagation is based on the total internal reflection phenomena.

- True Wave REACH fiber fabricated by Kurukawa Company provides optimal Raman amplification performance over long distance with higher capacity. This fiber allows more effective coupling of the optical transmitted signal and the pump signal in DRA. In addition, it provides zero dispersion wavelength and low attenuation by reducing the (OH^-) ions peak. Thus, using True Wave REACH fiber minimizes the higher power requirements and also reduces cost.

- Investigating the effect of channel spacing and to achieve the optimal DWDM network design. Increasing channel spacing decreases the network to a certain optimal channel spacing. Beyond this optimal spacing the network cost increases.

- Although DRA has been used to achieve a broadband amplification gain profile, EDFA gain profile is not linear for all the channels. Hence, some channels receive less amplification compared to other channels. This means OSNR for all the channels may not be the same. Suitable OSNR algorithms can be written to optimize channel placement to maximize OSNR in all the channels.

- Experimental verification of the simulation results which could not be performed due to unavailability of proper instrumentation in our laboratory.